THE THERMAL DECOMPOSITION OF SILVER OXIDE.

by

P. J. HERLEY B.Sc. (Hons.) (Rhodes).

A thesis submitted in part-fulfilment of the requirements for the Degree of Master of Science of Rhodes University.

Department of Chemistry,
Rhodes University,
Grahamstown,
South Africa.

June, 1959.

ACKNOWLEDGEMENTS.

The author wishes to express his appreciation to Dr. E.G. Prout, M.Sc., Ph.D., (S.A.), of Rhodes University, under whose careful guidance this research work was conducted and to thank him for his valuable criticism and keen interest in all aspects of the work.

The author is also indebted to Mr. F. van der Water for his assistance with the technical aspects of the work and to Messrs. African Explosives and Chemical Industries Limited, for a grant held throughout the tenure of this work.

CONTENTS.

1. INTRODUCTION.

The thermal decomposition of solids is characterized by the formation and growth of nuclei at sites on the surface of the solid or within the crystal lattice. Such nuclear formation is favoured by disorganisation of the crystal either by mechanical damage, or by the presence of impurities[1]. Disorganisation results in positions which have a high thermodynamic instability. The nuclei are likely to be formed initially at the corners and the edges of the crystal since these are more prone to damage. Careful handling[2] and storage in vacuo often leads to a large reduction in their number, while deliberate scratching[3] of the surface facilitates their production.

The number of potential sites for nuclear formation is also increased by pre-irradiation with ultra-violet light, though there are indications that a different type of nucleus may be produced[4]. Nucleation can be facilitated by pre-irradiation with electrons[5], neutrons[6], X-rays[6], gamma-rays and atomic particles[7].

The nature of the nuclei is not always clearly defined, but it is generally accepted that they are composed of solid reaction product; e.g. in the decomposition of barium azide[8] and silver oxalate[9], nuclei of metallic barium and silver, respectively, are formed.

Types of Nuclei.

In general, two types of nuclei are identifiable i.e. compact and diffuse nuclei. The latter are not directly observable as they spread uniformly throughout the whole crystal; e.g. as with

mercury/...

mercury fulminate[10] which turns brown throughout due to the decomposition product, and with nickel sulphate heptahydrate[11] where two dimensional diffuse bands of the product are formed.

Compact nuclei are confined mainly to the crystal surface. Their characteristics depend upon the relative crystal structures of the parent and product phases, the particular faces on which they are formed and the activation energy of nuclear formation and growth.

PLATE A illustrates the variety of nuclear shapes which have been observed. The dehydration of copper sulphate pentahydrate[2] affords an excellent example of the formation of compact nuclei. With this substance, as dehydration proceeds, nuclei are formed and grow to a star-shaped form. The shape is attributed to the preferential movement of the reaction/product interface along certain planes within the crystal. Chrome alum[12], too, possesses compact spherical nuclei of an interesting nature. The interior growth rate is less rapid than the surface growth rate and the nett result is the production of flattened hemispheres. However, cavities are formed early on in these centres and the nuclei tend to develop diffuse characteristics. A further example of spherical nuclei is found in the decomposition of barium azide[13]. In certain cases, e.g. the decomposition of potassium hydrogen oxalate[14], hexagonal nuclei result. Nuclei obeying a branching chain mechanism have been postulated for the decomposition of potassium permanganate[15]. The suggestion that the decomposition of silver oxalate[16] proceeds by a system of branching plate-like nuclei has also been proposed.

Classification/...

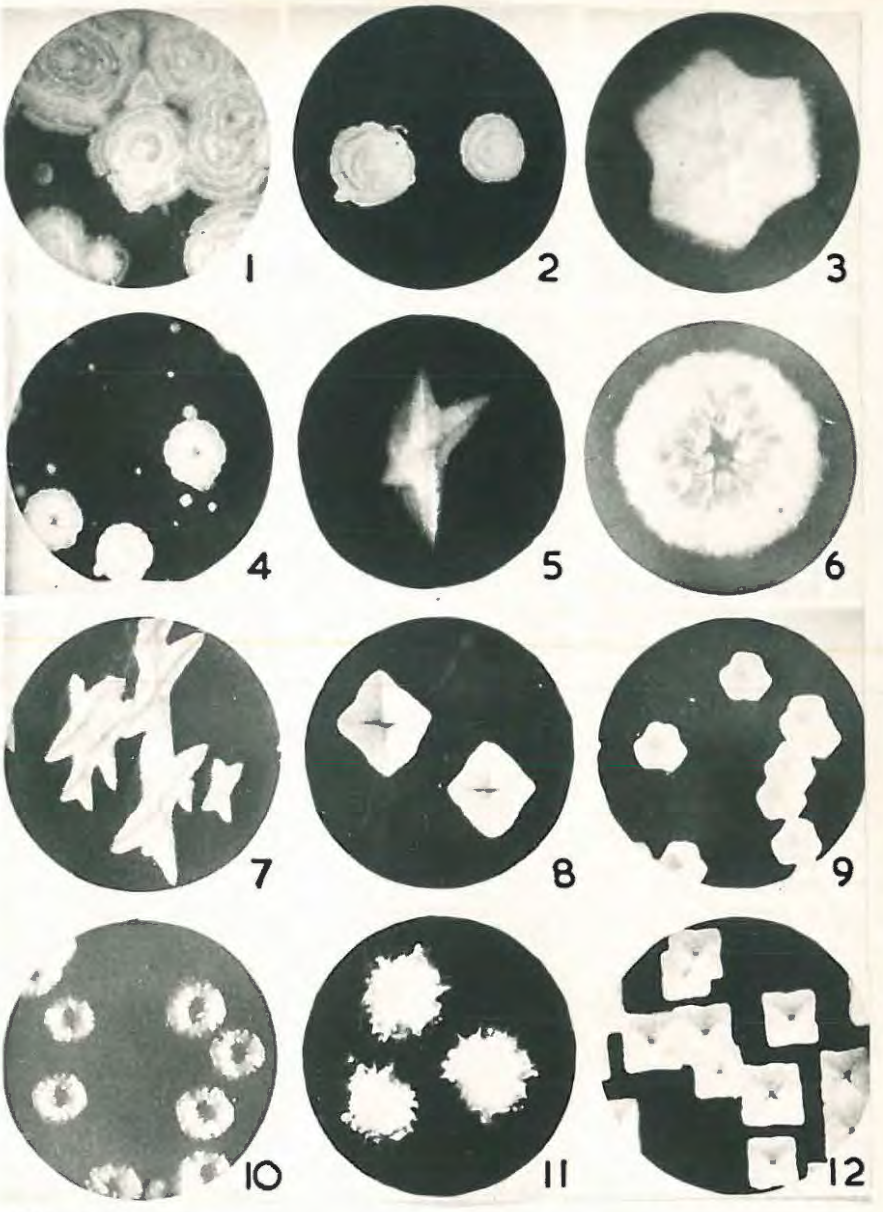

PLATE A.

1, 2, 4. —— MIXED ALUMS.
3, 9. —— COMMON ALUM, III FACE.
6. —— CHROME ALUM, III FACE.
5. —— $CuSO_4.5H_2O$.
7. —— $CuSO_4.5H_2O$ IN VACUO.
8. —— COMMON ALUM, OII FACE.
10. —— $CuSO_4.5H_2O$ IN H_2O.
11. —— AMMONIUM ALUM + H_2O.
12. —— COMMON ALUM, OOI FACE.

Classification of solid decompositions.

The experimental study of thermal decompositions involves the measurement of the overall decomposition and the plotting of rate/time, pressure/time or α/time curves where α is the fraction of the solid decomposed. A study of the mathematical relationships applying to the curves, in association with any characteristics found by visual observations of the decomposing solid, often allows of a description of the mode of decomposition of the solid.

The majority of the reactions studied are of the type:-

A (solid) = B (solid) + C (gas) ..... (1.01).

The character of the p/t curves depends mainly on:-

(i) the mechanism of formation of the nuclei of phase B,

(ii) the shape of the nuclei and

(iii) their mode of growth.

The plots of α against t can be classified into four main types, as shown in DIAGRAM B. In group (a) they are generally sigmoid curves indicating an autocatalytic reaction, and possess an induction period during which time little or no measurable decomposition occurs. Curves of this type are found for the decomposition of whole crystals of potassium permanganate[15], barium azide[13] and salt hydrates.

For some substances, e.g. lead styphnate[17] and mercuric oxalate[18], the initial acceleratory period is of relatively short duration while the decay period is more pronounced i.e. type (b). Substances in group (c) are such that their most rapid rate of reaction

occurs/...

DIAGRAM B.

occurs near the beginning of the decomposition. This is typical of cases where the nucleation process is very efficient and there is rapid coverage of the external surface with small nuclei e.g. lead azide[19].

In group (d) there occurs a small initial evolution of gas which is most rapid at the beginning of the heating e.g. whole crystals of potassium azide[20] and lithium aluminium hydride[21]. This is followed by a period of slow decomposition which leads to an accelerating decomposition. This latter is then succeeded by a period of decay.

In general, the decomposition/time curves studied can be interpreted in terms of a three stage process:-

(i) An initial reaction occurring on the surface of the solid.

(ii) The formation of nuclei of the new phase, B.

(iii) A reaction occurring at the interface between phase A and phase B.

Experimental procedure.

It is obvious that very few solid reactions can be studied by visual or optical methods and it is thus necessary to consider other experimental methods for obtaining the overall decomposition rate. In those cases where the crystals are too small for direct observation, the α/t curves mentioned above are obtained by two experimental procedures. For example, the loss in weight of carbonates and hydrates is measured by means of a quartz spiral balance, while with azides and fulminates it is the pressure of the gaseous product which is measured.

The early studies of solid decompositions concen-

trated/...

trated on the growth and increase in number of the nuclei with time. The reactions associated with the formation of decomposition centres was not explained until Mott and Gurney[22], in their classical work on the photolysis of silver halides, dealt with this aspect of the problem. Nevertheless, valuable contributions to the field of thermal decompositions were made by the early theoretical and practical studies from which the laws of nuclear formation and growth were derived. The laws of nucleation may be divided into nucleation involving a single step, or into more than one step, as follows:-[22a.]

(a) Nucleation involving a single step.

It is assumed that the decomposition of a single molecule results in the formation of a nucleus.

The probability of this happening is

$$k_1 = \nu \exp(-\Delta G_1/RT) \quad \ldots\ldots\ldots\ldots\ldots\ldots \quad (1.02).$$

where ν = the frequency of the lattice vibrations

and ΔG_1 = the free energy of activation for nucleus formation.

For condensed phases,

$$\Delta G_1 \simeq \Delta U_1 - T\Delta S_1$$
$$= E_1 - T\Delta S_1 \quad \ldots\ldots\ldots\ldots\ldots\ldots \quad (1.03).$$

so that equation (1.02) may be rewritten as

$$k_1 = S_1 \nu \exp(-E_1/RT) \quad \ldots\ldots\ldots\ldots\ldots\ldots \quad (1.04).$$

where S_1 = the entropy factor, $e(\Delta S_1/R)$.

If there are N_o potential nucleus forming sites, the rate of nucleus formation is

$$\frac{dN}{dt} \simeq k_1 (N_o - N) \quad \ldots\ldots\ldots\ldots\ldots\ldots \quad (1.05).$$

where/...

where N = the number of nuclei present at time, t.

Neglecting ingestion of potential sites by growing nuclei, on integrating equation (1.05) we obtain;

$$N = N_o (1 - e^{-k_1 t}) \quad \ldots\ldots\ldots\ldots\ldots\ldots\ldots \quad (1.06).$$

and hence, from equation (1.05),

$$\frac{dN}{dt} = k_1 N_o e^{-k_1 t} \quad \ldots\ldots\ldots\ldots\ldots\ldots\ldots \quad (1.07).$$

This is known as the Exponential Law.

In the early stages of the reaction, if ΔG_1 is very large and k_1 small, we can expand the exponential term in equation (1.07) to obtain the approximate relationship

$$N = k_1 N_o t \quad \ldots\ldots\ldots\ldots\ldots\ldots\ldots \quad (1.08).$$

or

$$\frac{dN}{dt} = k_1 N_o \quad \ldots\ldots\ldots\ldots\ldots\ldots\ldots \quad (1.09).$$

i.e. the number of nuclei increases linearly with time. This has been found to occur in the initial stages of the dehydration of copper sulphate pentahydrate[2] and of chrome alum[12].

(b) Nucleation involving multiple steps.

Powers of t greater than unity in equation (1.08) above, e.g. nickel sulphate heptahydrate[11], barium azide[13] and silver oxalate[23], can be accounted for in two ways.

Either a stable nucleus may result from a bimolecular process involving the combination of two active intermediaries, each of which is formed at a constant rate, or several successive decompositions may be required to form a stable nucleus. Both hypotheses lead to the same power law. (Bagdassarian[32]).

i.e./...

i.e. $\frac{dN}{dt} = D.B.t^{B-1}$ ..... (1.10).

where D = a constant

B = the number of successive decompositions (2nd theory)

or $B-1$ = the number of separate entities required (1st theory).

The formation of a nucleus, however, does not guarantee that the centre will grow to a size where it will, in effect, represent appreciable decomposition of the solid.

Consider a reaction of the type,

A (solid) = B (solid) + C (gas) ..... (1.01).

The probability of formation of a fragment of the new phase B at special points in the matrix of A depends not only on statistical energy fluctuations, but also on the possible deformation arising if B has a different molecular volume to that of A. This local deformation in the lattice of A is associated with a certain strain energy, γ, per unit area.

Consider a fragment of B containing m molecules. The free energy change when the fragment is formed is

$\Delta G_1 = m\Delta G_B + \sigma\gamma$ ..... (1.11).

where σ = the shape factor, ($4\pi r^2$ for a spherical interface),

and, if v_m = the volume per molecule of B,

then, for spherical fragments

$m = \frac{4\pi r^3}{3 v_m}$ ..... (1.12).

and equation (1.11) becomes

$\Delta G_1 = m\Delta G_B + \gamma(36\pi v_m^2)^{\frac{1}{3}} m^{2/3}$ ..... (1.13).

$= am^{2/3} - bm$ ..... (1.14),

where/...

where a is proportional to the strain energy

and b is the negative bulk free energy change per molecule.

Thus, when γ is positive, ΔG_1 must pass through a maximum at $m = m^*$; a fragment has the critical size to be in equilibrium with its surroundings. This is illustrated in DIAGRAM C below.

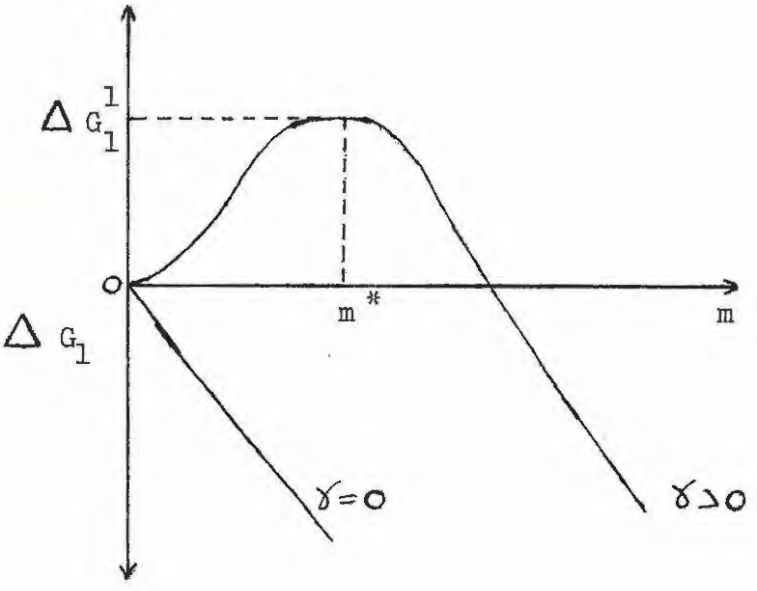

DIAGRAM C.

As can be seen from the plot, the induced strain tends to cause small fragments of B to revert to A, whereas larger fragments ($m > m^*$) are irreversible with respect to the transformation $A(s) = B(s) + C(g)$. Hence, further reaction tends to take place at the interface rather than produce a large number of sub-microscopic fragments of B, and the reaction spreads outwards from its "initial commencement points" or nuclei.

If the activation energy of nucleus growth is less than that required for nuclei formation, rapid growth of nuclei

occurs/...

occurs at certain localised spots on the crystal, resulting in the auto-catalytic nature of curve (a). Wischen[13] confirmed this for barium azide.

However, if the activation energies of nucleus growth and nucleus formation are both of the same order, a large number of small nuclei are formed as in curve (b). A reduction in, or the virtual removal of, the acceleratory period by grinding or crushing yields curve (c). Curve (d) is simply a combination of (a) and (c) and represents two phases of the reaction, one of which is initiated extremely rapidly.

It has been shown that one or more of three main stages may occur in a decomposition viz. an induction period, an acceleratory period and a decay period. The last two periods have been exhaustively studied and mechanisms of decomposition have been postulated. No general mechanism covering all decompositions has, as yet, been obtained. This is unlikely, since experimental observations have indicated that nearly all substances decompose in a manner peculiar to themselves. A few generalisations have, however, been made.

The acceleratory period.

Firstly, we will consider the acceleratory period, where nucleus growth is of importance. Four main mechanisms of decomposition over this period have been postulated. They are:-

(i). The power law.

(ii). The exponential (or logarithmic) law.

(iii). The Prout-Tompkins equation.

(iv). The modified Prout-Tompkins equation.

(i)/...

(i). The power law.

The growth of nuclei can be considered as follows:-

Let r = a size parameter

= the length of the nucleus for one dimension,

or = the radius of a circular nucleus or side of a square nucleus for two dimensions,

or = the mean radius for three dimensions.

Let $G(t)$ = a growth function.

Then the size of the nucleus which commenced growing at $t = y$ is

$$r(t,y) = \int_y^t G(x)\,dx \quad \ldots\ldots\ldots\ldots\ldots\ldots\ldots\ldots \quad (1.15).$$

Thus, the volume of the nucleus is

$$v(t,y) = \sigma\,[r\,(t,y)]^{\lambda} \quad \ldots\ldots\ldots\ldots\ldots\ldots\ldots\ldots \quad (1.16).$$

where σ = a shape factor $= \frac{4}{3}\pi$ for a spherical nucleus.

and λ = 1, 2 or 3 depending on the number of dimensions of the nucleus.

The total volume of all nuclei, V_t, at time, t, is therefore

$$V\,(t) = \int_0^t v(t,y) \left[\frac{dN}{dt}\right]_{t=y} dy \quad \ldots\ldots\ldots\ldots\ldots\ldots \quad (1.17).$$

which, on substituting in equations (1.15) and (1.16) becomes

$$V\,(t) = \int_0^t \sigma \left[\int_y^t G(x)\,dx\right]^{\lambda} \left[\frac{dN}{dt}\right]_{t=y} dy \quad \ldots\ldots\ldots \quad (1.18).$$

When $\frac{dN}{dt}$ or its appropriate form, as well as $G\,(t)$, is known, we can evaluate $V\,(t)$ and hence the degree of decomposition. For example, assuming a power law nucleation and a constant growth rate, the degree of decomposition can be shown to be

α /...

$$\alpha = C^{*}t^{n} \quad \ldots\ldots\ldots\ldots\ldots\ldots\ldots\ldots\ldots\ldots \quad (1.19).$$

where C^{*} = a constant

and $n = B + \lambda$

Since $\alpha = p/p_f$ where p is the pressure of evolved gas at time, t, and p_f is the final gas pressure, equation (1.19) becomes

$$p = Ct^{n} \quad \ldots\ldots\ldots\ldots\ldots\ldots\ldots\ldots\ldots\ldots \quad (1.20).$$

Aged mercury fulminate[24] has been shown to obey the power law with n = 3 i.e. spherical nuclei are formed. For the formation of compact, spherical nuclei according to a linear law, n should be equal to 4. For aged silver oxalate a value of n between 3 and 4 was found, corresponding to a mainly two dimensional growth with some tendency to form compact nuclei. Small crystals of barium styphnate monohydrate[25] decompose rapidly on dehydration, leaving an open lattice in which nucleation is rapid; i.e. n = 2, two dimensional growth occurs.

(ii) The exponential law.

The decomposition of some substances, notably mercury fulminate[10] and silver oxalate[16], cannot be explained by the above theory. Garner and Hailes[10] derived the concept of linear branching chains to apply to these exceptions, and further postulated a constant branching coefficient, k_2, assuming that the rate of nucleation is effectively constant. Hence the nett rate of nuclei production is

$$\frac{dN}{dt} = k_1N + k_2N \quad \ldots\ldots\ldots\ldots\ldots\ldots\ldots\ldots\ldots\ldots \quad (1.21).$$

from/...

from which it can be shown that,

$$p = C^{l}e^{k_2 t} \quad \ldots\ldots\ldots\ldots\ldots\ldots\ldots\ldots\ldots\ldots \quad (1.22).$$

The linear branching chains would, however, separate the crystal into mosaic blocks which would decompose slowly. This led to the postulation of branching plate-like nuclei. The general exponential relationship still held.

(iii). The Prout-Tompkins equation.

In the above treatment, however, interference of chains during growth was neglected and Prout and Tompkins[15] in their work on potassium permanganate evolved the following mechanism to allow for this factor.

It is assumed that there are N_o nuclei originally present in the crystal, consisting of molecules of reactant whose decomposition is highly favoured. They are present mainly on the surface but some may be present within the mass e.g. at internal cracks. The reaction is therefore mainly initiated on the external surface, and leads to the formation of an array of product molecules which, in general, have unit cells differing in geometric form and dimensions from that of the reactant. The effect of such an array of product molecules will result in the formation of lateral strains similar to those resulting in the formation of Smekal cracks[26] but of a much greater magnitude. These strains produce cracks, at the mouths of which nuclear formation will be favoured. The result is that, as the reaction proceeds, the inner surfaces of the crevices will be progressively covered with product molecules of different dimensions. This array will produce further cracking

perpendicular/...

perpendicular to the inner surface. The evolved oxygen escapes through the crevices created by the penetration of the reaction into the crystal. It is therefore thought that the production of planes of strain or deformation are brought about by the surface array of product molecules; along these planes the deformation effect of the product on the electronic structure of an adjacent molecule of potassium permanganate will be a maximum and here decomposition is favoured. Such deformation can be transmitted over short distances by induction so that there will be a number of potentially reactive reactant molecules associated with such planes and, on the average, there will be a certain time interval between the creation of the conditions necessary for reaction and the actual decomposition of the molecule. The depth of such planes can be regarded as being fairly constant, at least in the initial stages, since they will be extended at the forward edge at the same rate as the reaction proceeds at its rear.

Now, if k_2 is the probability of branching occurring and if k_3 is the probability of termination of the nuclei,

$$\frac{dN}{dt} = k_1 N_o + (k_2 - k_3) N \quad \ldots\ldots\ldots\ldots\ldots\ldots \quad (1.21A).$$

Soon after the reaction commences, the potential nucleus forming sites, (N_o), are exhausted and equation (1.21) becomes

$$\frac{dN}{dt} = (k_2 - k_3) N \quad \ldots\ldots\ldots\ldots\ldots\ldots \quad (1.22A).$$

The rate of decomposition, $d\alpha/dt$, may be supposed to be proportional to the number of nuclei present i.e.

$$\frac{d\alpha}{dt} = k^1 N \quad \ldots\ldots\ldots\ldots\ldots\ldots \quad (1.23).$$

For/...

For a symmetrical p/t curve, as for potassium permanganate, certain boundary conditions may be applied since, at the inflexion point, $\alpha_i = \frac{1}{2}$,

Thus,

at $t = o$, $\alpha = o$, $k_3 \therefore = 0$.

at $t = t_i$, $\alpha = \alpha_i = \frac{1}{2}$, $d\alpha/dt$ is a maximum,

and $k_2 = k_3$ since dN/dt changes sign.

i.e. the boundary condition is

$$k_3 = k_2 \frac{\alpha}{\alpha_i} \quad \ldots\ldots\ldots\ldots\ldots\ldots\ldots\ldots\ldots\ldots \quad (1.24).$$

Hence equation (1.21) becomes

$$\frac{dN}{dt} = k_2 \left[1 - \frac{\alpha}{\alpha_i} \right] N \quad \ldots\ldots\ldots\ldots\ldots\ldots \quad (1.25).$$

or

$$\frac{dN}{d\alpha} = k \left[1 - \frac{\alpha}{\alpha_i} \right] \quad \text{where } K = \frac{k_2}{k^1} \quad \ldots\ldots\ldots \quad (1.26).$$

On integration of equation (1.26) we obtain

$$N = k \left[\alpha - \frac{\alpha^2}{2\alpha_i} \right] \quad \ldots\ldots\ldots\ldots\ldots\ldots\ldots \quad (1.27).$$

and using equation (1.23) this transorms to

$$\frac{d\alpha}{dt} = k_2 \alpha (1 - \alpha) \quad \ldots\ldots\ldots\ldots\ldots\ldots\ldots\ldots \quad (1.28).$$

Letting $\alpha_i = \frac{1}{2}$, on integration we get

$$\log \frac{\alpha}{1-\alpha} = k_2 t + c_2 \quad \ldots\ldots\ldots\ldots\ldots\ldots\ldots\ldots \quad (1.29).$$

or, since $\alpha = p/p_f$

$$\log \frac{p}{p_f - p} = k_2 t + c_2 \quad \ldots\ldots\ldots\ldots\ldots\ldots\ldots\ldots \quad (1.30).$$

Equation (1.30) is known as the Prout-Tompkins equation and has been found valid for potassium permanganate[15], nickel formate[27], ammonium

perchlorate/...

perchlorate[28], caesium and rubidium permanganates[29] and lead oxalate[36].

(iv). The modified Prout-Tompkins equation.

With silver permanganate, Prout and Tompkins[30] found that equation (1.30) could be applied to the acceleratory period only up to $\alpha \approx 0.1$, but that the results were well fitted by a modified form of this equation. This equation results when the branching coefficient, k_2, is not constant but varies inversely with time, so that

$$k_2 = k_2^1/t \quad \ldots\ldots\ldots\ldots\ldots\ldots\ldots\ldots\ldots\ldots \quad (1.31).$$

Equation (1.25) would become

$$\frac{dN}{dt} = \frac{k_2^1}{t} N (1 - 2\alpha) \quad \ldots\ldots\ldots\ldots\ldots\ldots\ldots \quad (1.32).$$

whence

$$t \frac{d^2\alpha}{dt^2} = k_2^1 (1 - 2\alpha) \frac{d\alpha}{dt} \quad \ldots\ldots\ldots\ldots\ldots\ldots \quad (1.33).$$

Integrating both sides of equation (1.33) we have; (since $\alpha = o$ at $t = o$),

$$t \frac{d\alpha}{dt} - \alpha = k_2^1 (\alpha - \alpha^2) \quad \ldots\ldots\ldots\ldots\ldots\ldots\ldots \quad (1.34).$$

and $\therefore$

$$\log \frac{\alpha}{(k_2^1 + 1) - k_2^1\alpha} = (k_2^1 + 1) \log t + c^1 \quad \ldots\ldots\ldots\ldots\ldots \quad (1.35).$$

which reduces to

$$\log \frac{\alpha}{1 - \alpha} = k_2^1 \log t + c^1_2 \quad \ldots\ldots\ldots\ldots\ldots\ldots\ldots \quad (1.36).$$

when k_2^1 is very large, i.e. t is very much greater than $1/k_2^1$.

Since $\alpha = p/p_f$, equation (1.36) becomes

log/...

$$\log \frac{p}{p_f - p} = k_2^1 \log t + c^1_2 \quad \ldots\ldots\ldots\ldots\ldots\ldots\ldots \quad (1.37).$$

The induction period.

The induction period, where present, has received relatively little attention. This is probably the most difficult part of a decomposition to explain. In the decomposition of the permanganates, Sole[31] considers that the induction period represents the time during which the product is either forming or thickening on the surface of the crystal. When the strain created by this coating of product is high enough, cracks occur in the reactant interface and the acceleratory period begins.

In the case of azides and hydrates, the induction period is assumed to represent an abnormally slow growth of nuclei due to high interfacial tension and consequently a high activation energy for nuclear growth.

The decay period.

The extensive overlap of compact nuclei in the later stages of any solid decomposition results in the formation of a contracting interface of complex shape, enclosing blocks of reactant. If the interface remains intact, the Avrami[33] - Erofeyev[34] equation,

$$\alpha = 1 - \exp(-k_4 t^3) \quad \ldots\ldots\ldots\ldots\ldots\ldots\ldots \quad (1.38).$$

holds.

Groocock and Griffiths[35], in their work on α - lead azide, showed that the decay period followed from the point

of/...

of coalescence of the increasing nuclei on the crystal surface, and subsequent decomposition would be controlled by the rate of penetration of the lead/lead azide interface into the crystal. At nucleus coalescence, the particles can be considered to be identical spheres of undecomposed azide, surrounded by a metallic layer.

If the interface moves at a constant velocity i.e. $dr/dt = -k_5$, where r is the radius of each sphere at time, t, the rate of decomposition is

$$\frac{d\alpha}{dt} = 4\pi r^2 (dr/dt)\, c\rho \quad \ldots\ldots\ldots\ldots\ldots\ldots\ldots \quad (1.39).$$

where c is the number of particles in unit weight of the sample and ρ is the density of lead azide. If the radius of the particles is a at time, τ, it can readily be shown that

$$\left(\frac{d\alpha}{dt}\right)^{\frac{1}{2}} = (4\pi c\rho k_5)^{\frac{1}{2}} (a + k_5\tau) - (4\pi c\rho)^{\frac{1}{2}} k_5^{3/2} t \ldots\ldots \quad (1.40).$$

and a plot of $(d\alpha/dt)^{\frac{1}{2}}$ against t should give a straight line, as was experimentally found in this case. These facts and the supporting evidence, e.g. the microscopic evidence for a lead/lead azide interface, indicate a contracting interface mechanism.

In the thermal decomposition of potassium permanganate, Prout and Tompkins[15] suggested that, during the decay period, the rate controlling factor becomes the number of remaining, unreacted potassium permanganate molecules, which is proportional to $(p_f - p)$. Not all these molecules are favourably situated for decomposition, since this requires that a molecule of product be adjacent to an unreacted potassium permanganate molecule, because contiguity facilitates decom-

position/...

position. Therefore, the rate of reaction is

$$\frac{dp}{dt} = k_6 (p_f - p) \delta \quad \ldots\ldots\ldots\ldots\ldots\ldots\ldots\ldots \quad (1.41).$$

where δ denotes the probability of this favoured situation. From geometric considerations based on the type of branching postulated, it is reasonable to assume that δ is determined by the fraction of the number of product molecules to the total number of all molecules present, i.e. by p/p_f - this has the desired property of approaching unity as p tends to p_f. Thus, during the decay period,

$$\frac{dp}{dt} = k_6 \frac{(p_f - p)}{p_f} p \quad \ldots\ldots\ldots\ldots\ldots\ldots\ldots\ldots \quad (1.42).$$

which, on integration between limits, reduces to equation (1.30) except that k_2 is replaced by k_6. This treatment has been successfully applied to lead oxalate[36] and ammonium dichromate[37].

Hydrates.

In certain cases, notably the loss of water from hydrates, rates can be predicted by simple geometrical considerations. Thus, for copper sulphate pentahydrate[38], the linear rate of interface propagation may be derived by the application of a contracting rectangular parallelepiped formula[39].

If l is the length of each crystal, d, the thickness, and, v, the volume of each crystal, (l.d), and, if t is the time after the arbitrary zero, and u is the linear propagation rate, then

$$\alpha = v - \frac{(l - 2ut)^2 (d - 2ut)}{v} \quad \ldots\ldots\ldots\ldots\ldots\ldots \quad (1.43).$$

or/...

or

$$\alpha = \frac{2ut(l^2 + 2dl) - 4u^2t^2(2l + d) + 8u^3t^3}{l^2d} \quad \ldots\ldots(1.44).$$

The dehydration of manganous oxalate trihydrate[39] has been successfully treated in a similar manner where, however, over the decay period, reaction particles are assumed to be spherical.

Such an elementary consideration neglects the fact that in a decomposition, nucleation need not occur simultaneously in all crystals. Account has been taken of this in the dehydration of calcium carbonate hexahydrate[40]. Microscopic observations of the decomposition of thin plates of the hydrate under water show that a crystal does not diminish in length and breadth but rather in thickness. Coupled with an almost negligible induction period, it follows therefore, that, since the time interval from the incidence of nucleation until complete surface coverage is negligible, nucleation occurs simultaneously in the upper and lower parallel faces, and the resulting interface traverses the crystal before noticeably spreading from the vertical faces.

The overall reaction rate, consequently, can be derived as follows:-

Let there be n_o crystals of uniform shape and size in the form of thin plates of thickness, d, with upper and lower parallel faces of area, A. The reaction interface proceeds with a linear velocity, u, in a direction perpendicular to the major faces.

The number of crystals nucleated at a time, t, from the start of the reaction, in the interval, dt, is $k_7 n_o e^{-k_7 t}\, dt$.

Now/...

Now at a time, t_2, the volume of resultant, dv, produced from a crystal nucleated at time, t, is

$$dv = 2A\,u\,(t_2 - t) \quad \ldots\ldots\ldots\ldots\ldots\ldots\ldots\ldots \quad (1.45).$$

and thus for n_t particles nucleated at time, t,

$$dV = 2A\,u\,n_o\,k_7 \int_0^{t_2} (t_2 - t)\, e^{-k_7 t}\, dt \quad \ldots\ldots\ldots \quad (1.46).$$

$$= 2A\,u\,n_o \left(t_2 + \frac{e^{-k_7 t_2} - 1}{k_7}\right) \quad \ldots\ldots\ldots\ldots\ldots \quad (1.47).$$

But,

$$\alpha_{t_2} = \frac{Vt_2}{n_o.A.d.} \quad \ldots\ldots\ldots\ldots\ldots\ldots\ldots\ldots\ldots \quad (1.48).$$

Hence

$$\alpha_{t_2} = \frac{2u}{d}\left(t_2 + \frac{e^{-k_7 t_2} - 1}{k_7}\right) \quad \ldots\ldots\ldots\ldots\ldots \quad (1.49).$$

which is valid until $t_2 = \frac{d}{2u}$, when it is assumed that the crystal which was nucleated at zero time will be completely decomposed. After t_2, the values given by the equation will be greater than the true values, the excess at t_3 (greater than $\frac{d}{2u}$), being equal to the decomposition occurring in the interval,

$$t = o \longrightarrow t = \left(t_3 - \frac{d}{2u}\right) \quad \ldots\ldots\ldots\ldots\ldots\ldots \quad (1.50).$$

i.e. the excess equals

$$\frac{2u}{d}\left[t_3 - \frac{d}{2u} + \frac{e^{-k_7(t_3 - d/2u)} - 1}{k_7}\right] \ldots\ldots \quad (1.51).$$

Thus the fractional decomposition at time, t_3, is

$$\alpha_{t_3} = \frac{2u}{d}\left[\frac{d}{2u} + \frac{e^{-k_7 t_3}\,(1 - e^{kd/2u})}{k_7}\right] \ldots\ldots\ldots\ldots \quad (1.52).$$

or/...

or

$$\alpha_{t_3} - 1 = \frac{2u}{k_7 d} \left(1 - e^{k_7 d/2u}\right) e^{-k_7 t_3} \quad \ldots\ldots\ldots\ldots \quad (1.53).$$

which only applies when t is greater than $\frac{d}{2u}$.

k_7, the nucleation constant, is obtained from

$$\log_{10} (1 - \alpha_{t_3}) = - 0.4343\, k_7 t_3 + C_7 \quad \ldots\ldots\ldots\ldots\ldots \quad (1.54).$$

Apart from a slight deviation in the early stages of the decomposition, attributed to the assumption of instantaneous surface coverage of the crystal after nucleation has begun, the agreement between the theoretical and the experimental curves is good.

The foregoing considerations on nuclear growth enable one to deduce, from the mathematical analysis of the p/t plots, the progress of the reaction through the solid. It is possible to define the existence of two dimensional or three dimensional nuclei, growing from (i) a fixed number of centres or (ii) from centres which are increasing in number as a power of the time. Similarly, if the nuclei grow by a branching chain mechanism, the mathematical equations describing the characteristics of the p/t plot will indicate this mechanism. For a large number of substances such as the permanganates and certain oxalates, it is not possible, as yet, to describe the reactions accompanying the progression of the reactant/product interface, or to describe the exact mechanism which gives rise, in the first instance, to the nucleus of product. However, this shortcoming has been largely overcome with substances which are sensitive to ultra-violet light or cathode rays.

Historically/...

Historically, this important development was initiated by the study of the photolysis of silver bromide by Mott and Gurney[22]. They concluded that, on illumination by light of a definite wavelength, the solid absorbs a photon with the formation of a free electron. This results in a positive hole on the surface. This hole forms a neutral bromine atom which is then absorbed elsewhere on the surface. The electron is mobile and becomes trapped on the surface where it reacts with a migrating interstitial silver ion from a Frenkel defect to form a silver atom. When a second photon falls on the surface, the hole produced forms another bromine atom which combines with the one previously formed and bromine gas escapes from the surface of the solid. The remaining electron adds on to the silver atom to form Ag^- which attracts another interstitial cation to form Ag_2. This process is continuous and the silver specks, initially formed, grow in size.

Mitchell[41] extended this work to include the effects of impurities on the formation of nuclei. Sheppard[42,43] had put forward a theory of the formation of "sensitivity specks" of sulphur from the gelatin emulsion on the surface of the solid. These, then, acted as nuclei during the photolytic process. The "specks" were thought to consist of minute crystals of silver sulphide. Mitchell suggested that the silver halides dissolve silver sulphide which ionises in the solid to form a S^- ion and an F-centre. Plate-like aggregates of colloidal silver are formed and, if sufficiently large, break away from the halide matrix. These aggregates correspond to the

"sensitivity/...

"sensitivity specks" of Sheppard's theory. On illumination, the transference of electrons from the F-centres to the aggregates starts a process of ionic migration. The aggregates thus increase in size. The ionic migration process may be summarised as, either a transport of cations as described by Mott and Gurney[22], or the motion towards the centre of vacant anion sites which may result from the removal of electrons from F-centres or which may initially be present as Frenkel defects.

The transfer of these concepts to the field of thermal decompositions was done by Mott[44] in his work on the decomposition of barium azide. Barium azide is considered to be an ionic conductor at room temperature. In the thermal treatment, the electron traps are produced by a surface evaporation of azide ions during the induction period, resulting in a slow linear evolution of nitrogen with time, during this period. cp., potassium azide[20]. The surface evaporation frees metal atoms which go into solid solution. Since these will dissociate, the effect of heating is to increase the concentration of interstitial ions already present and also to provide free electrons. These electrons are finally trapped and the nuclei grow by a process of electrolysis.

Nuclei formed in silver bromide, by the trapping of an electron and the subsequent attachment of an ion, are not stable over indefinite periods, since the electron will escape and thus the centre is destroyed. Stability may be achieved, however, if another electron attaches itself to the atom before the first escapes, in which case, the nucleus will have a chance to build itself

up/...

up to a size so large that it will be stable. Exactly the same thing may be expected to happen in barium azide, and Mott has shown that the number of nuclei, N_t, present at time, t, will be given by

$$\left[\frac{S.Q}{V}\right]^{n} \cdot \frac{t^{n+1}}{n+1} \quad \ldots\ldots\ldots\ldots\ldots\ldots\ldots \quad (1.55).$$

where S is the surface area of a crystal, Q, a constant at a given temperature, V, its volume and, n, the number of electrons necessary to form a stable nucleus. For barium azide at 100°C, N_t is proportional to $t^{3\frac{1}{3}}$, i.e. n = 2, or a nucleus of two electrons and one interstitial ion is stable. At higher temperatures, N_t varies as a higher power of t, corresponding to a much larger nucleus.

Ultra-violet light increases the number of nuclei observed after a given time and also the value of x in $p = Ct^x$ from 6 to 8. The first effect is in accord with Mott's theory, since ultra-violet light causes a surface evaporation of azide ions and thus increases the existing number of electron traps. The higher value of x is due to an increase in the number of barium atoms required to form a nucleus as a result of irradiation, according to Garner and Maggs[4]. They suggest that the ultra-violet light increases the number of centres at which nuclei can be formed linearly with the time of illumination, τ. The number of nuclei created during thermal treatment will, therefore, vary as t_i^p, where (p - 1) is the number of barium atoms required to form a stable nucleus; is then equal to

$$\text{constant}/t_i^{\,p+3} \quad \ldots\ldots\ldots\ldots\ldots\ldots\ldots \quad (1.56).$$

where t_i is the length of the induction period.

For/...

For powdered strontium and barium azides, the slope of $\log \tau / \log t_i$ is 8 - 9, i.e. 4 - 5 barium atoms are required to form a stable nucleus; the figure of Garner and Maggs (4 - 5) is thus apparently in error, since 2p must represent the number of barium atoms in the nucleus. The correct value (2 - 3) then agrees well with the value of x = 8 found by use of the equation $p = Ct^x$. After prolonged illumination, the value of x falls and approaches the value of 3, due to the formation and growth of nuclei by light. The volume of each nucleus and, therefore, the pressure, will then increase as t^3, during heating.

Thomas and Tompkins[45], however, discarded Mott's theory for barium azide since the azide did not show photoconductance. Consequently, the production of free electrons was unlikely. Its conductance is due mainly to anion migration. They concluded that the growth rate of nuclei in the solid was far too high to be accounted for by any mechanism[46] involving both cation and electron processes. They proposed instead their exciton theory outlined on page 26, paragraph 4, of this thesis, where the effects of pre-irradiation are considered.

Mitchell's[41] theory, involved the aggregation of F-centres present initially in barium azide because of $CO_3^=$ impurities. The approximate mobility of these F-centres would be given by

$$\text{constant.}\ c.\ e^{-E/RT} \quad \ldots\ldots\ldots\ldots\ldots\ldots \quad (1.57).$$

where c = the concentration of anion vacancies,

and E = the activation energy for their mobility.

The rate of formation of double F-centres would therefore be

constant/...

$$\text{constant. } c.\ e^{-E/RT}.\ K^2 \quad \ldots\ldots\ldots\ldots\ldots\ldots \quad (1.58).$$

where K = the concentration of single F-centres at $t = 0$.

The number of double centres formed after a time, t, is

$$\text{constant. } c.\ e^{-E/RT}.\ K^2.t \quad \ldots\ldots\ldots\ldots\ldots\ldots \quad (1.59).$$

If N = constant. t^3, then for a four centre complex nucleus the number present is

$$\text{constant. } c^3\ e^{-3E/RT}.\ K^4.t^3 \quad \ldots\ldots\ldots\ldots\ldots\ldots \quad (1.60).$$

The above theories for the decomposition of barium azide serve to illustrate the method of approach which can be adopted for light-sensitive solids - an approach which has been singularly successful in explaining the photographic processes and the thermal and photochemical decomposition of silver oxalate, potassium azide and cuprous azide[47].

The effects of pre-irradiation on thermal decompositions.

An inadequate explanation of the physical characteristics of nucleation often results on consideration of the facts obtained from "straight" thermal decompositions. However, the induction period and subsequent decomposition of certain solids, notably the azides, is affected by pre-irradiation, and the results have given us a clearer picture of nucleation processes. These effects were initially studied by Garner and Moon[48], and Maggs[49]. They found a decrease in the length of the induction period and an increasing reaction rate for barium azide on pre-bombardment of the solid by electrons.

Thomas and Tompkins[45] studied the effects of ultra-violet light on barium azide. Barium azide, on decomposition,

yields/...

yields nitrogen, the pressure of which can be expressed as a function of the heating time, t. viz:-

$$p = C.(t - t^1)^n \quad \ldots\ldots\ldots\ldots\ldots\ldots\ldots\ldots \quad (1.61).$$

where C = a constant

t^1 = the slow growth correction

and n = the slope of the plot of log p against log $(t - t^1)$.

If τ was the irradiation time, it was noted that ultra-violet pre-irradiation increased the value of C to C_τ, which was found to be proportional to $I\tau$ where I is the intensity of the irradiation. Ultra-violet pre-irradiation also shortened the induction period.

The product of pre-irradiation is undoubtedly an anionic vacancy as suggested by Mott[44]. During irradiation, an electron is ejected from a surface azide ion and is trapped at a deep impurity centre. The mobile hole is trapped at a cation vacancy where it may react with an activated adjacent anion to give gaseous product, forming an anion vacancy and an F-centre. The F-centre is destroyed during the warming up period preceeding thermal decomposition, by its electron tunnelling to other mobile holes present at the surface, giving an azide ion and a further anion vacancy. The acceleration of the thermal rate is due to the anion vacancies rendering the F-centres created thermally, mobile, thereby allowing them to form nuclei. As the number of impurity centres is limited, for larger energies of pre-irradiation the anion vacancies compete for the ejected electrons, and F-centres are formed. For a low value of $I\tau$, the establishment of sites for nuclei formation is initially proportional to $I\tau$, and, for those

nuclei/...

nuclei which grow, the resulting mechanism in the subsequent thermal process is unchanged. i.e.

$$p = C.(t - t^1)^6 \quad \ldots\ldots\ldots\ldots\ldots\ldots\ldots\ldots \quad (1.62).$$

Larger energies result in F-centre formation and those with existing vacancies are rendered mobile and either C increases more rapidly than linear with I or, n decreases finally from 6 to 3, since the thermal process during irradiation is such that nuclei aggregation predominates.

Groocock and Tompkins[5] made a detailed study of the bombardment of sodium and barium azides by electrons. They concluded that, for pre-irradiation, the primary effect of the treatment was an increase in the concentration of the sites of anionic vacancies at a rate proportional to $I\tau$. These vacancies are responsible for the movement of the F-centres produced in the thermal decomposition. The greater the anion vacancies, the greater the mobility of the F-centres and the faster their aggregation rate to form nuclei.

However, for variable electron flux bombardment, the following discrepancies arose:-

(i) for the bombardment, C increases as the square of the electron flux (i) and then becomes constant, independent of i, but for pre-irradiation, C varies with $I\tau$.

(ii) n remains approximately 6 for all pre-bombardments, while n = 6 for small ultra-violet irradiation energies only and tends to 3 for high $I\tau$.

These difficulties were overcome by considering

that/...

that, since no nuclei are created during pre-bombardment (n = 6) and electron ejection from the azide ion is the primary act of the beam, sufficient energy for photo-emission is available. Because of the large electron excess present, surface anion vacancies are converted to F-centres which, however, are rendered stationary, since their mobility depends on the simultaneous presence of anion vacancies. Hence nucleus formation is improbable. Regeneration of azide ions and vacancies results during warming up from holes and F-centres. These vacancies which were greatly increased after the irradiation process, assisted in accelerating the thermal reaction by nucleus formation. Since their increase depends on the square of the beam current, they indicated that a bimolecular process would occur which involved a pair of positive holes.

Neutron, electron and gamma-ray bombardment of several inorganic azides was carried out by Bowden and Singh[6]. They found decreased induction periods and an increase in the maximum rate when lithium azide was bombarded with thermal neutrons. The work, however, was mainly concerned with the problem of "hot spots" in explosives.

Prout and Tompkins[18] found that, for mercuric oxalate, a higher initial rate of decomposition resulted from electron pre-bombardment and ultra-violet pre-irradiation, when the material was subsequently decomposed. This suggested a saturation of surface effects, from which they concluded that pre-irradiation affected the individual molecules, and that it penetrated at least two or three molecular layers.

The/...

The primary act of the irradiation is the emission of an electron from the surface oxalate radical, and its subsequent capture by a mercury ion in the second molecular layer i.e. electron transfer followed by an intramolecular change which resulted in the formation of mercurous oxalate. Thus no evolution of gas is necessary or was found.

The decomposition of α-lead azide after pre-irradiation by X-rays, was studied by Groocock[50] who found similar effects to those found for barium azide. After the initial increase of the maximum decomposition rate for small irradiations, a decrease in the maximum decomposition rate with increased dosage was found.

Flanagan[51] observed no effects by gamma-rays from ^{60}Co on the subsequent thermal decomposition of lead styphnate monohydrate. However, the decomposition rate was greatly influenced by neutrons, and he presumed that the fast particles caused such radiation damage that decomposition began from a large number of evenly distributed sites. The unirradiated material decomposed from a smaller number of sites, proceeding via grain boundaries, cracks and other defects of a more localised nature. No detailed explanation of the effects was given.

Prout[7] found unusual irradiation phenomena in his study of the thermal decomposition of pre-irradiated potassium permanganate crystals. Irradiations were carried out in B.E.P.O., the thermal column of B.E.P.O. and in a ^{60}Co "hot spot". He evolved a new approach to the ideas of radiation damage by stating that the acceleration of the decomposition was caused by the formation of "radiation

nuclei"/...

nuclei" during heating. These appear to be independent of nuclei ordinarily operative in the unirradiated solid. He suggested an annealing mechanism for the point defects over the induction period. Prout and Sole[52] extended this theory to silver permanganate and found that the activation energy for point defect migration over the induction period is 1.09 eV. X-ray studies indicated strain and fragmentation within the irradiated crystal at the end of the induction period.

2. PREVIOUS WORK ON THE THERMAL DECOMPOSITION OF SILVER OXIDE.

Lewis[53] studied the thermal decomposition of several preparations of silver oxide in oxygen at atmospheric pressure. He measured dp/dt values at various times for the decompositions at temperatures in the range 320°C - 350°C. The reaction system was connected to a differential water manometer with which pressures were determined. He particularly stated that the rapidity and temperature of drying of his preparations had an influence on the decomposition rate.

He considered the reaction to be autocatalytic; being dependent on the amount of catalyst present. The reaction rate increased with increased temperature and the reaction obeyed the relationship

$$dx/dt = k_g x\ (1 - x) \quad \ldots\ldots\ldots\ldots\ldots\ldots\ldots\ldots \quad (2.01).$$

where x is the fraction of silver produced.

The temperature coefficient of the velocity constants was measured, from which a value of the activation energy was calculated as 31.8 kcal.mole^{-1}.

Initially, he used Merck's silver oxide, one specimen of which decomposed with extremely long induction periods. It was impossible to repeat this determination with any other specimens. His first Merck preparation took 24 hours to decompose completely at 327.5°C, while the decompositions of other Merck prepared silver oxide specimens were completed in three hours at 340°C. Reproducibility on any one specimen was not obtained; varying maximum rates, times for

complete/...

complete decomposition, and other abnormal irregularities were found for decompositions at a particular temperature. He suggested that the reason for this might be due to the presence of impurities or to variations in the physical condition of the powder, e.g. grain size.

Three laboratory preparations were used as well. They were:-

(i). Sodium carbonate solution was added to a dilute silver nitrate solution; the silver nitrate used was twice recrystallised. The precipitated carbonate was then washed by repeated decantation with distilled water; the final washings took 24 hours each. The precipitate was then dried for 24 hours by heating at 240°C to remove all water and carbon dioxide. However, no details were given of storage or of subsequent handling of the preparation.

(ii). A dilute solution of the silver nitrate prepared above, was added to a clear solution of barium hydroxide, both solutions being kept at room temperature.

(iii). As for (ii) above except that both solutions were maintained at 100°C.

For preparations (ii) and (iii) he stated no more than that the reaction was completed with the exclusion of carbon dioxide. The precipitates were carefully washed, and dried at 240°C, but again, no details of handling or storage of the samples were given.

He obtained a slow maximum rate of decomposition; slower than any previous decompositions which he had examined. The

oxide/...

oxide prepared in the cold decomposed even more slowly than preparation (iii) above.

Hood and Murphy[54] used essentially the same decomposition procedure as Lewis, but with the difference that air replaced oxygen. Lewis' results were verified. The method consisted of intimately mixing 0.01 g. of electrolytically precipitated silver with 0.15 g. of Mallinckrodt's U.S.P.IX silver oxide. The mixture was allowed to stand exposed to the air while the apparatus heated up. Rate curves were plotted, the rate being measured only after an initial 10 minutes had elapsed.

The equation,

$$\ln x/(1 - x) = k_9 t + c_9 \quad \ldots\ldots\ldots\ldots\ldots\ldots\ldots\ldots \quad (2.02).$$

was derived by integration of equation (3.01) where x is the fractional number of moles of silver oxide decomposed and k_9 is the reaction rate constant.

This equation was applied to the rate plots. From the values of k_9 at various temperatures, an activation energy of 25.6 kcal. mole^{-1} was obtained. The ratio of rate constants per 10°C temperature difference was 1.50 compared to that of the value of 1.53 found by Lewis.

Benton and Drake[55] prepared an active silver surface by reducing precipitated silver oxide with hydrogen at low temperatures. They investigated the oxidation of this silver and also the dissociation of the surface oxide layer. They obtained dissociation at about 200°C. The thermal decomposition obeyed the normal interface

relationship/...

relationship for balanced reactions at a constant interface i.e.

$$d[O_2]/dt = k_{10} (1 - p/p_e) \quad \ldots\ldots\ldots\ldots\ldots\ldots\ldots \quad (2.03).$$

where p is the pressure of the oxygen at time, t, and p_e is the equilibrium dissociation pressure. They derived values for the activation energies of both the forward and reverse reactions of;

$$2\,Ag_2O = 4\,Ag + O_2 \quad \ldots\ldots\ldots\ldots\ldots\ldots\ldots \quad (2.04).$$

and found that they differed by the heat of reaction. The energy of activation for the forward reaction was 35 - 36 kcal. $mole^{-1}$.

Pavlyuchenko and Gurevich[56] prepared silver oxide in darkness but in the presence of air (at 5°C), by the addition of an aqueous solution of potassium hydroxide to an aqueous solution of silver nitrate at 5°C. The precipitated silver oxide was dried at room temperature. The sample was thermally decomposed in vacuo, and the rate of pressure increase with time was followed. The curves gave a maximum rate of decomposition at the beginning of the reaction. This rate then rapidly decreased, the reaction being completed in about 75 minutes at 190°C. The sample was extremely light sensitive; the rate of decomposition being considerably increased by pre-exposure to ultraviolet light. They obtained a low activation energy of 10.2 kcal. $mole^{-1}$.

Iijima[57] studied the thermal dissociation of silver oxide at relatively low temperatures (230°C - 270°C) using a thermal balance. The decomposition was found to begin in the range 230°C - 270°C. The reverse reaction i.e. the oxidation of silver to silver oxide did not occur at any temperature when the oxygen pressure was taken below 760 mm. mercury pressure, and the reverse reaction velo-

city/...

city of the dissociation equilibrium at these low temperatures was too small to be detected.

Averbukh and Chufarov[58] decomposed silver oxide on a spring balance in atmospheres of oxygen, hydrogen or oxygen and hydrogen from pressures of (10 - 760) mm. mercury, and the decrease in weight was determined. V, the rate of dissociation, became noticeable at 300°C. V was determined for a constant degree of dissociation and an apparent energy of activation of 29.0 kcal. $mole^{-1}$ was found.

Garner and Reeves[59], using preparations similar to Lewis', decomposing in vacuum and measuring the oxygen pressure on a McLeod gauge, found that the maximum rate occurred at the beginning of the reaction and that the decompositions at a fixed temperature were highly irreproducible. No long induction periods or curves of an autocatalytic type were obtained at decomposition temperatures of 300°C - 330°C. They showed, too, that at temperatures of 180°C - 220°C silver oxide is converted to silver in the presence of cylinder oxygen.

They then prepared samples of silver oxide by Lewis' methods and heated these in a thick walled bulb at 200°C - 300°C at pressures of (23 - 30) atmospheres to remove, as they presumed, any nuclei of metallic silver produced in the course of the preparation. They obtained a dense, polycrystalline solid with particles approximately 0.3 mm. in diameter. They found that the decomposition in vacuo commenced on the surface of the solid. The p/t curves were fitted by the equation

$$p^{\frac{1}{3}} = k_{11}t + c_{11} \quad \ldots\ldots\ldots\ldots\ldots\ldots\ldots\ldots \quad (2.05).$$

A/...

A negative intercept on the t axis was obtained when $p^{\frac{1}{3}}$ was plotted against t. They obtained a value of 43.0 kcal. $mole^{-1}$ for the activation energy. The value of k_{11} was increased four times by grinding and the percentage decomposition at the maximum rate was reduced from (20 - 25)% to about 12% of the total decomposition. Pre-irradiation by ultra-violet light had no effect on the decomposition.

3. OBJECTS OF THE RESEARCH.

The data available on the decomposition of silver oxide is conflicting. There are discrepancies between the activation energies, the form of the pressure/time curves and the mathematical relationships describing such plots. In addition, there is disagreement as to the effect of the decomposition products and pre-irradiation by light. Furthermore, the mathematical relationships applied by Lewis[53], Hood and Murphy[54] and Garner and Reeves[59] did not in any instance describe the complete decomposition curve.

In the present work, the objects have been to distinguish between the various treatments and results, and to find some equation which is applicable over the complete reaction. As well, it was of interest to extend the study of pre-irradiation effects of silver oxide.

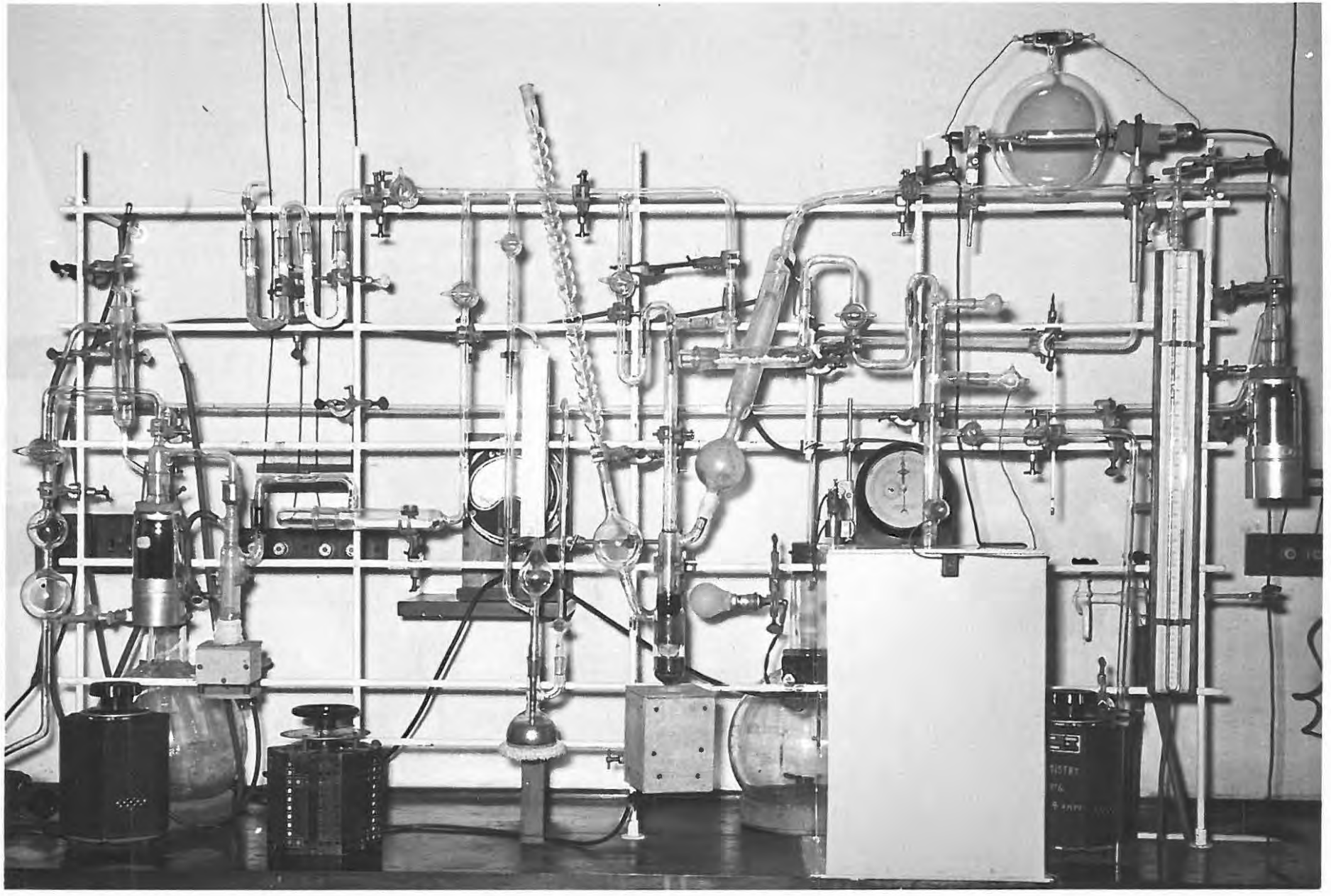

4. APPARATUS AND EXPERIMENTAL PROCEDURES.

4.1. DESCRIPTION OF THE APPARATUS.

The apparatus (see Plate following page 38) is shown diagrammatically in FIG.I. and can be divided into three main sections; the pumping system, the pressure gauge and the decomposition chambers.

The Pumping system.

It consists of a single stage mercury diffusion pump, B, backed by a Hyvac, rotary oil pump,A. The Hyvac oil pump, A^1, was used during pretreatment of the silver oxide. The two pumps, A and B, are separated by a cold trap, C, and an oil trap, D.

E is a safety device controlling the flow of the cooling water to the condenser in B. It consists of a 2 inch diameter vertical tube which accomodates a 1 inch diameter test tube, containing approximately 5 ml. of mercury. Two diametrically opposed tubes of $\frac{1}{4}$ inch diameter are placed high up on the larger tube which tapers at its lower end to an outlet. This outlet is connected to the condenser of B. One lead of the electric mains to B^1 is connected through the mercury when the flow rate of the water is sufficiently high. Any excess water passes out of the overflow tube, opposite the inlet tube. Should the rate of flow of water at any time drop, the inner tube would no longer maintain its equilibrium position and would drop, breaking the electric circuit and thus switching off the heater, B^1.

B^1/...

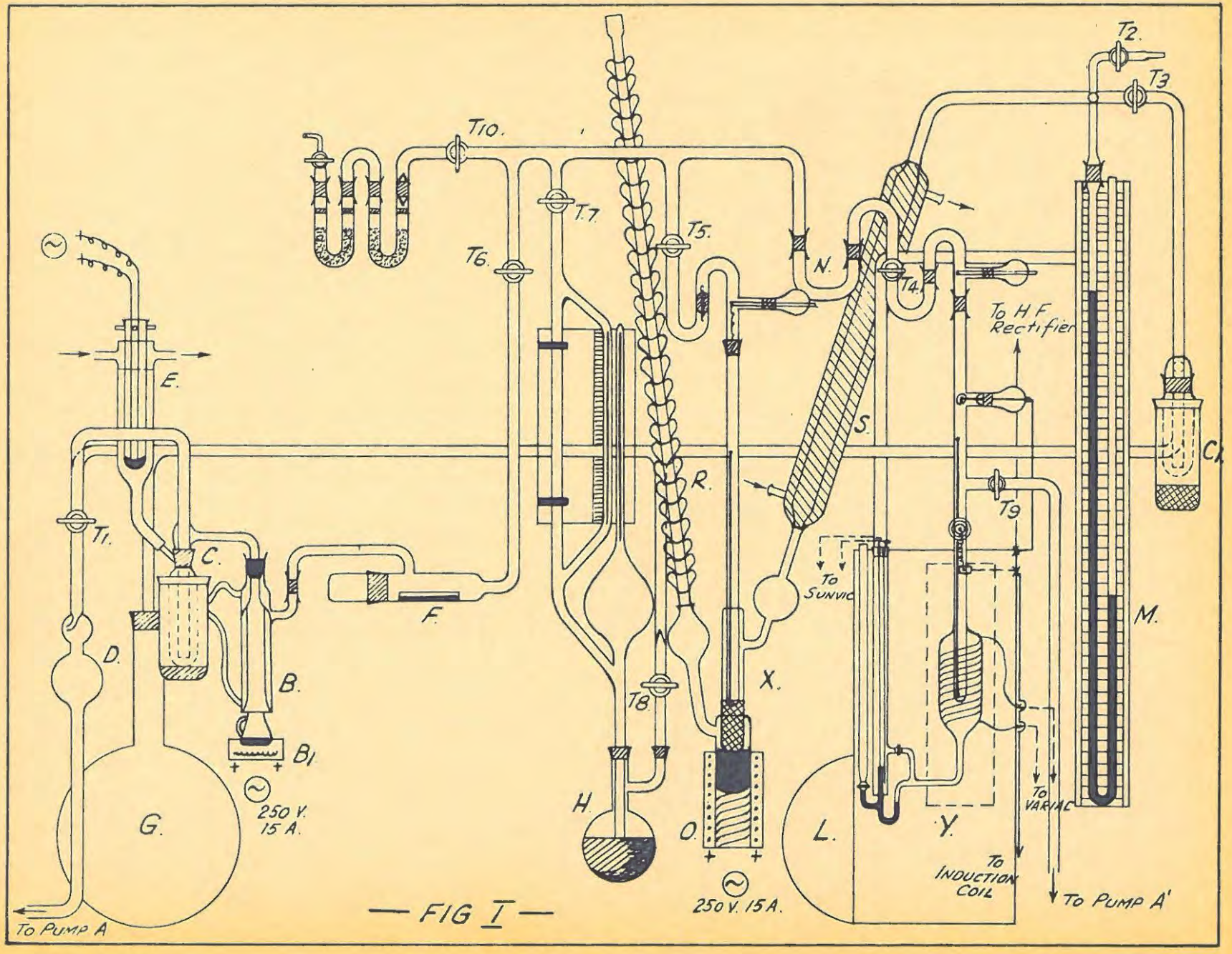
T10.
T7
T6.
T5.
N.
T4.
T2.
T3
To H F Rectifier
C1
S.
R.
T9
E.
T1.
C.
F.
D.
B.
B1
250 V. 15 A.
G.
To Pump A
T8
H.
O.
X.
250 V. 15 A.
To Sunvic
M.
L.
Y.
To Varic
To Induction Coil
To Pump A'

— FIG I —

B^1 consists of an asbestos box with lid, containing a horizontal, 100 watt, coiled heater which is connected to the mains through a Variac. Any mercury vapour from the diffusion pump condenses in the low temperature trap, C. The phosphorus pentoxide trap, F, is used to remove traces of water vapour. The vacuum reservoir, G, which is used to lower the mercury level in the McLeod gauge, H, is connected to A through the double-oblique tap, T_1, and isolated from the decomposition system, X, by tap, T_3. Another cold trap, C_1, prevents any vapours from leaving the system, X.

The McLeod pressure gauge.

This is connected to F by way of tap, T_6. The tap, T_{10}, connects the vacuum system to the atmosphere through two U-tubes, containing potassium hydroxide pellets and "Carbasorb" pellets, respectively. The tap, T_7, is used to isolate the McLeod gauge from the rest of the system, while the operation of tap, T_8, raises or lowers the mercury in H.

The decomposition chambers.

The pumps and pressure gauge are connected to the decomposition chambers, X and Y, through taps, T_5 and T_4, respectively. Between T_7 and T_4 is a removeable tube, N, which contains either potassium hydroxide pellets, cadmium turnings or phosphorus pentoxide powder, depending on the experiment.

The decomposition chamber, X, (FIG.III.) consists of a pyrex tube of 19 mm. internal diameter, sealed into a double

boiling/...

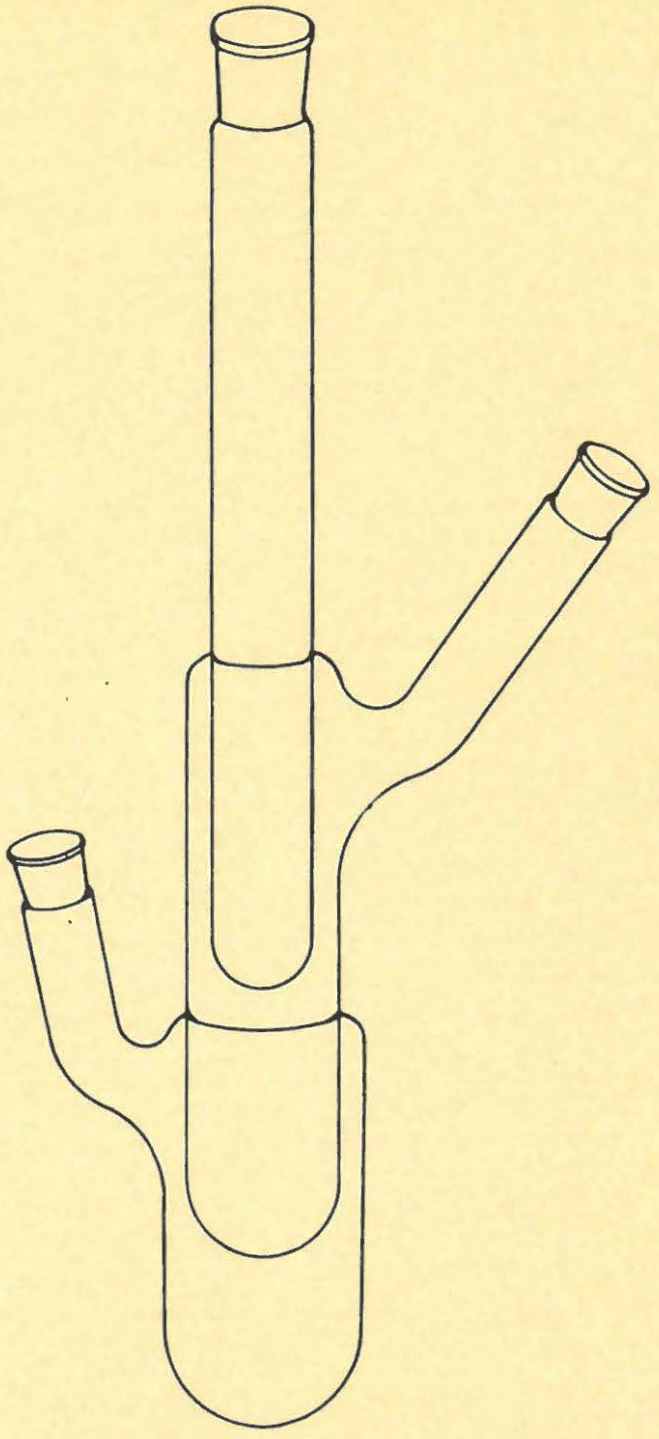

— FIG. III —

boiling system; the outer boiler contains mercury while the inner boiler contains benzyl benzoate. To ensure a constant check over the temperature of decomposition, a calibrated thermometer is placed in X and attached to the side of the tube by means of vacuum wax. The outer liquid is heated by the furnace, O.

The condensers, R and S, remove the mercury and organic vapours respectively. S is connected to either the atmosphere or to the pumps through taps, T_2 and T_3, respectively. Fine adjustment of the pressure over the inner liquid in X is achieved by capillary connections on these two taps, and by the presence of the 10 litre flask, L, connected to the condenser, S. By this means it was possible to achieve fine adjustment of the decomposition temperatures. The pressure is recorded on the mercury manometer, M.

The other decomposition chamber was used for higher decomposition temperatures in the range 330°C - 380°C.

4.2. CONSTRUCTION AND CALIBRATION OF THE McLEOD GAUGE.

The capillary tubes of the McLeod gauge were constructed of Veridia precision-drawn tubing of 2 mm. internal diameter. The closed tube was sealed off by inserting a tight-fitting, flat-ended, glass rod into the tube and carefully sealing it in with the flat end maintained.

Bulb volumes of the McLeod were determined by weighing the empty bulb and capillary tube assembly and then reweighing it when it was filled with water at a known temperature. The

results/...

results are tabulated below in TABLE 1.

TABLE 1.

Wt. of assembly + water. (g).	191.397	191.497	191.537	191.696
Wt. of assembly. (g).	83.257	83.257	83.257	83.257
∴ Wt. of water. (g).	108.140	108.240	108.280	108.439
Temperature of water. (°C).	12.1	12.8	13.0	13.0
Density of water. ($g.cc^{-1}$.)	0.9995	0.9994	0.9994	0.9994
Volume of assembly.(cc.)	108.30	108.34	108.38	108.44

Mean volume of assembly:- 108.36 cc.

The McLeod gauge was tested by measuring the same pressure of gas with the mercury level in the closed limb at different positions down the tube. The top of the mercury meniscus was read The pressures were calculated according to

$$P = \frac{\left[\pi r^2 l - (\pi r^2 r - 2/3 \pi r^3)\right] \triangle h}{V} \text{ cm. mercury .... (4.01).}$$

where V = the total volume of the bulb and sealed Veridia tube.

l = the height of displacement of mercury down the Veridia tube, in cms.

r = the radius of the Veridia tube, in cms.

and $\triangle h$ = the difference in mercury levels between the outer and inner Veridia tubes, in cms.

A table of values of $\frac{\left[\pi r^2 l - (\pi r^2 r - 2/3 \pi r^3)\right]}{V}$ for different values

of/...

of 1 was drawn up for convenience in calculation.

At increasing distances down the capillary tube, for the same pressure, a typical series of readings was:-

$8.556, 8.553, 8.563, 8.578 \times 10^{-3}$ cm. mercury.

The percentage deviation from the arithmetic mean for the highest and lowest pressures, respectively, was 0.30% and 0.22%

4.3. CONSTRUCTION OF THE CONSTANT TEMPERATURE REACTION VESSEL, Y.

The reaction vessel, X, has already been described. Such a system gives a temperature control of approximately $\pm$ 0.05°. This system is limited in its use by the availability of suitable liquids and cannot be used for temperatures above 310°C.

Therefore, in order to follow the decomposition at temperatures greater than 310°C, a constant temperature electric furnace was constructed. This is shown in FIG.II. It consists of a wide-bore pyrex tube, A, of 19 mm. internal diameter, internally sealed into an air jacket of 11.4 cm. external diameter and 22.5 cm. length, B, the outlet of which is joined to a capillary tube of 2 mm. internal diameter. This tubing was chosen so as to limit the volume of gas outside the furnace. The tap, T_1, sealed into this tube, allows air to escape from the furnace when open, via the outer tube, D, which is open to the atmosphere through a slit in the rubber stopper, S. Tap, T_2, controls the volume of mercury in the U-bend, K. The levels of the mercury in the two arms of K, Z_1 and Z_2, rise or fall according as the gas in B expands or contracts with T_1 closed. The mercury pool, P, inside the temperature control tube is connected to the mercury in Z_2 by means of a small piece of platinum wire, X,

sealed/...

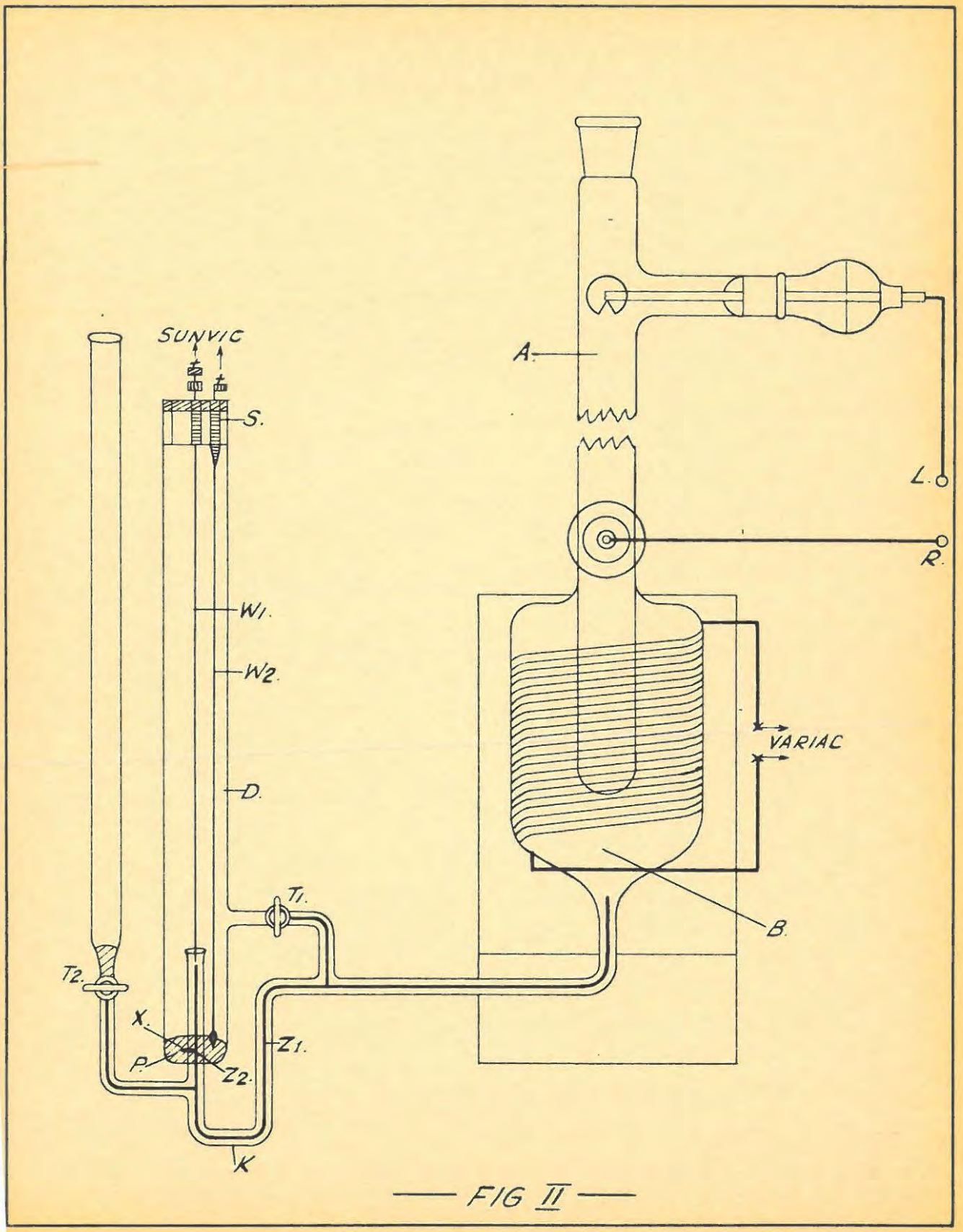

— FIG II —

sealed into Z_2. The mercury inside the capillary tube is in contact with an adjustable platinum wire, W_1, while another fixed platinum wire, W_2, dips into P.

An electric furnace of resistance 100 ohms is wound around the outer air jacket, B. The windings are separated from the glass by asbestos paper, thinly coated with plaster of Paris; heat losses are minimized by a thick layer of the plaster over the wire followed by an external wrapping of thick asbestos cord. The furnace is connected to the output of a Variac.

W_1 and W_2 are connected to the control terminals of a Sunvic hot-wire control which, in turn, regulates the Variac. The whole furnace system, excluding the constant temperature control device, is contained in a close-fitting asbestos box, well insulated with asbestos wool. The complete assembly is surrounded by the larger fibreboard box as shown in FIG.I. and thermal insulation is obtained by a vermiculite packing. The resulting temperature control is approximately $\pm$ 0.1° at 350°C for a period of 5 - 7 hours, which is considered highly satisfactory.

4.4. THE APPARATUS FOR PRE-IRRADIATION BY CATHODE RAYS.

An apparatus for the production of cathode rays was incorporated in the decomposition chamber of furnace, Y. Two side arms (FIG.II.), L and R, 20 cm. apart, were sealed into the decomposition tube, A. The lower one ended in a ground glass joint, sealed into which was a heavy platinum rod (anode), centrally placed in the tube

and/...

and with its tip just protruding into the decomposition chamber proper. A similar platinum rod (cathode) was sealed into the upper joint. A platinum disc was welded to this rod, as indicated in the diagram. The disc could be rotated so as to allow free descent of the bucket, the groove in the disc allowing free passage of the platinum suspension wire.

The discharge was produced, at a residual carbon dioxide-free oxygen pressure of 1.0×10^{-3} cm. mercury, by means of an accelerating potential of 20 kV which was supplied by an induction coil operating from a 60 volt supply. A cadmium trap was inserted in position N of the vacuum line to remove the mercury vapour. The electrode system also contained a helium-filled, high-voltage rectifier in series with the discharge tube. The voltage of the induction coil was maintained constant for all irradiations. The "dark space" extended the distance between the electrodes. The gas pressure was maintained by pumping off the gas between the periods of irradiation.

The salt (20 mg.) was uniformly spread over the bottom of a glass bucket, preheated in vacuo at 280°C for three hours and then raised to the required position for irradiation. After the pressure had been increased to 1.0×10^{-3} cm. mercury by the introduction of carbon dioxide-free oxygen, irradiation was commenced. After irradiation, the vacuum line was pumped hard, the temperature of the furnace raised and the specimen decomposed at 350°C.

4.5. PROCEDURE FOR A DECOMPOSITION.

After removal of the section containing T_4, the ground glass winch, the ground glass joints and the platinum suspension

wire/...

wire, the joints were freed from grease by means of carbon tetrachloride. The platinum bucket and cap were boiled with concentrated nitric acid, rinsed with distilled water and finally dried at red heat over a bunsen flame.

The platinum bucket and its loose-fitting, conical cap, when cool, were weighed in a deep weighing-bottle with a ground glass cap. The bucket was suspended by means of a hook on the glass cap. The bottle was then refilled with nitrogen and as quickly as possible, approximately 20 mg. of silver oxide were placed into the bucket from the silver oxide container; the whole operation taking place in an atmosphere of nitrogen. The bucket and cap were then returned to the nitrogen atmosphere of the weighing bottle, which was then reweighed.

The bucket was transported in this bottle to the vacuum line. The decomposition tube was filled with nitrogen, the lid removed from the weighing bottle, the bucket hooked on to the platinum suspension wire and the regreased winch system pushed down into position. The ground glass joints were pulled up by small springs which were attached to their sides. The tap, T_4, was slowly opened and the nitrogen pumped off. The evacuation was continued until the McLeod gauge failed to register any gas pressure.

To commence the run, tap T_6 was closed, the winch rotated until the platinum wire became slack; the decomposition chamber tapped to ensure that the bucket was at the bottom of the decomposition tube, and the stopwatch started. The pressures were read at various times by means of the McLeod gauge. The final pressure, p_f, was determined/...

mined by allowing the decomposition to continue for a further period of half an hour beyond the apparent end point.

Since liquid air and solid carbon dioxide were not available as refrigerants, the apparatus was tested for its vacuum-holding properties. The apparatus was evacuated for twenty-four hours and then the decomposition and pressure gauge systems were isolated from the pumps for six hours. The pressure developed was less than 1% of the final gas pressure arising from a typical decomposition.

4.6. PRE-IRRADIATION DOSES.

(i). Pile irradiations:- These irradiations were performed in B.E.P.O. The specimens were exposed to a thermal neutron flux of 2×10^{11} neutrons. cm^{-2}. sec^{-1}. at an ambient temperature of $30 \pm 5^{\circ}C$.

(ii). Gamma-rays:- Gamma-ray irradiations were carried out at room temperature in a ^{60}Co "hot spot"[61] of total activity 439 curies. The dose rate, as measured by ferrous-ferric methods, was 1.6×10^{6} r.e.p. hr^{-1}. ^{60}Co emits gamma-rays of 1.33 and 1.17 MeV.

(iii). Fast neutrons:- Fast neutron bombardment was carried out at $50^{\circ}C$ in a hollow uranium slug in B.E.P.O. The fast neutron flux was 3×10^{11} neutrons. cm^{-2}. sec^{-1}.

4.7. THE CALIBRATION OF VOLUMES.

Known pressures of dry air were expanded from the calibrated bulb of H into the evacuated decomposition system, and the resultant pressures were measured after temperature equilibrium had been attained. The volumes were then calculated using the gas laws.

5/...

5. PREPARATIONS.

5.1. THE PREPARATION OF SILVER OXIDE.

Different methods of preparation of silver oxide were used by previous workers, e.g. Lewis[53] used a preparation manufactured by Merck's Chemicals, Darmstadt, while Hood and Murphy[54] used Mallinckrodt's U.S.P. IX, another commercially obtainable chemical. In both cases the specimens were exposed to light and air. Garner and Reeves[59] and Lewis[53] prepared silver oxide from solutions of barium hydroxide and silver nitrate, with no special precautions against contamination of the silver oxide by carbon dioxide or exposure of the silver oxide to light. (VIDE Preparation B below).

The quantitative work of Garner and Reeves was done on a specimen of silver oxide, prepared in a way comparable to the second and third preparations of Lewis, viz. by precipitation of silver nitrate with barium hydroxide, followed by prolonged drying of the precipitate in a vacuum desiccator. The specimens of this, and three similar-type precipitations; differing only in temperature and conditions of precipitation and drying, were heated in oxygen in a thick-walled glass bulb at temperatures between 200°C - 300°C, and at pressures of oxygen ranging from 28 - 33 atmospheres, for eight to ten days. Throughout this treatment, the pressures were kept appreciably above those given by the equation of Keyes and Hara[60].

The preparations used in this work were as follows:-

Preparation/...

Preparation A.

Merck's "Pro Analysi" silver oxide. The bottle had been left standing on the reagent shelf for some time and had been previously used.

Preparation B.

A sample of silver oxide, equivalent to Garner and Reeves' preparation B, was prepared. This is also similar to the second and third preparations of Lewis; the precipitation of silver oxide was done by the addition of a saturated, aqueous solution of barium hydroxide to an aqueous solution of silver nitrate, at room temperature. The saturated solution of recrystallised Merck's barium hydroxide was prepared in boiled distilled water and, after allowing the precipitate to settle, was added dropwise to a flask containing an N/10 solution of A.R. silver nitrate in boiled distilled water, until no more turbidity occurred on the addition of the saturated solution. The precipitate was then washed by decantation, and filtered through a G_4 pyrex, sintered glass crucible, and stored in a silica gel desiccator. The methods of drying, prior to decomposition, are discussed later.

Preparation C.

The apparatus used for this preparation is illustrated in FIG.IV.

All glass apparatus used in this preparation was pre-cleaned with conc. nitric acid and conc. hydrochloric acid, followed by aqua regia and prolonged steaming out with conductance water.

A two litre, flat-bottomed flask, A, contained a

saturated/...

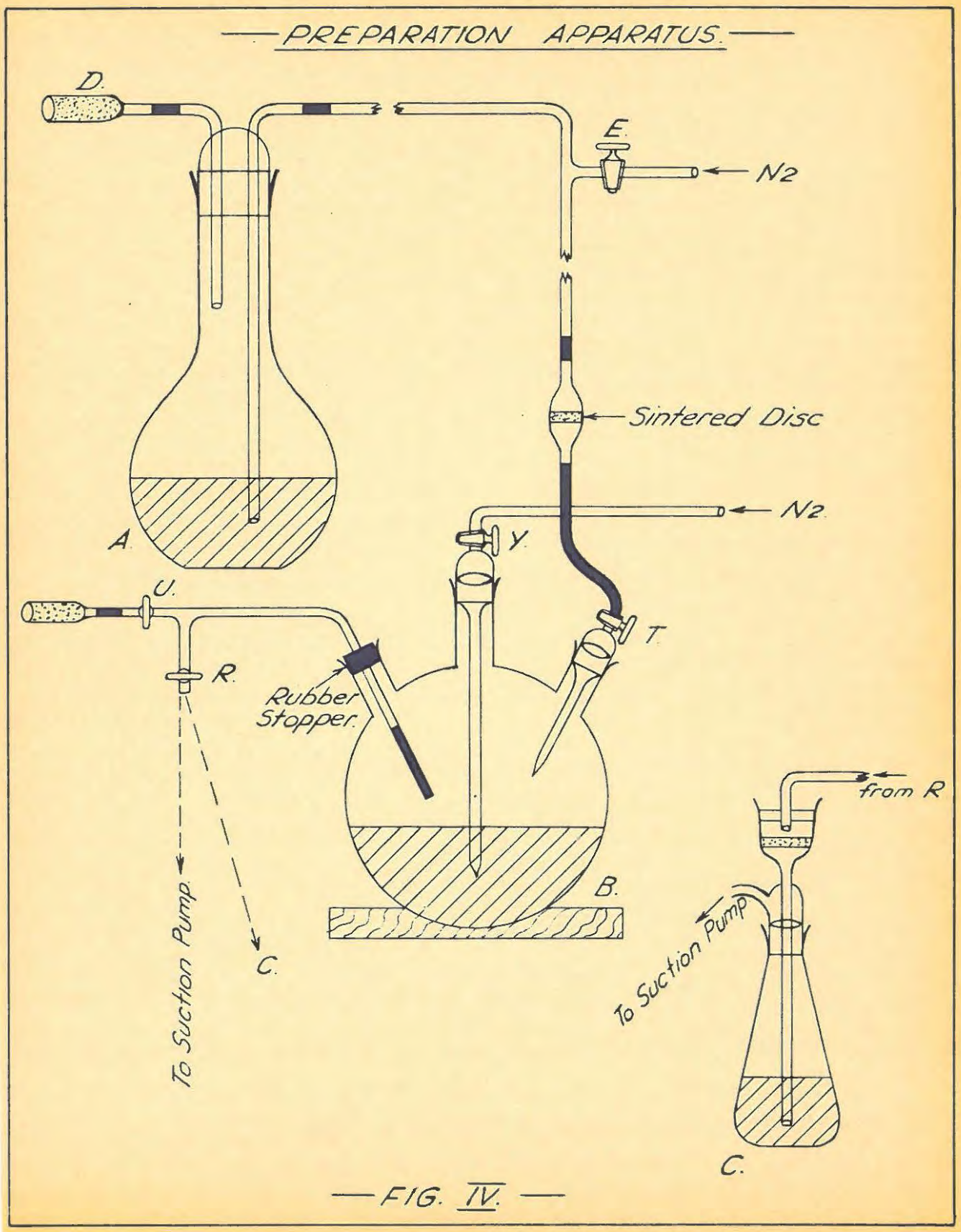
PREPARATION APPARATUS.
D.
E.
N2
Sintered Disc
N2
A.
Y.
U.
T.
R.
Rubber Stopper.
B.
To Suction Pump.
C.
from R
To Suction Pump
C.

FIG. IV.

saturated, aqueous solution of recrystallised Merck's barium hydroxide. The water used throughout the preparation was prepared in the still constructed by Gledhill[62]. The ground glass neck of A permitted two inlet tubes; one connected to a decarbonating tube, D, the other to a "T-piece", E. The transverse section of E was connected, by way of a tap, to a nitrogen inlet, while the remaining section was connected to a very fine sintered glass disc (160 G_4/10 Jena glass), and this, in turn, was joined by polythene tubing (which was used throughout the apparatus) to the Tap, T, in one neck of the three-necked, 5 litre, round-bottomed flask, B. The nitrogen used in the apparatus was elaborately purified[63].

Flask B contained an approximately N/10 solution of A.R. silver nitrate in conductivity water into which dipped the centre inlet tube, Y, of the flask. The remaining neck of the flask contained a rubber stopper through which passed a "T-piece" ending in 5 cms. of polythene tubing. The second outlet of the "T" was connected to a "Carbasorb" tube via tap, U. The remaining outlet was connected to a water suction pump via a two-way tap, R; one lead of which went direct to the water pump, the other via the sintered glass filtering apparatus, C.

Procedure for the preparation of silver oxide (specimen C).

The whole of this procedure was carried out in red light. Flask B was filled with about 1½ litres of conductivity water and nitrogen was allowed to bubble via E, through the water for 3 days, at the rate of 3 bubbles per minute. The water after this

treatment/...

treatment had a conductance at 25°C of 60 nanomhos. (10^{-9} ohm^{-1} cm^{-1}). The tap, T, was kept closed. For the 1 litre of conductance water in B, nitrogen similarly entered through Y with the tap, T, closed and tap, U, open.

After this bubbling time had elapsed, recrystallised Merck's barium hydroxide was introduced into A in excess, and approximately twenty grams of A.R. silver nitrate was introduced into B as quickly as possible. The bubbling of nitrogen was continued throughout these additions. After a further 43 hours bubbling, the tap at B was closed and the barium hydroxide allowed to settle for about another five to six days. The resulting solution was clear and absolutely free from turbidity.

Tap, U, was then closed and tap, R, directly opened to the suction pump. By suitable adjustment of Y and T, the flow of nitrogen and barium hydroxide solution was adjusted, so as to allow a slow, steady flow of barium hydroxide into B, via the sintered disc which removed any fine particles of barium hydroxide. After a few minutes, the precipitate in B was allowed to settle, and the process repeated until no more turbidity was visually noticeable in the red light. The flask was stirred by hand swirling.

When the precipitation was complete (the total time of precipitation was approximately three to four days), the flask, A, was removed and another attached containing nitrogen-bubbled, carbon dioxide-free, conductance water. For washing by decantation, the supernatant liquid in B was removed by pushing the "T-piece" tubing, containing/...

taining R, further through the rubber stopper, so that the polythene tubing dipped into the solution and a gentle suction was applied through R, until all the supernatant liquid was sucked off, nitrogen being bubbled in slowly. Nitrogen was allowed to enter B until atmospheric equilibrium pressure was reached, when tap U was opened to allow free escape of the gas. Then tap R was opened, tap U closed and tap T opened. By suitable adjustment of the bubbling rate and inflow of water through T, a sufficient quantity of water for washing was allowed to pour slowly into B, by water suction through R. The flask was then swirled to wash the precipitate and then allowed to stand to let the precipitate settle, and then decanted as above.

As the whole precipitation process was carried out in red light, it was extremely difficult to note when all the precipitate had settled. Hence a partial loss of some fine particles occured during the removal of the supernatant liquid. The washings were continued until the supernatant liquid was free from Ba^{++} ions.

The precipitate was filtered by connecting the tap, R, to the suction flask, C, and the polythene tubing inside the flask, B, was pulled with its end flush with the stopper in the neck of the flask. This flask was then tilted on its side and constantly agitated by swirling. Nitrogen was admitted to balance the suction pressure if this became too great, and the liquid and silver oxide precipitate were sucked through into the suction flask, and filtered through the G_4 pyrex, sintered glass filter of C.

The suction flask assembly was contained in a

glove-box/...

glove-box filled with nitrogen, containing traps of carbon dioxide absorbent. The flask assembly was rinsed twice with carbon dioxide-free conductance water admitted through R. Nitrogen was then drawn through the silver oxide on the sintered glass funnel for about two days. The glass-sinter funnel was then removed in the nitrogen atmosphere, and quickly placed in a nitrogen-filled vacuum desiccator, the whole procedure being carried out in a nitrogen atmosphere. Evacuation of the desiccator was then continued for four days.

After drying, the sample was removed from the funnel in the above-mentioned glove-box i.e. a nitrogen atmosphere and carbon dioxide absorbents present, as a finely-divided, brown powder. It was then placed in a clean, dry, dark bottle filled with nitrogen in a blackened, nitrogen-filled desiccator in the glove-box. The desiccator contained silica gel and "Carbasorb". This was sample C.

Preparation D.

This was similar to that used by Lewis where silver carbonate was used as a source of silver oxide.

5.2. THE PREPARATION OF SILVER CARBONATE.

An aqueous solution containing 500 ccs. of exactly N/10 silver nitrate was placed in a 2 litre round-bottomed flask and cooled to approximately 5°C. An exactly equivalent amount of N/10 sodium carbonate solution was then slowly added, by a dropping funnel, into the cold solution, with no stirring. After addition, the silver carbonate precipitate was filtered through a G_4 sintered glass funnel at

the/...

the pump, and dried in vacuo over silica gel for three days. Great care was taken to exclude all light during this preparation.

6. RESULTS

Extreme care was taken to exclude light during all these determinations. All weighing, drying and handling procedures were carried out in red light, and, at all times, the sample was kept in a dark container. All pressures are recorded in cm. mercury and times in minutes.

6.1. THE DECOMPOSITION OF PREPARATION A.

The initial run was carried out with approximately 20 mg. of the sample at 350°C, in a platinum bucket, with a loosely-fitting, conical, platinum cap. The results are given in TABLE 2 and FIG.V shows the p/t plots. It was noted that decomposition 3, where the sample was taken from the bottom of the bottle, yielded a curve with a peculiar flattened decay. The runs were irreproducible.

TABLE 2.

RUN 1.			
t.	p x 10^3.	t.	p x 10^3.
0.5	0.407	63	148.4
3	8.799	75	169.4
6	14.14	90	183.6
9	16.61	126	189.6
15	30.11	150	196.7
30	60.78	p_f	197.5
54	126.7		

TABLE 2(continued)/...

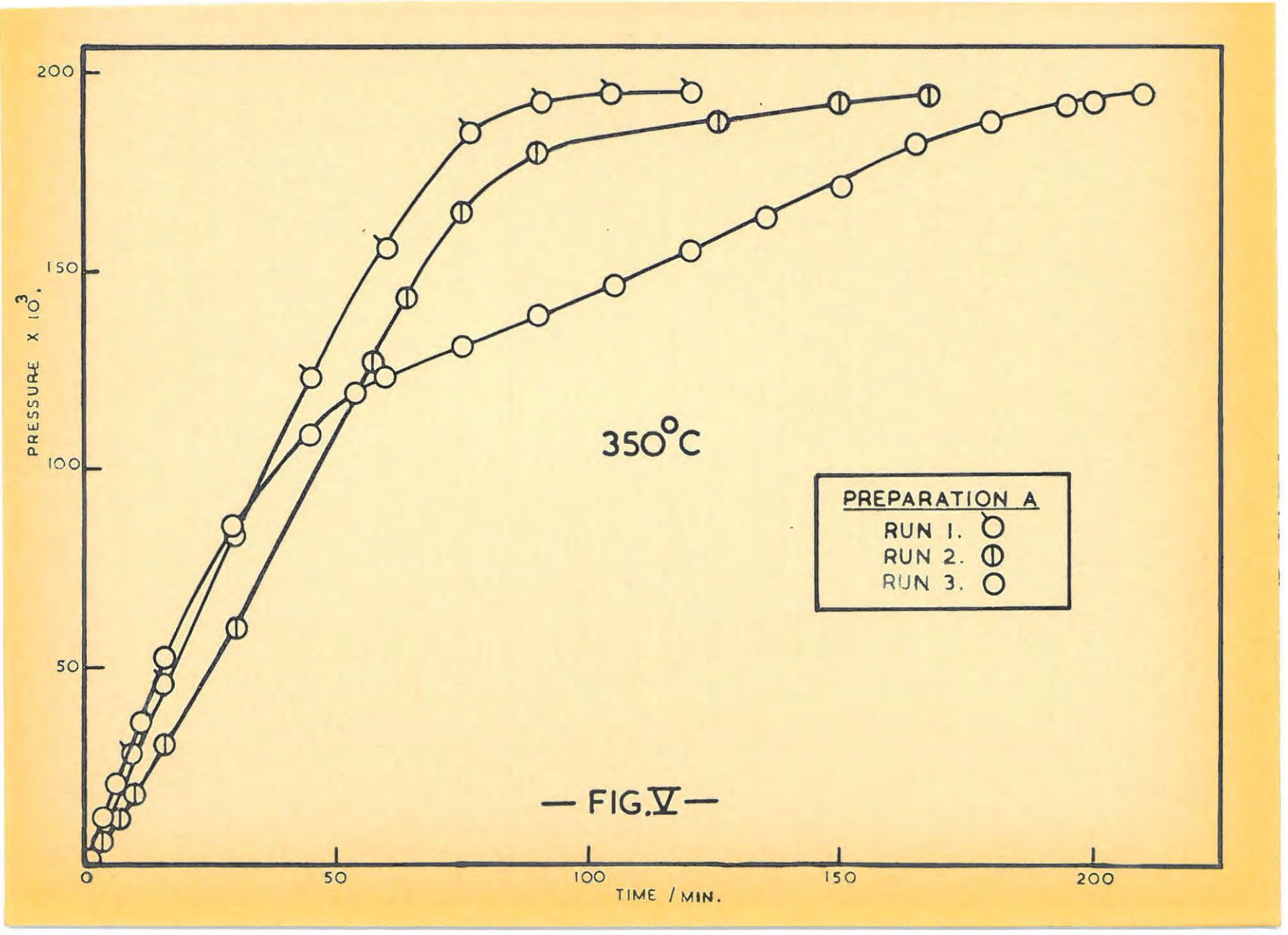
200
150
100
50
0
50
100
150
200
PRESSURE X 10^3.
TIME / MIN.
350°C
PREPARATION A
RUN 1.
RUN 2.
RUN 3.

— FIG. V —

TABLE 2. (continued)

RUN 2.			
t.	p x 10^3.	t.	p x 10^3.
0.5	2.352	60	161.8
3	10.11	75	186.7
6	19.17	90	195.3
9	28.75	105	196.7
15	47.63	123	196.9
30	83.57	p_f	197.5
45	125.7		

RUN 3.					
t.	p x 10^3.	t.	p x 10^3.	t.	p x 10^3
0.5	0.581	45	109.8	150	175.4
2	5.633	60	126.6	165	185.9
3	10.40	75	133.9	180	191.4
6	17.66	90	142.6	195	194.6
9	34.56	105	151.0	200	196.0
15	52.56	120	158.8	215	197.2
30	86.54	135	167.0	p_f	197.5

6.2./...

6.2. THE DECOMPOSITION OF PREPARATION B.

This, too, was carried out at 350°C in the platinum bucket. The results are given in TABLE 3. Runs 3 and 4, in FIG.VI were done on preparation B dried in vacuo at room temperature, while runs 1 and 2 were done on preparation B dried at 100°C for three hours in vacuo.

TABLE 3.

RUN 1.					
t.	p x 10^3.	t.	p x 10^3.	t.	p x 10^3.
0.5	7.463	33	68.36	84	149.3
3	33.84	39	76.40	90	158.8
6	42.06	45	86.20	96	169.0
9	43.59	54	99.42	102	178.2
12	46.72	60	108.5	111	189.6
15	47.60	66	118.0	120	194.2
21	53.06	73	129.9	129	197.3
27	59.34	79	141.3	p_f	197.5

It is noticeable from the curves that

(i). irreproducibility of results persists for room temperature drying,

(ii). drying at 100°C for three hours does improve the reproducibility and

(iii). the initial maximum rate is still present after drying at 100°C for three hours.

These/...

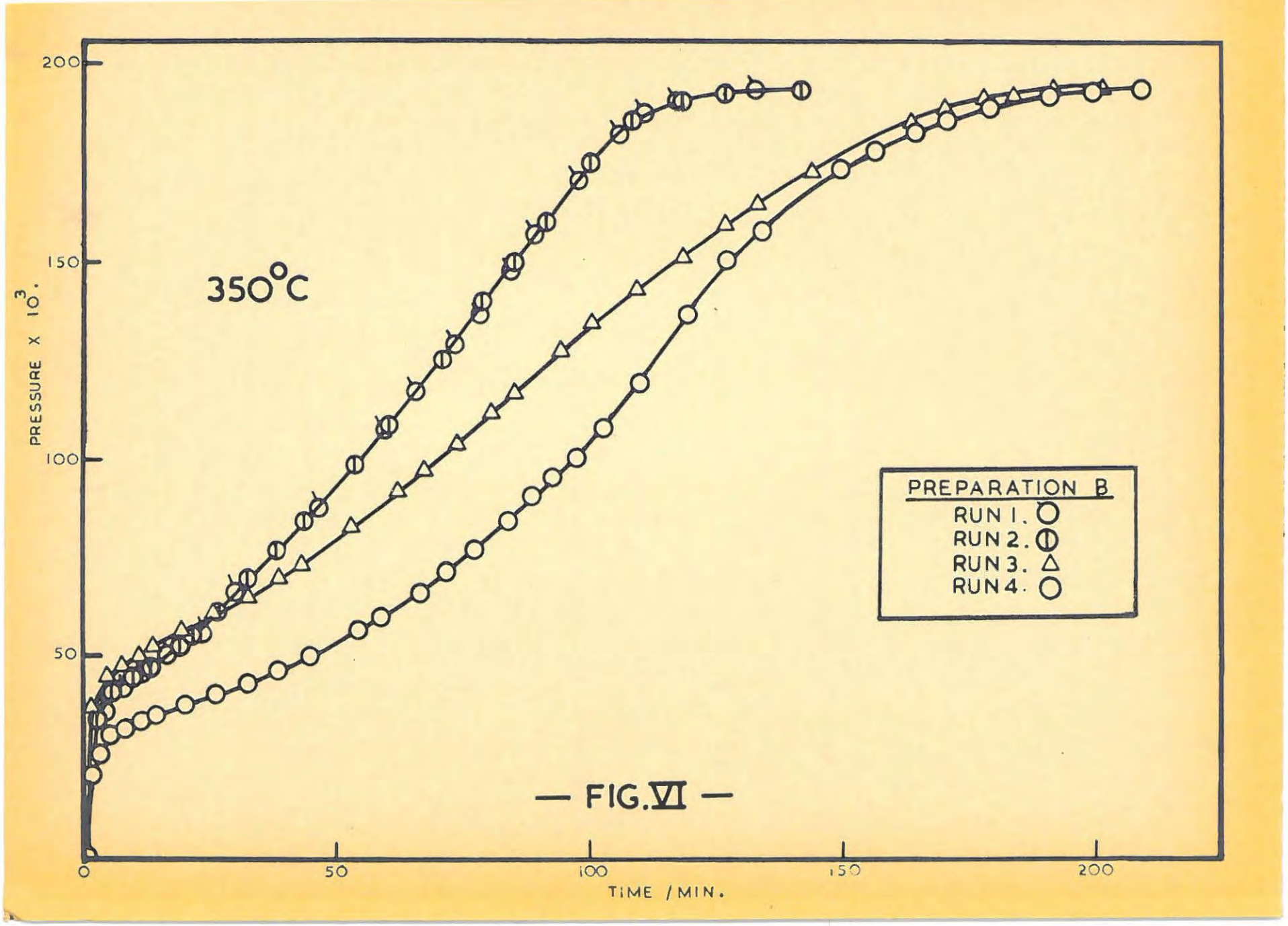
200
150
100
50
0
50
100
150
200
PRESSURE X 10^3.
TIME / MIN.
350°C
PREPARATION B
RUN 1.
RUN 2.
RUN 3.
RUN 4.

— FIG. VI —

TABLE 3. (continued)

RUN 2.					
t.	p x 10^3.	t.	p x 10^3.	t.	p x 10^3.
0.5	6.969	33	65.60	84	147.8
3	31.39	39	74.04	90	158.5
6	38.57	46	83.37	97	169.6
9	41.73	54	96.58	105	181.7
12	43.93	60	106.7	135	197.0
15	45.07	66	116.9	p_f	197.5
21	50.64	72	128.4		
27	59.10	78	139.7		

RUN 3.					
t.	p x 10^3.	t.	p x 10^3.	t.	p x 10^3.
0.5	5.401	54	84.86	129	162.7
3	34.88	60	91.80	135	169.5
6	42.80	66	97.63	144	175.7
9	46.00	72	105.5	150	179.2
12	48.61	78	112.4	156	181.8
15	51.49	84	117.0	165	183.4
21	56.16	90	124.3	171	188.2
27	60.49	96	131.0	180	192.4
33	64.96	102	136.4	186	195.7
39	70.16	111	146.7	192	197.0
45	75.62	120	155.0	p_f	197.5

TABLE 3. (continued/...

TABLE 3. (continued)

RUN 4.					
t.	p x 10^3.	t.	p x 10^3.	t.	p x 10^3.
0.5	4.53	54	57.32	129	153.0
3	22.56	60	63.02	135	160.6
6	28.66	66	71.26	144	173.9
9	29.94	72	74.28	150	179.2
12	32.90	78	81.54	156	183.3
15	34.38	84	88.51	165	188.2
21	35.37	90	95.48	171	190.2
27	39.06	96	103.7	180	192.5
33	42.20	102	109.6	186	197.4
39	45.97	111	126.5	p_f	197.5
45	50.47	120	138.6		

These facts are in conformity with those reported by Garner and Reeves[59]. They reported irreproducibility for specimens dried at room temperature, and a maximum rate at the beginning of the reaction, but no experimental results were given to support these statements.

The initial fast reaction is of interest, and experiments were carried out to study this part of the decomposition.

Drying with continuous pumping in the high vacuum apparatus, prior to decomposition, was carried out at various

temperatures/...

temperatures. In all the experiments the specimen was initially "dried" in vacuum at room temperature, and was then accurately weighed into the platinum bucket, introduced into the high vacuum system, and pumped at the stated temperature and time, prior to decomposition in vacuum at 350°C.

From the results tabulated in TABLE 4 and illustrated in FIG.VII, it is obvious that drying at temperatures above 200°C gives fairly reproducible curves, apart from the initial fast rate, and that this fast rate disappears at a drying temperature between 265°C and 300°C. There is a large change in the initial rate between 100°C and 200°C, suggesting that the removal of the major part of the material causing the fast rate occurs between these temperatures.

TABLE 4.

TEMPERATURE OF DRYING:- 23°C.			
t.	$p \times 10^3$	t.	$p \times 10^3$
0.5	14.63	60	150.4
3	40.95	75	179.5
6	48.50	90	196.9
9	55.46	98	197.2
15	68.25	108	197.4
30	95.54	p_f	197.5
45	121.4		

TABLE 4.(continued/...

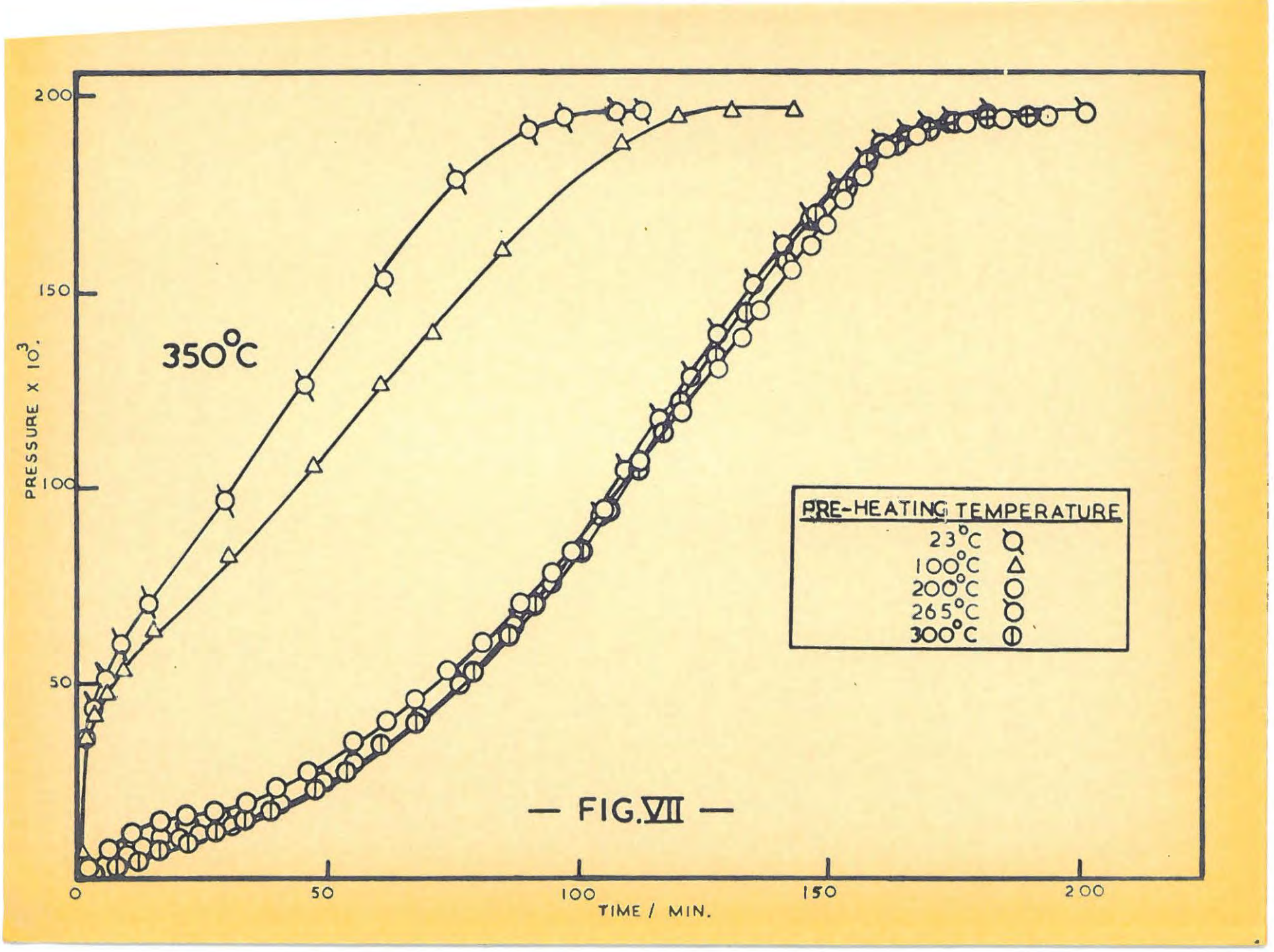
200
150
100
50
0
50
100
150
200
PRESSURE X 10^3.
TIME / MIN.
350°C
PRE-HEATING TEMPERATURE
23°C
100°C
200°C
265°C
300°C

— FIG.VII —

TABLE 4. (continued)

TEMPERATURE OF DRYING:- 100°C.					
t.	p x 10^3.	t.	p x 10^3.	t.	p x 10^3.
0.5	6.969	33	65.60	84	147.8
3	31.39	39	74.04	90	158.5
6	33.57	46	83.37	97	169.6
9	41.73	54	96.58	105	181.7
12	43.93	60	106.7	135	197.4
15	45.07	66	116.9	p_f	197.5
21	50.64	72	128.4		
27	59.10	78	139.7		

TEMPERATURE OF DRYING:- 200°C.					
t.	p x 10^3.	t.	p x 10^3.	t.	p x 10^3.
0.5	0.1133	60	41.13	126	131.5
3	3.334	66	46.26	129	137.1
6	8.149	72	52.82	135	149.3
9	10.37	78	59.82	141	159.2
15	12.96	84	66.15	147	169.3
21	15.34	90	74.49	153	176.3
27	17.21	96	82.12	159	186.9
33	18.51	102	91.39	165	192.1
39	23.48	108	101.2	p_f	197.5
45	27.17	114	111.4		
54	35.51	120	121.4		

TABLE 4. (continued/...

TABLE 4. (continued)

TEMPERATURE OF DRYING:- 265°C.					
t.	p x 10^3.	t.	p x 10^3.	t.	p x 10^3.
0.5	0.2904	48	22.62	120	124.8
3	3.208	54	28.20	126	137.6
6	4.348	60	33.25	132	149.2
9	6.209	66	38.75	138	161.4
12	7.943	74	48.15	144	170.3
15	9.177	78	53.75	150	179.8
18	10.62	84	62.66	156	186.8
21	11.92	90	70.65	162	191.7
24	12.61	96	82.04	168	194.4
30	14.64	102	90.45	174	195.7
36	15.92	108	99.72	180	197.3
42	19.35	114	113.2	p_f	197.5

TABLE 4. (continued)/...

TABLE 4. (continued)

TEMPERATURE OF DRYING:- 300°C.					
t.	p x 10^3.	t.	p x 10^3.	t.	p x 10^3.
0.5	0.5503	60	33.16	132	147.1
3	0.7725	66	38.89	138	157.7
6	1.365	75	47.74	144	168.4
9	2.869	78	52.07	150	178.2
12	4.480	84	60.74	156	183.7
15	6.023	90	68.19	162	190.1
21	9.497	96	79.43	168	193.6
27	13.14	102	87.44	174	196.3
33	16.66	108	99.97	180	197.3
39	20.15	114	110.4	p_f	197.5
45	23.15	120	121.6		
54	28.66	126	135.0		

The/...

The following runs (TABLE 5) were performed in an attempt to determine whether or not this removal was time dependent. FIG.VIII indicates various drying times at 280°C(approximately midway between 265°C and 300°C).

TABLE 5.

TIME OF DRYING (HOURS):- 1.75.					
t.	p x 10^3.	t.	p x 10^3.	t.	p x 10^3.
0.5	33.55	66	69.08	144	153.6
3	38.57	72	74.42	150	166.3
6	39.67	78	79.95	156	172.4
9	41.24	84	84.57	162	178.2
12	42.09	90	91.91	168	184.0
17	43.91	96	99.31	174	187.6
21	45.38	102	106.0	180	190.5
27	47.56	108	112.9	186	192.8
33	50.23	114	119.3	192	194.1
39	52.23	120	129.6	201	195.0
45	54.78	126	139.1	216	195.9
54	60.68	132	144.6	p_f	197.5
60	64.43	138	150.0		

TABLE 5.(continued)/...

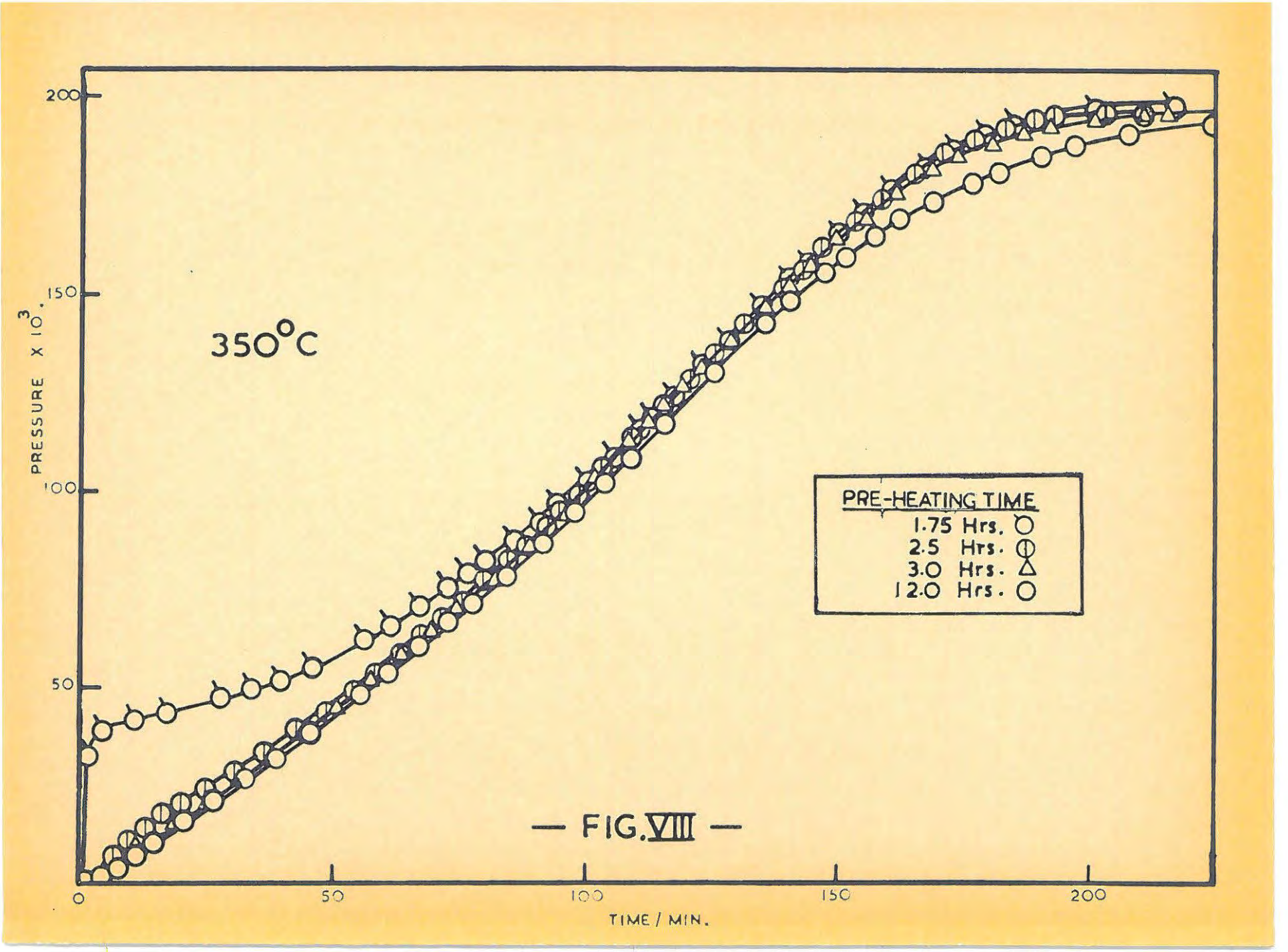
200
150
100
50
PRESSURE X 10.3
350°C
PRE-HEATING TIME
1.75 Hrs.
2.5 Hrs.
3.0 Hrs.
12.0 Hrs.
0
50
100
150
200
TIME / MIN.

— FIG. VIII —

TABLE 5. (continued)

TIME OF DRYING (HOURS):- 2.50.					
t.	$p \times 10^3$.	t.	$p \times 10^3$.	t.	$p \times 10^3$.
0.5	0.1742	57	47.62	132	144.1
3	3.514	63	55.46	144	157.7
6	6.592	69	63.02	150	165.2
9	9.874	75	69.84	159	174.3
12	12.40	84	79.02	168	182.9
15	14.63	90	84.22	174	187.0
21	15.13	96	94.66	183	191.6
27	23.37	102	104.0	192	195.2
33	27.70	108	112.4	201	196.3
39	31.08	114	120.2	213	197.2
45	36.18	120	127.7	p_f	197.5
51	43.07	126	135.9		

TABLE 5. (continued)/...

TABLE 5. (continued)

TIME OF DRYING (HOURS):- 3.0.					
t.	p x 10^3.	t.	p x 10^3.	t.	p x 10^3.
0.5	0.0465	63	55.33	144	156.1
3	0.6215	69	60.77	150	165.8
6	2.718	75	69.52	156	171.8
9	5.181	84	79.11	162	177.0
12	8.537	90	83.24	169	183.2
15	9.734	96	102.9	174	187.1
21	15.13	102	109.3	180	190.1
27	20.57	108	112.3	186	192.6
33	26.28	114	118.9	192	193.6
39	32.29	120	127.2	201	195.5
45	38.68	127	137.1	210	196.5
51	42.81	135	147.8	p_f	197.5
57	49.14	138	150.3		

TABLE 5. (continued/...

TABLE 5. (continued)

TIME OF DRYING (HOURS):- 12.0.					
t.	$p \times 10^3$.	t.	$p \times 10^3$.	t.	$p \times 10^3$.
0.5	0.1046	66	56.62	144	153.1
3	0.6389	72	61.86	150	161.2
6	1.974	78	67.95	156	164.4
9	4.182	84	75.51	162	170.2
12	6.738	90	82.75	168	174.0
15	9.380	96	89.45	174	177.9
21	13.88	102	97.57	180	181.8
27	18.21	108	106.0	189	186.2
33	22.04	114	113.9	208	191.6
39	29.04	123	127.5	230	195.7
54	42.61	132	140.0	240	196.3
60	48.20	138	147.8	p_f	197.5

The/...

The curves show that three hours drying at 280° is approximately the minimum time required for the removal of the initial fast reaction.

Experiments were now carried out to determine the chemical nature of the gas evolved during the fast reaction. A run was carried out where the drying was commenced in vacuo and the apparatus isolated from the pumps. Pressure readings were taken of this process. (TABLE 6.)

TABLE 6.

t.	p x 10^3.	t.	p x 10^3.	t.	p x 10^3.
0.5	2.325	25	43.29	123	47.41
5	35.43	30	43.35	150	47.88
10	37.59	45	44.24	180	48.09
15	40.97	63	44.40	p_f	48.15
20	42.35	102	44.94		

The p/t curve of the evolution of the initial gas at 280°C resembles in shape that for preparation A, (FIG.V, 1 and 2.), decomposed at 350°C, in vacuo.

The run was then repeated but with a phosphorus pentoxide trap present in position N in the apparatus to trap any moisture which evolved. The results are tabulated in TABLE 7. The curve obtained was similar to the previous one.

It/...

It was thus concluded that the gas evolved at 280°C contains little or no water vapour.

TABLE 7.

t.	p x 10^3.	t.	p x 10^3.	t.	p x 10^3.
0.5	0.1851	45	34.60	150	34.53
6	19.29	75	35.12	180	39.98
9	24.18	90	36.26	p_f	40.69
15	31.26	105	38.16		
30	33.39	125	39.47		

A blank run was done using only the platinum bucket and its lid but the gas evolved (due to the adsorption of air on the platinum) was negligible.

It was therefore concluded that the initial fast rate for specimens decomposed at 350°C and subjected to a pre-treatment at temperatures up to and including 265°C did not represent the evolution of water vapour. This conclusion was verified by carrying out a decomposition at 350°C, in the presence of phosphorus pentoxide, on a specimen previously dried for three hours at 200°C in vacuum. The results are shown below in TABLE 8. The p/t plots still showed the initial fast reaction and were similar in shape.

TABLE 8./...

TABLE 8.

WITH P_2O_5 TRAP PRESENT.					
t.	p x 10^3.	t.	p x 10^3.	t.	p x 10^3.
0.5	0.6504	54	29.39	120	110.1
3	1.870	60	34.34	129	121.0
6	5.860	66	41.37	141	137.7
9	7.879	72	46.80	153	151.7
12	9.419	78	53.23	165	163.5
15	10.99	84	60.12	177	175.5
21	13.31	90	67.74	189	184.4
27	15.16	96	75.09	201	191.5
33	17.87	102	84.50	213	196.0
39	20.33	108	91.43	p_f	197.5
45	22.94	114	100.0		

Having established the absence of water vapour, it seemed possible that the evolved gas might contain carbon dioxide. The above runs at 200°C in a closed system were thus repeated, but with a trap of potassium hydroxide pellets present in the place of the phosphorus pentoxide trap. The evolved gas was all absorbed and was thus presumed to be carbon dioxide. With a potassium hydroxide trap present, the decomposition of a specimen at 350°C, which had been dried for three hours at 200°C in vacuo, with continuous pumping, gave the results tabulated in TABLE 9, shown in FIG.IX. FIG.IX also shows the same run without/...

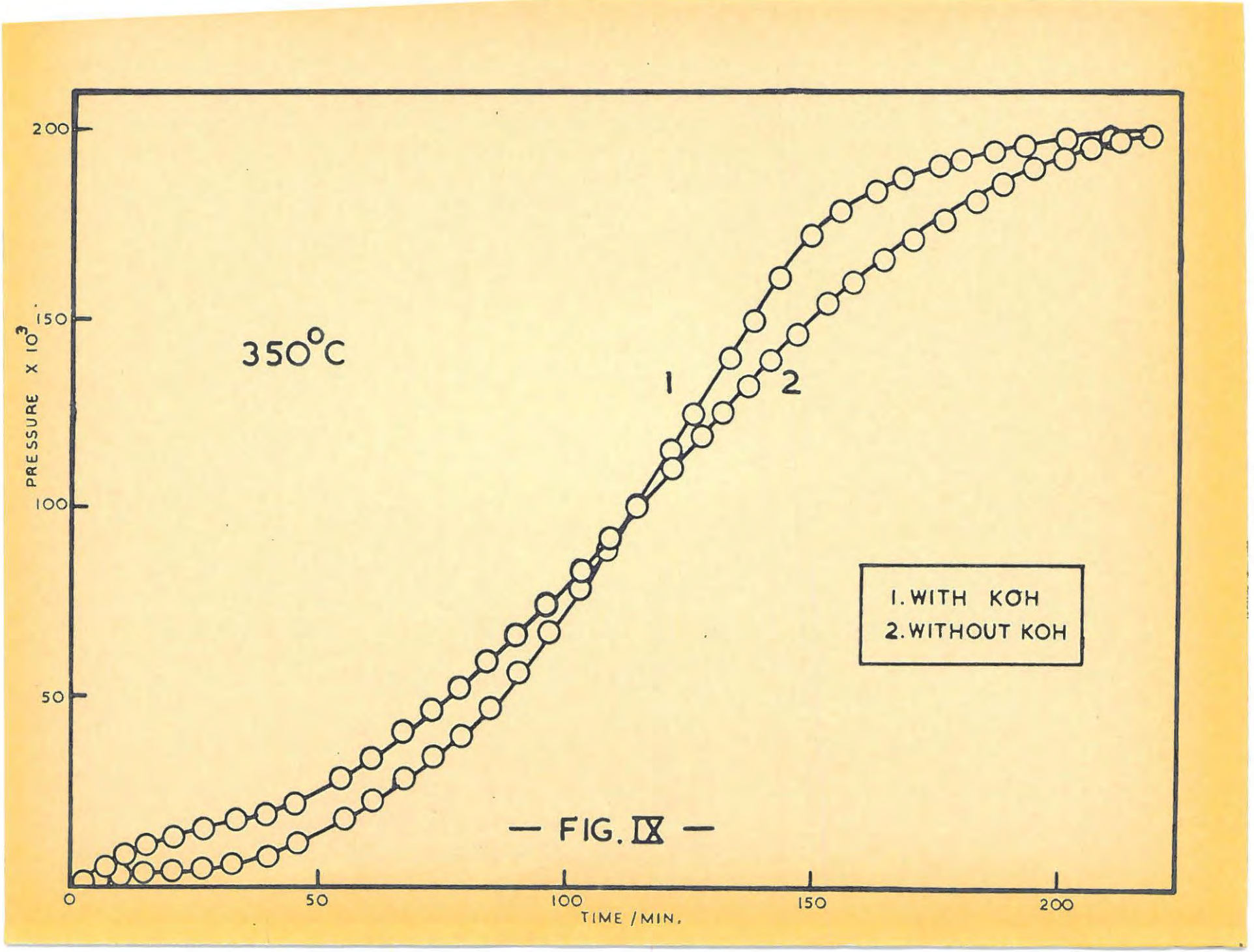
200
150
100
50
PRESSURE X 10^3
350°C
1
2
1. WITH KOH
2. WITHOUT KOH
0
50
100
150
200
TIME / MIN.

— FIG. IX —

out the potassium hydroxide trap. (TABLE 9).

TABLE 9.

WITH KOH TRAP PRESENT.					
t.	p x 10^3.	t.	p x 10^3.	t.	p x 10^3.
0.5	0.0116	66	28.45	144	163.9
3	0.7028	72	34.45	150	170.3
6	1.801	78	41.47	156	178.3
9	2.788	84	47.79	162	182.9
12	3.485	90	58.08	168	187.6
15	3.950	96	67.44	174	190.6
21	4.646	102	80.21	180	192.9
27	5.518	108	36.69	186	195.1
33	6.795	114	101.0	192	195.9
39	8.712	120	112.9	201	196.6
45	11.50	126	124.7	p_f	197.5
54	17.60	132	136.4		
60	23.05	138	149.0		

From these curves it can be seen that potassium hydroxide removes the initial "bump" completely. It can thus be concluded that the initial burst of gas is due to the evolution of carbon dioxide, and that this carbon dioxide can be removed by trapping with potassium hydroxide during the run, or by heating at a higher temperature i.e. 280°C for three hours, prior to the run.

A run/...

TABLE 9. (continued)

WITHOUT KOH TRAP PRESENT.					
t.	p x 10^3.	t.	p x 10^3.	t.	p x 10^3.
0.5	0.5053	69	52.01	156	163.3
3	6.222	75	58.99	162	170.0
6	10.36	81	64.76	168	172.8
9	13.01	87	74.87	174	177.8
12	14.03	93	82.56	180	181.0
15	15.37	99	90.65	186	184.8
21	17.32	108	101.5	192	187.7
27	19.55	114	111.6	198	191.0
33	22.11	120	119.3	204	193.4
39	24.92	126	127.3	210	194.9
45	29.27	132	132.6	216	196.3
51	33.75	138	143.2	p_f	197.5
57	42.44	144	150.8		
63	45.04	150	156.8		

A run was also carried out with the specimen dried in vacuo at room temperature, but decomposed at 350°C with the potassium hydroxide trap. The curve resembled plot 1. FIG.IX - no initial fast rate was now present.

The effect of the contamination of silver oxide by atmospheric carbon dioxide was now shown on the thermal decom-

position/...

position. This explained many of the results obtained by previous workers. It will also be more fully considered in the Discussion.

An attempt was then made to prepare silver oxide, free from $CO_3^=$, by decomposing silver carbonate.

6.3. THE DECOMPOSITION OF PREPARATION D.

The result of initially heating a sample of D, in vacuo for three hours, at 200°C with continuous pumping, (to decompose the silver carbonate into silver oxide), and then decomposing in vacuo at 350°C, can be seen in FIG.X, and is tabulated in TABLE 10 below.

TABLE 10.

WITHOUT KOH TRAP PRESENT.					
t.	p x 10^3.	t.	p x 10^3.	t.	p x 10^3.
0.5	0.071	46	47.18	114	174.2
3	1.734	54	56.84	120	134.1
6	6.923	60	65.27	126	190.5
9	11.81	66	75.75	132	194.1
12	14.17	72	85.43	138	195.9
15	17.34	78	96.72	144	196.6
21	22.42	84	109.1	150	197.1
27	28.12	90	121.7	p_f	197.5
33	33.40	96	137.7		
39	39.71	102	149.1		

TABLE 10.(continued)/...

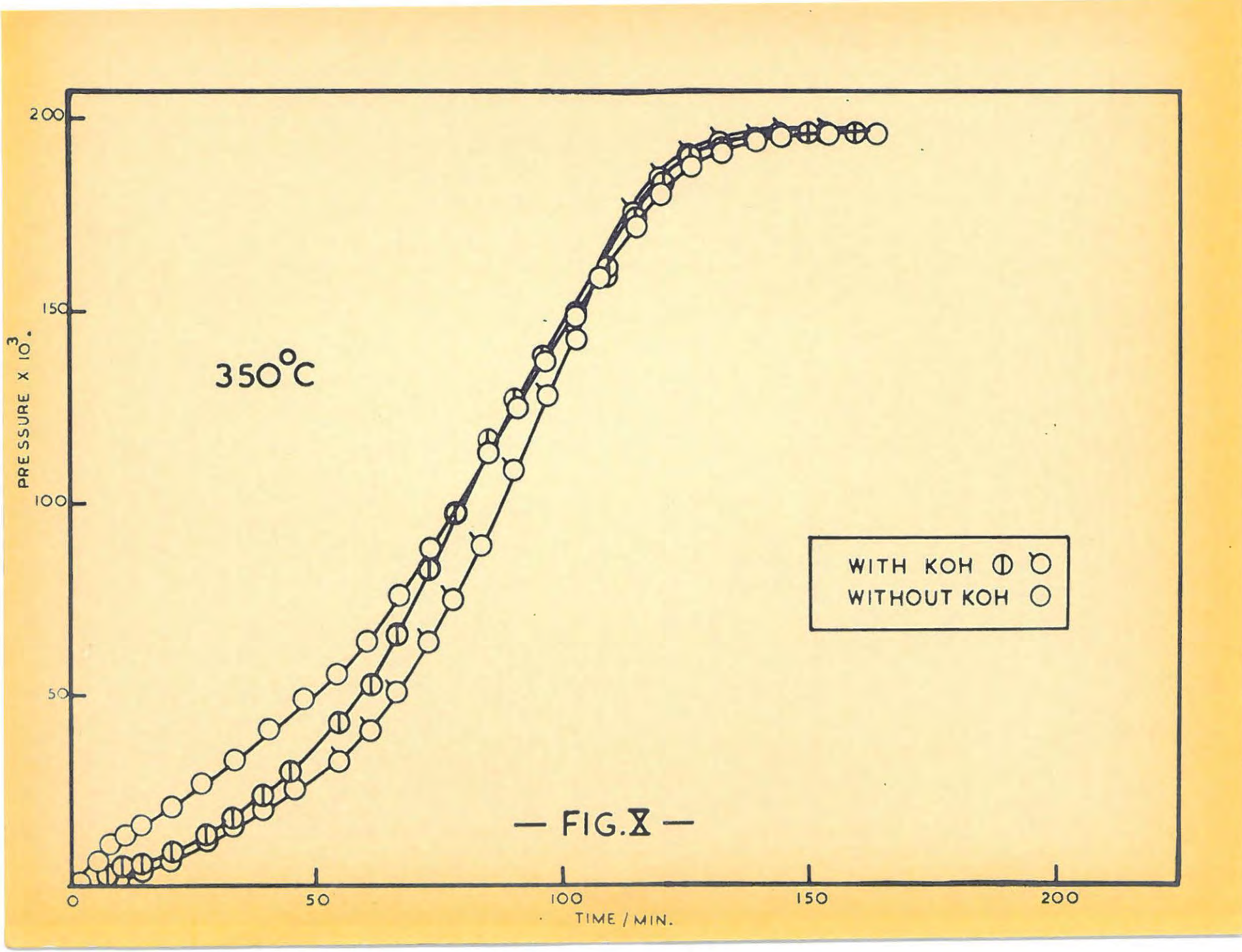
200
150
100
50
0
50
100
150
200
PRESSURE X 10^3.
TIME / MIN.
350°C
WITH KOH
WITHOUT KOH

— FIG.X —

TABLE 10. (continued)

WITH KOH TRAP PRESENT.					
t.	p x 10^3.	t.	p x 10^3.	t.	p x 10^3.
0.5	0.0181	39	19.97	97	129.2
3	0.0543	45	26.11	102	144.2
6	0.7049	54	35.20	108	161.7
9	1.993	60	45.19	114	178.0
12	3.050	66	54.68	120	186.6
15	3.796	72	65.61	126	194.3
21	6.416	78	77.71	132	197.0
29	12.43	84	93.99	138	197.2
33	15.18	90	109.8	p_f	197.5

WITH KOH TRAP PRESENT.					
t.	p x 10^3.	t.	p x 10^3.	t.	p x 10^3.
0.5	0.0155	39	23.80	96	139.6
3	0.7864	45	31.39	102	151.7
6	1.977	54	42.94	108	163.8
9	3.210	60	55.78	114	175.4
12	4.967	66	69.02	120	185.3
15	6.421	72	81.47	126	193.1
21	9.432	78	96.32	132	196.6
27	13.04	84	111.5	138	196.9
33	18.02	90	128.0	p_f	197.5

The/...

The initial acceleration is again present. Identical runs were then carried out with the same initial preparatory treatment, and the samples decomposed with potassium hydroxide present. (TABLE 10, FIG.X). The curves are now sigmoid although the agreement is not good.

It was then decided to prepare a specimen of "carbonate-free" silver oxide, and to exclude, as far as possible, any contamination of the silver oxide by carbon dioxide. The preparation was performed as previously described, and this sample was used throughout the subsequent work. The sample was stored in an atmosphere of nitrogen, and light was excluded. Air was excluded as far as possible during all handling and weighing operations.

The precipitate of silver oxide was brown in colour and very finely divided.

6.4. THE DECOMPOSITION OF PREPARATION C.

A run was done under ordinary conditions i.e. no preheating and no traps present. (FIG.XI, TABLE 11). The initial fast rate was still present. It was, however, greatly reduced in magnitude and represented only a very small fraction of the complete decomposition.

Thus, despite the careful preparation, storage and handling, the sample was still very slightly contaminated with carbon dioxide. It was felt that the contamination probably occurred during the weighing procedure. A specimen of this preparation was then decomposed at 350°C with a potassium hydroxide trap in the line and the initial

acceleration/...

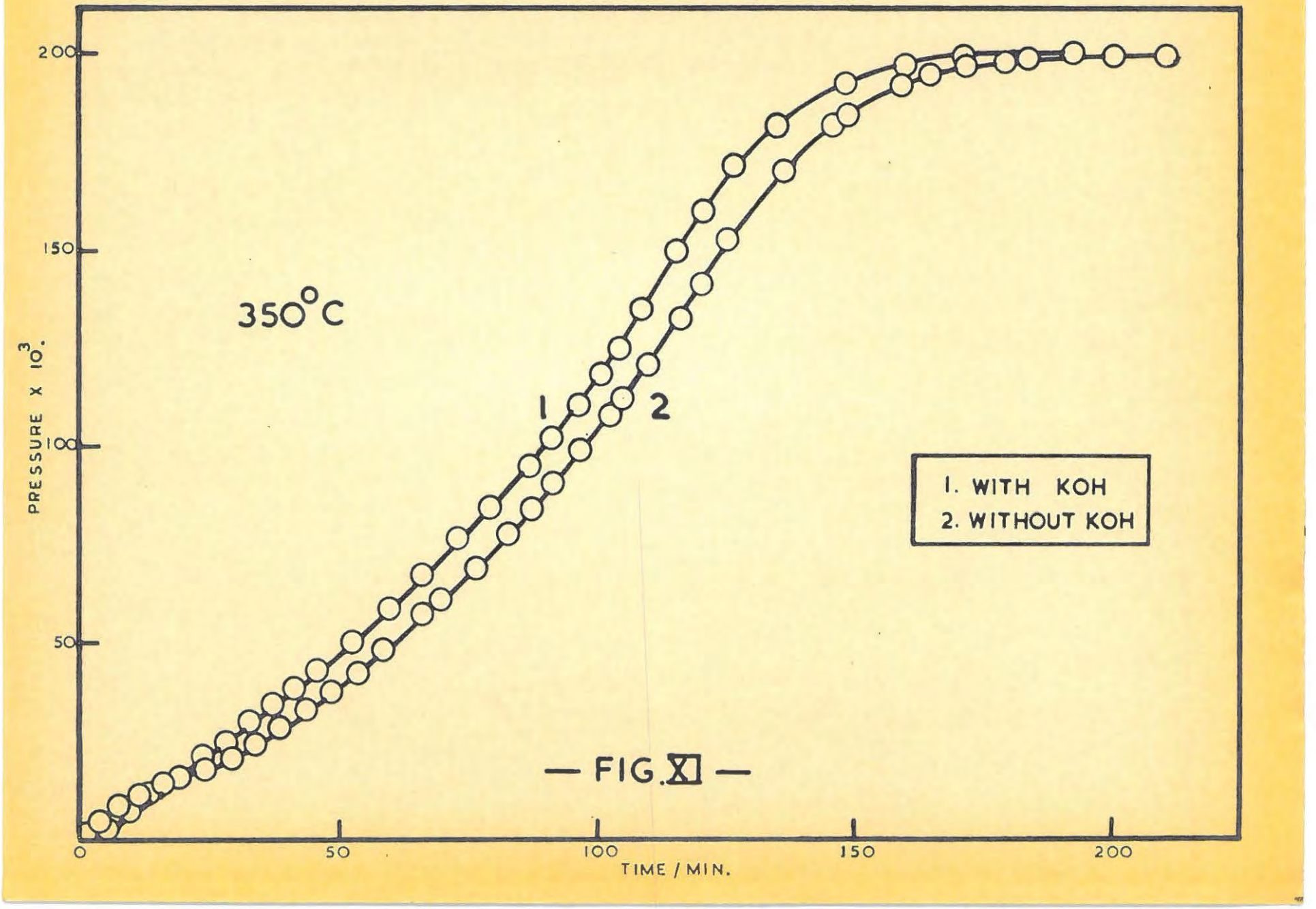
200
150
100
50
PRESSURE X 10.3
350°C
1
2
1. WITH KOH
2. WITHOUT KOH
0
50
100
150
200
TIME / MIN.

— FIG. XI —

acceleration was eliminated (FIG.XI, TABLE 12). Reproducibility was, however, not satisfactory using this method of decomposition.

TABLE 11.

t.	p x 10^3.	t.	p x 10^3.	t.	p x 10^3.
0.5	0.2567	40	25.45	115	131.2
2	1.302	45	30.46	126	151.0
5	3.567	54	39.44	136	163.2
10	7.352	57	41.30	145	180.3
16	10.76	69	57.05	159	194.5
22	14.19	75	65.52	164	195.1
30	18.02	87	77.00	179	196.3
36	21.57	105	109.6	p_f	197.5

TABLE 12.

t.	p x 10^3.	t.	p x 10^3.	t.	p x 10^3.
0.5	0.0291	37	31.65	101	120.2
3	0.3712	43	38.04	108	134.7
5	3.435	43	43.56	114	146.4
6	4.066	53	49.95	120	156.8
9	6.098	53	55.18	125	165.0
12	9.293	66	65.34	147	189.3
15	11.62	74	76.67	159	195.1
21	13.94	81	85.96	170	197.0
27	16.26	89	98.16	181	197.4
33	22.07	96	110.4	p_f	197.5

Runs/...

Runs were then performed at 350°C, after preheating at 280°C for three hours with pumping. The p/t plots are shown in FIG.XII and the results in TABLE 13.

6.5. REPRODUCIBILITY.

TABLE 13.

t.	p x 10^3.	t.	p x 10^3.	t.	p x 10^3.
0.5	0.0133	60	42.55	132	153.3
3	0.1371	66	48.45	138	164.2
6	0.9141	72	54.86	144	173.2
9	2.194	78	62.16	150	181.0
12	4.251	84	69.47	156	187.0
15	6.080	90	78.61	162	189.3
21	10.65	96	87.30	168	192.2
27	14.31	102	96.90	174	194.0
33	19.01	108	107.6	180	195.6
39	24.36	114	118.9	189	195.9
45	29.07	120	130.7	198	196.6
54	36.80	126	143.1	p_f	197.5

It is evident that the results are now singularly reproducible. The preheating at 280°C for three hours was again done in a closed evacuated system and the evolved gas was expanded into an evacuated potassium hydroxide trap. All the gas was absorbed. This showed that no measurable decomposition of the silver oxide had occurred during the preheating.

This/...

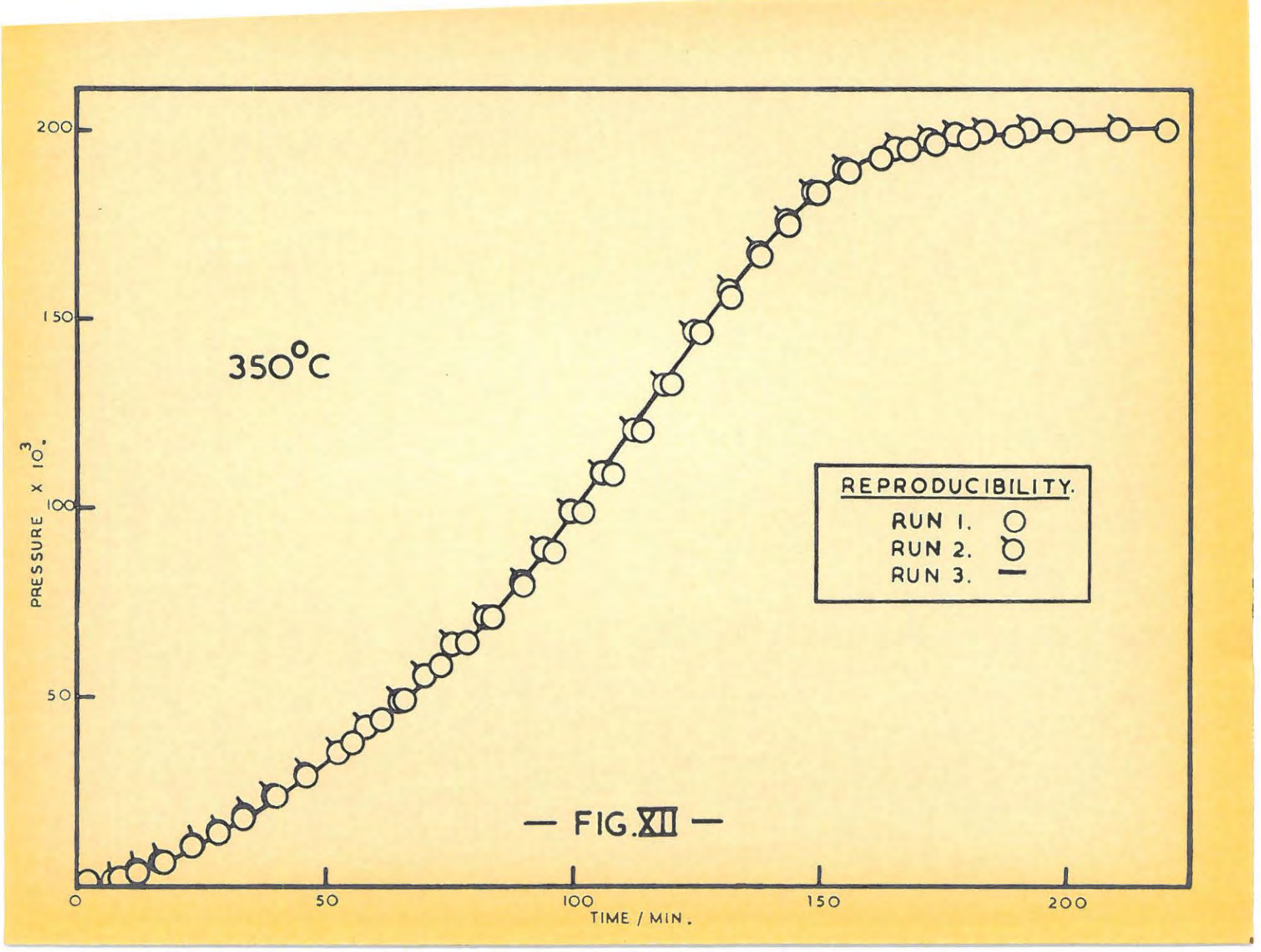
200
150
100
50
0
PRESSURE X 10^3.
350°C
REPRODUCIBILITY.
RUN 1.
RUN 2.
RUN 3.
50
100
150
200
TIME / MIN.

— FIG. XII —

This preheating was then a standard procedure for all runs.

TABLE 13. (continued)

t.	p x 10^3.	t.	p x 10^3.	t.	p x 10^3.
0.5	0.0022	57	37.44	130	154.4
3	0.0416	63	42.51	135	163.6
6	0.5654	69	50.02	141	172.4
9	2.039	75	56.99	147	178.9
12	3.994	82	65.32	153	184.8
15.5	5.971	87	73.60	159	188.9
22	9.645	93.5	83.43	165	191.1
28	13.61	99	93.85	171	194.0
33	16.97	105	105.4	177	195.9
39	21.56	111	117.9	183	196.2
45	26.37	117	129.5	192	197.1
51	31.64	123	141.3	p_f	197.5

TABLE 13. (continued)/...

TABLE 13.(continued)

t.	p x 10^3.	t.	p x 10^3.	t.	p x 10^3.
0.5	0.0146	57	38.33	129	151.0
3	0.1536	63	42.98	135	161.4
6	2.353	69	50.23	141	170.8
9	3.514	75	58.08	147	178.3
12	4.908	85	69.69	153	184.7
15	6.621	87	73.47	159	188.5
21	11.59	93	81.32	165	191.6
27	14.41	99	92.92	171	194.0
33	18.09	105	104.6	180	195.7
42	24.89	112	118.5	189	196.9
45	26.75	117.5	128.9	198	197.3
51	31.78	123.5	140.6	p_f	197.5

6.6. PERCENTAGE PURITY OF THE SILVER OXIDE.

A sample of silver oxide was heated at 280°C for three hours, and a portion of this was weighed out in a nitrogen atmosphere/...

atmosphere and dissolved in 0.2 N nitric acid solution. This solution was then titrated with 0.1040 N ammonium thiocyanate solution using ferric ammonium sulphate as an indicator, (Volhards method). Triplicate results are given below:-

Weight of silver oxide (mg).	Titre (mls) of ammonium thiocyanate.	Percentage Purity (on dried weight).
130.9	10.71	99.89
127.2	10.40	99.96
131.7	10.80	99.97

6.7. THE EFFECT OF USING A QUARTZ BUCKET.

Since irradiations of the silver oxide in B.E.P.O. and with ultra-violet light and gamma-rays, had to be done in quartz containers, it was necessary to study the effect of replacing the platinum bucket and cap by a similar quartz assembly. The results are shown in FIG.XIII, TABLE 14.

As can be seen, a quartz bucket has no effect on the decomposition. This is in agreement with the result obtained by Garner and Reeves[59].

TABLE 14./...

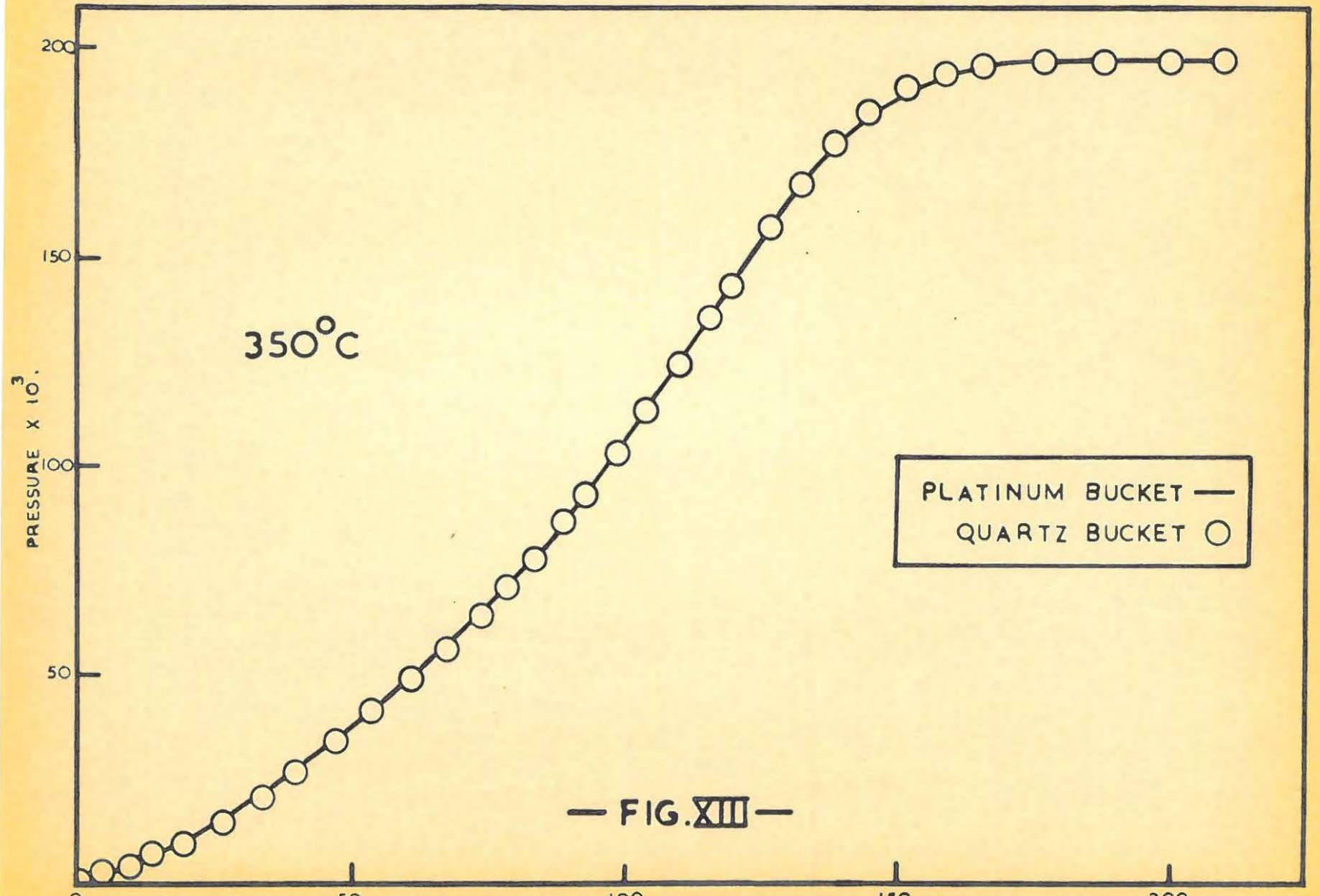
200
150
100
50
0
50
100
150
200
PRESSURE X 10^3.
TIME / MIN.
350°C
PLATINUM BUCKET —
QUARTZ BUCKET ○

— FIG. XIII —

TABLE 14.

t.	p x 10^3.	t.	p x 10^3.	t.	p x 10^3.
0.5	0.5224	55	41.82	120	141.7
3	1.510	60	47.92	126	151.3
6	3.435	68	55.46	132	160.1
10	4.646	72	58.39	138	171.4
12	7.551	78	63.83	144	179.5
15	9.393	84	76.95	150	184.2
21	12.75	90	86.54	157	189.3
27	17.68	96	95.83	171	194.0
33	22.04	102	106.0	180	195.0
39	28.18	111	123.7	195	195.8
45	31.95	114	128.0	p_f	197.5

6.8./...

6.8. THE EFFECT OF ULTRA-VIOLET IRRADIATION.

20 mg. of silver oxide were placed in a small quartz capsule, which was to be the decomposition bucket, and heated in the furnace, in darkness, for three hours at 280°C. The decomposition chamber was then filled with nitrogen, the capsule carefully extracted, and the open end sealed by means of an oxy-hydrogen flame. These quartz capsules were used for the ultra-violet irradiations.

TABLE 15.

(The pressures are corrected to a constant weight of 22.9 mg. of sample).

RUN 1.					
t.	p x 10^3.	t.	p x 10^3.	t.	p x 10^3.
0.3	0.0244	60	33.11	132	119.3
3.5	0.3945	66	38.33	138	126.9
6	1.208	72	42.40	145	130.7
9	2.661	78	47.92	150	135.1
12	4.356	84	55.18	156.5	138.6
15	5.373	90.5	60.98	162.5	141.8
21	8.712	96	69.11	168	142.9
27	12.20	102	78.02	174	143.4
33	15.10	108	85.37	180	143.7
39	17.71	114	92.34	195	144.0
45	22.66	120	101.6	p_f	145.1
54	28.75	126	109.7		

Duplicate/...

Duplicate filled-capsules were placed 3 cms. from a quartz mercury arc lamp. These samples were irradiated, with intermittent shaking, for a period of four and a half hours and then decomposed in vacuo at 350°C. A blank run was also carried out where the irradiation was omitted. The results are shown in FIG.XIV.

TABLE 15. (continued)

RUN 2.					
t.	p x 10^3.	t.	p x 10^3.	t.	p x 10^3.
0.5	0.0822	57.5	32.23	129	114.1
3	1.024	63	36.59	135	122.3
6	1.481	69.5	40.95	141	123.6
9	2.294	75	46.17	147	133.9
12	4.820	81	52.35	153	133.6
16	7.028	87	58.66	163	142.3
22	9.699	93	65.63	171	142.6
27	12.14	99.5	75.73	180	143.4
33	16.41	105	82.75	198	143.8
40	19.16	111	89.74	p_f	144.6
45	22.66	117	98.45		
51	23.83	123	106.6		

TABLE 15.(continued)/...

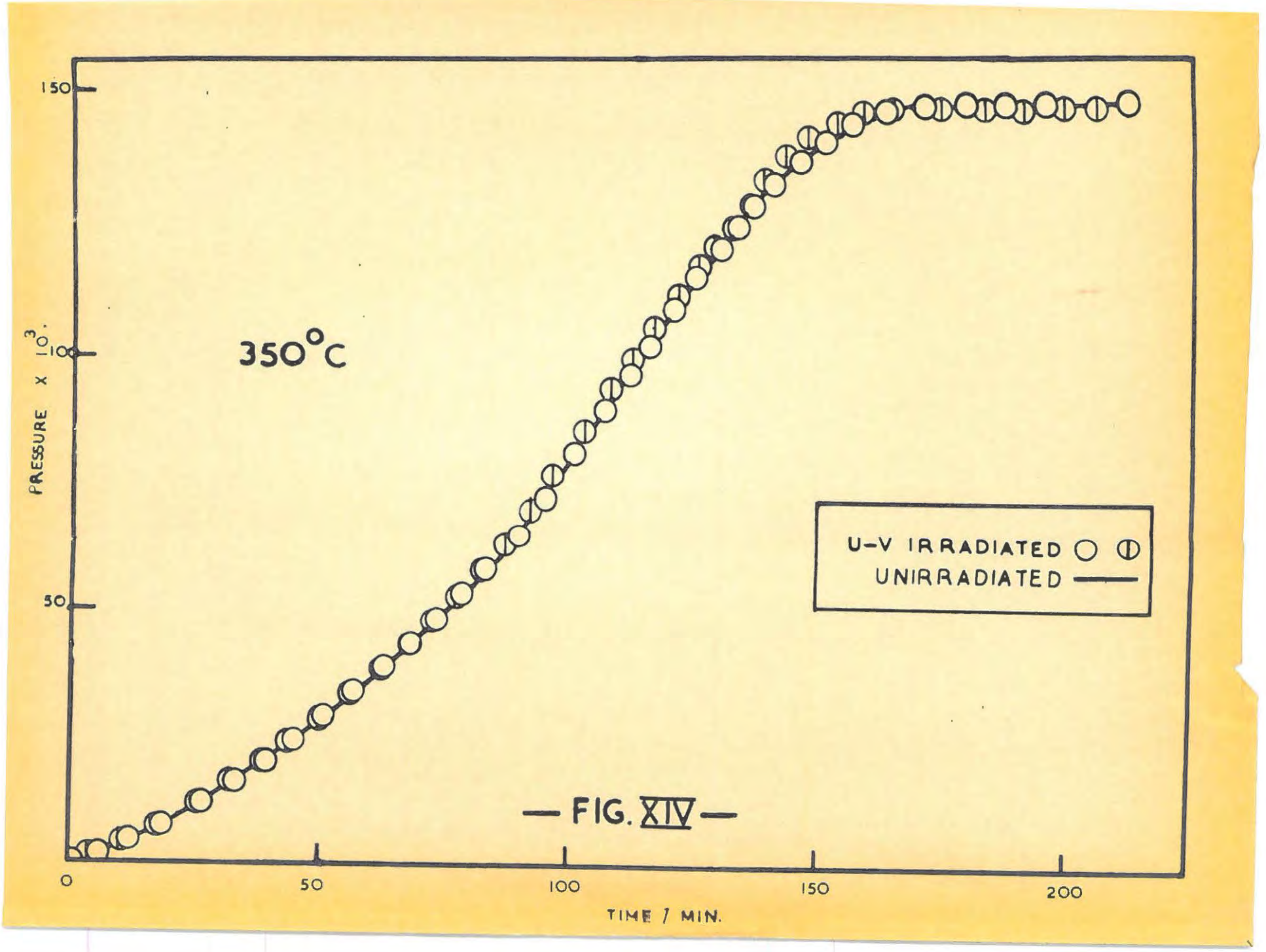
150
100
50
0
PRESSURE X 10^3.
350°C
U-V IRRADIATED
UNIRRADIATED
50
100
150
200
TIME / MIN.

— FIG. XIV —

TABLE 15. (continued)

BLANK RUN.					
t.	p x 10^3.	t.	p x 10^3.	t.	p x 10^3.
0.5	0.0035	57	34.85	129.5	116.1
3	1.024	63	39.20	135	124.6
6	2.758	69	43.56	141	130.5
9	4.298	75	47.92	147	134.2
12	6.098	81.5	55.18	153	136.8
15	7.551	87.5	60.98	159	141.1
21	11.32	93	66.79	166	143.4
27	13.07	99	76.67	177	144.6
33	16.27	105	84.50	189	144.9
39	20.32	111	91.47	p_f	145.7
45	23.81	117	99.31		
51	29.62	124	108.9		

The values of p and t are listed in TABLE 15 and show that the ultra-violet light has no effect. It now became possible, for the first time, to handle the specimen in ordinary light.

6.9. THE EFFECT OF PILE AND GAMMA-RAY PRE-IRRADIATION.

Several preheated, duplicate specimens were prepared, as above, in sealed, nitrogen-filled, quartz buckets. These

were/...

were subjected to gamma-ray and neutron irradiation. The results indicated that the following pre-irradiations had no effect on the decompositions at 350°C.

(i). Gamma-rays (^{60}Co); doses of 3.3, 15 and 30 Mrad. (TABLE 16).

(ii). Irradiation in B.E.P.O. for 15 hours and 48 hours. (TABLE 17).

(iii). Fast neutrons in a hollow uranium slug in B.E.P.O. for one week. (TABLE 18).

TABLE 16.

3.3 Mrad.					
t.	p x 10^3.	t.	p x 10^3.	t.	p x 10^3.
0.5	0.0523	57	35.72	132	131.8
3	0.3742	63	40.36	139	136.5
6	2.666	69	46.17	144	140.6
10	3.329	75	52.28	150.5	143.7
12	3.706	81	58.08	159	144.1
16	5.643	87	60.98	168	144.6
21	8.859	95	78.41	177	145.5
27	12.20	101	90.61	186	145.9
33	15.68	110	98.45	195	146.[illegible]
39	19.74	116.5	106.3	p_f	147.3
45	27.30	120	115.0		
51	32.23	126	123.7		

TABLE 16.(continued)/...

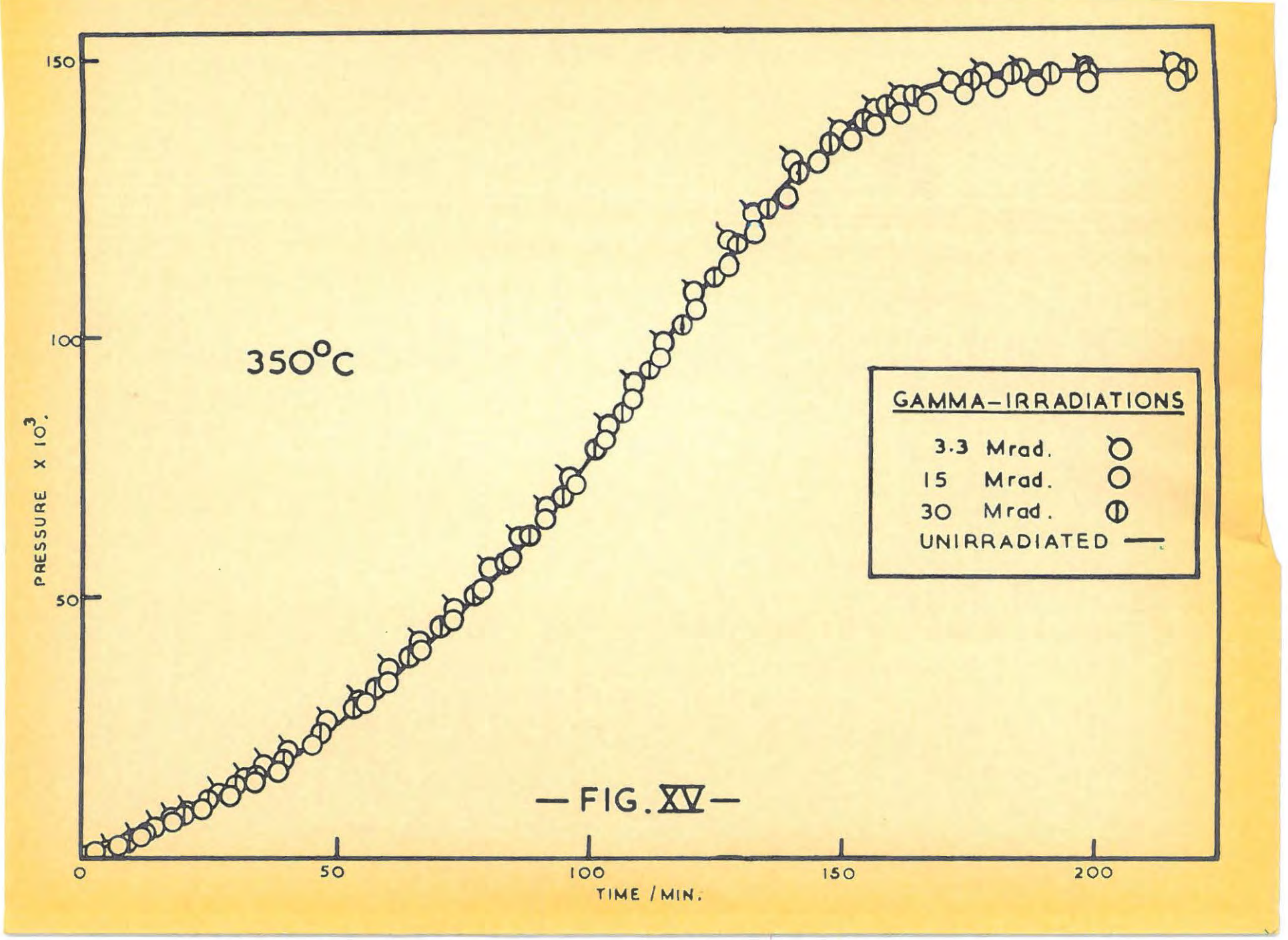
150
100
50
PRESSURE X 10^3.
350°C
GAMMA–IRRADIATIONS
3.3 Mrad.
15 Mrad.
30 Mrad.
UNIRRADIATED
0
50
100
150
200
TIME / MIN.

— FIG. XV —

TABLE 16. (continued)

3.3 Mrad.					
t.	p x 10^3.	t.	p x 10^3.	t.	p x 10^3.
0.5	0.0668	60	35.72	132	122.8
3	1.155	66	40.95	141	131.2
6	3.038	73	46.46	147	139.1
9	4.214	80	53.15	155	144.6
12	6.639	86	58.66	159	146.7
15	7.433	91	64.76	167	147.2
21	10.46	96	70.28	171	147.5
27	13.94	103	80.15	181	147.8
35	18.88	108	88.86	189	148.1
40	21.78	114	96.99	198	148.4
47	25.56	120	105.4	p_f	148.9
55	32.23	126	114.8		

TABLE 16. (continued)/...

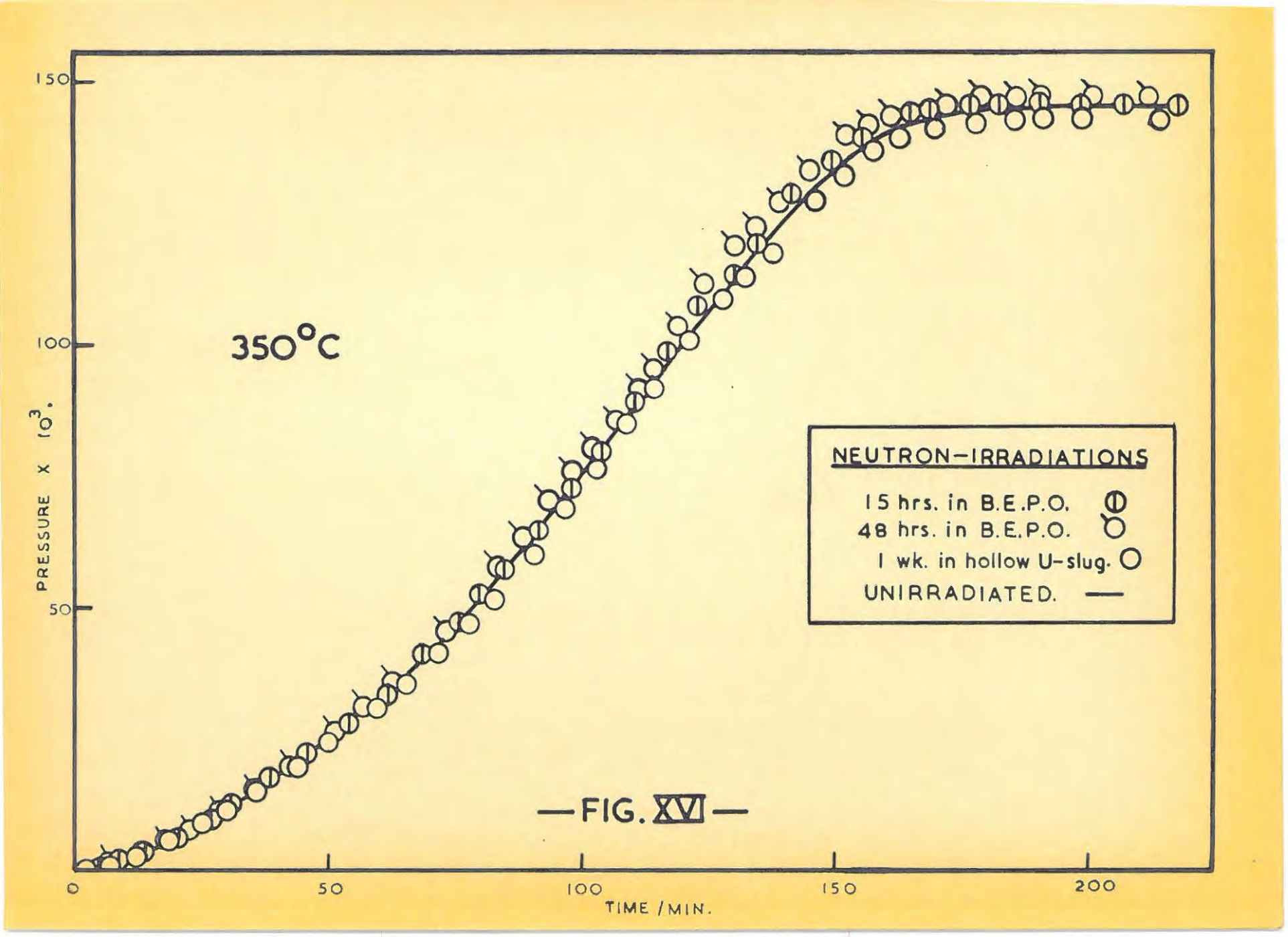
150
100
50
PRESSURE X 10^3.
350°C
NEUTRON–IRRADIATIONS
15 hrs. in B.E.P.O.
48 hrs. in B.E.P.O.
1 wk. in hollow U-slug.
UNIRRADIATED.
0
50
100
150
200
TIME / MIN.

—FIG. XVI—

TABLE 16. (continued)

15 Mrad.					
t.	p x 10^3.	t.	p x 10^3.	t.	p x 10^3.
0.5	0.0381	57	31.35	129	116.8
3	0.6215	63	35.72	138.5	128.9
6	1.743	69	40.07	149	138.2
9	3.486	75	45.30	158	142.9
12	4.356	81	51.40	165	144.6
15	7.259	87	59.24	174	144.9
21	9.583	93	66.20	183	145.2
27	13.07	99	73.18	191	145.7
33	16.55	106	82.75	200	146.3
39	20.04	111	91.47	p_f	146.7
45	24.68	117	100.2		
51	27.58	123	108.9		

TABLE 16. (continued)/...

TABLE 16. (continued)

15 Mrad.					
t.	p x 10^3.	t.	p x 10^3.	t.	p x 10^3.
0.5	0.2004	60	33.93	132	121.1
3	1.002	66	38.33	138	128.6
6	1.289	72	43.42	144	134.2
9	2.073	78	47.92	150	137.9
12	4.211	84	55.76	156	141.1
15	4.356	90.5	62.73	162	143.4
21	7.841	96.5	69.69	168	144.6
27	12.20	102	77.54	174	144.9
33	15.68	108	86.54	180	145.2
39	18.88	114	96.70	189	145.7
45	21.78	120	103.0	198	146.3
55	29.62	126	111.5	p_f	147.0

TABLE 16. (continued)/...

TABLE 16. (continued)

30 Mrad.					
t.	p x 10^3.	t.	p x 10^3.	t.	p x 10^3.
0.5	0.0134	57	32.23	139	129.2
3	1.155	63	36.59	145	135.9
6	1.852	69	40.95	151	140.3
9	2.944	75	46.17	157	143.7
12	4.214	81	52.23	163	144.6
18	7.968	87	60.98	169	145.2
21	8.545	93	66.21	175	145.7
27	12.28	99	74.04	184	146.3
33	15.73	106	83.64	196	147.0
39	19.45	112.5	93.80	p_f	148.1
45	22.94	117	99.31		
51	27.83	126	112.4		

TABLE 16. (continued)/...

TABLE 16. (continued)

30 Mrad.					
t.	p x 10^3.	t.	p x 10^3.	t.	p x 10^3.
0.5	0.1455	57	32.41	129	118.5
3	0.9705	63	36.59	135	126.3
6	2.317	69	41.85	141	132.6
9	3.283	76	47.92	147	137.7
12	4.771	82	54.01	153	142.0
15	6.089	87	59.24	159	143.7
21	8.343	93	67.08	165	145.2
27	13.31	99	74.08	175	146.3
33	16.63	105	82.79	134	147.0
39	19.23	111	92.32	193	147.2
46	23.80	117	100.4	199	147.8
52.5	28.20	123	108.9	p_f	148.4

TABLE 17. /...

TABLE 17.

15 hours.					
t.	p x 10^3.	t.	p x 10^3.	t.	p x 10^3.
0.5	0.1394	57	30.49	129	117.0
3	1.191	63	36.00	135	124.6
6	1.547	69	41.53	143	132.7
9	2.661	75	46.76	148	136.8
12	3.744	81	52.94	153	142.0
15	5.346	89	61.86	159	145.5
21	8.742	93	66.21	165	146.3
27	10.88	100	75.78	171	147.2
30	11.64	105	81.89	180	148.4
39	19.16	111	91.18	188	148.9
45	22.66	118	100.2	195	149.8
51	26.57	123.5	108.9	p_f	150.0

TABLE 17.(continued)/...

TABLE 17. (continued)

15 hours.					
t.	$p \times 10^3$.	t.	$p \times 10^3$.	t.	$p \times 10^3$.
0.5	0.1731	57	31.08	129	115.9
3	0.8626	63	36.59	135.5	124.0
6	1.742	70	42.40	141.5	130.7
9	2.370	75	46.98	147.5	136.8
12	3.753	81	53.43	153	141.1
15	4.926	87.5	60.98	159	143.7
21	8.015	93	67.08	165	145.5
27	10.77	99	74.33	174	147.0
33	14.74	106	83.07	183	147.3
39	17.54	112	91.47	192	147.9
45	21.05	117.5	99.15	201	143.4
51.5	26.13	123	107.2	p_f	148.9

TABLE 17. (continued)/...

TABLE 17. (continued)

48 hours.					
t.	p x 10^3.	t.	p x 10^3.	t.	p x 10^3.
0.5	0.3600	57	30.67	129	115.3
3	1.461	63	36.15	135	124.8
6	1.312	69	41.82	141	130.9
9	2.308	75	47.34	150	139.5
12.5	4.633	81	53.15	159	144.2
15	5.373	87	60.15	165	147.2
21	8.364	93	67.08	171	148.1
27	10.54	100	75.78	180	148.4
33.5	14.37	105	83.64	189	148.9
39	18.01	112	91.09	198	149.6
45	23.41	117	99.24	p_f	150.8
51.5	26.52	123	107.2		

TABLE 17. (continued)/...

TABLE 17. (continued)

48 hours.					
t.	p x 10^3.	t.	p x 10^3.	t.	p x 10^3.
0.5	0.4330	61	35.72	135	127.7
3	0.9991	66.5	40.70	144	136.2
6	2.004	72	44.86	159.5	145.5
9	3.455	79.5	53.43	165	147.1
12	4.646	84.5	58.52	171	148.1
15	6.098	90	66.24	177	148.4
21	9.353	97	74.09	186	148.9
27	14.00	102	81.87	191	149.4
33	17.51	109	90.63	197	149.6
39	20.96	114	96.96	p_f	150.7
45	24.53	120	106.3		
54	29.62	129	119.0		

TABLE 18./...

TABLE 13.

1 week.					
t.	p x 10^3.	t.	p x 10^3.	t.	p x 10^3.
0.5	0.0427	59	33.36	129	116.1
3	1.072	63	36.15	135	125.4
7	1.754	69	42.84	141	131.7
9	2.718	75	47.04	150	139.4
12	4.194	81	53.58	157	144.1
15	5.685	87	60.98	165	144.6
21	8.730	95	69.69	172	145.2
29	13.40	100	77.54	180	145.7
33.5	16.64	107	83.64	189	146.3
40	19.23	111	90.61	199	147.0
45	22.27	117	99.31	p_f	147.5
53	27.45	123	107.4		

TABLE 13. (continued)/...

TABLE 18. (continued)

1 week.					
t.	$p \times 10^3$.	t.	$p \times 10^3$.	t.	$p \times 10^3$.
0.5	0.0683	75	46.80	147	137.7
5	1.734	80	52.53	154	142.0
9	3.329	85	58.60	163	146.3
15	5.683	91	65.75	171	147.2
21	8.763	97	73.18	178	148.1
29	13.31	102	80.30	184	148.6
35	17.46	108	87.14	190	148.7
39	19.33	115	96.81	196	149.1
46	23.70	121	104.1	202	149.5
54	29.01	128	115.0	p_f	149.6
61	35.14	132	122.0		
68	40.58	140	131.6		

These/...

These results are illustrated in FIG.XV and FIG.XVI where the runs are normalised to a constant weight of 23 mg. of preparation C.

6.10. THE EFFECT OF INTERRUPTING A DECOMPOSITION.

FIG.XVII shows the effect of interrupting a decomposition after 36 and 63 minutes. The sample was initially pre-heated and then subsequently decomposed at 350°C. At the above-mentioned times, the bucket was removed from the furnace by means of the winch, and allowed to cool for three hours. The bucket was then lowered into the furnace and the run continued. The results are tabulated below in TABLE 19.

TABLE 19.

t.	$p \times 10^3$.	t.	$p \times 10^3$.	t.	$p \times 10^3$.
0.5	0.0357	33	20.90	57	42.11
3	0.1577	36	23.24	63	47.79
6	1.504	INTERRUPTED FOR		INTERRUPTED FOR	
9	3.514	3 HOURS		3 HOURS	
12	5.546	39	25.56	64	50.23
15	7.841	42	28.45	69	55.60
21	11.61	45	31.36		
27	16.26	51	36.29		

6.11./...

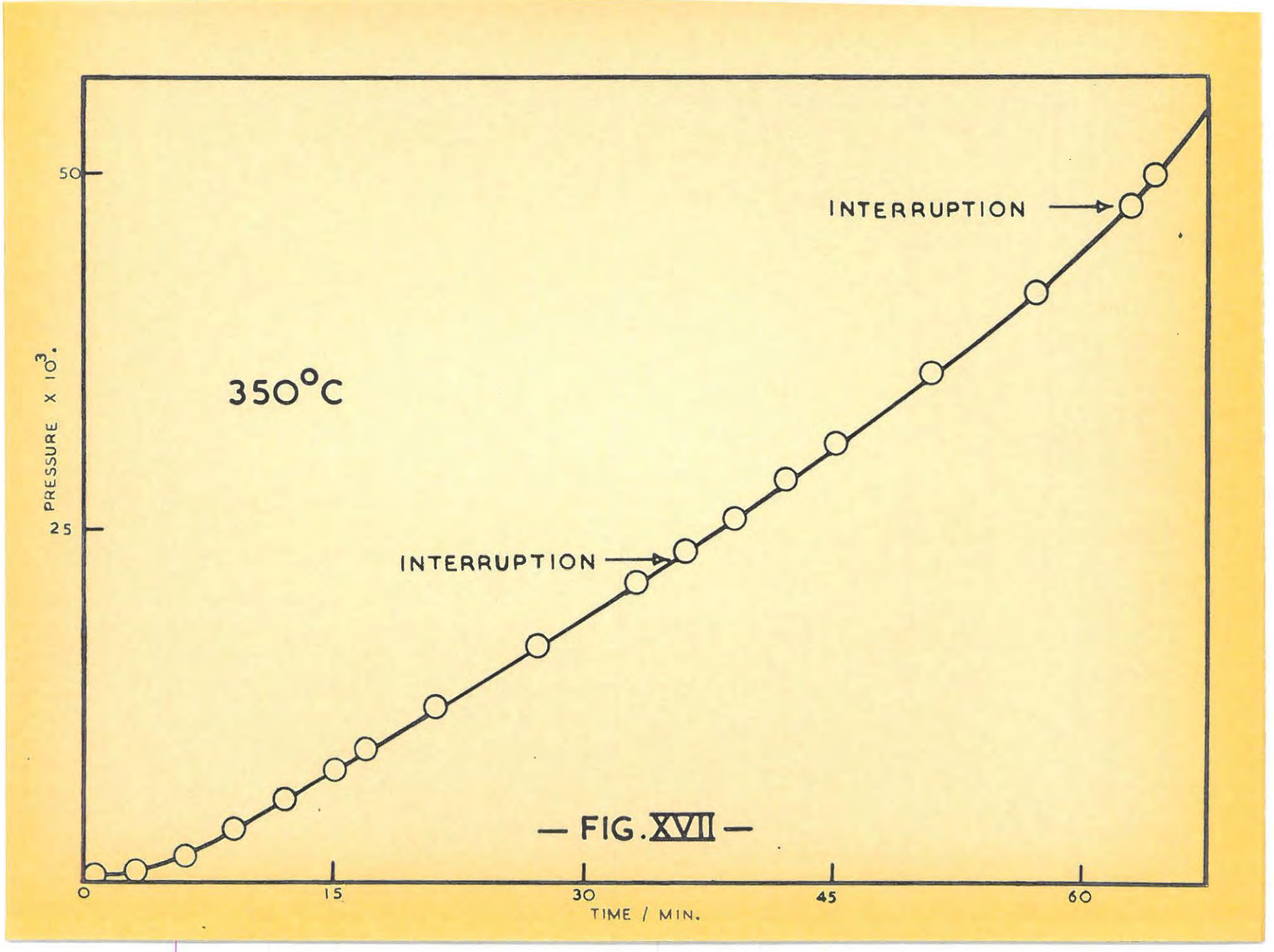
50
25
PRESSURE X 10^3.
350°C
INTERRUPTION
INTERRUPTION
0
15
30
45
60
TIME / MIN.

— FIG. XVII —

6.11. THE EFFECT OF CARBON DIOXIDE.

In order to demonstrate fully the reactivity of the silver oxide with carbon dioxide, specimens of pre-treated silver oxide were exposed to air, and carbon dioxide, both at one atmosphere pressure, and at room temperature, for various lengths of time. Decompositions were then carried out at 350°C with no potassium hydroxide trap present. The results, corrected to the same weight of 23 mg., are shown in FIG.XVIII, and are tabulated in TABLE 20 below.

TABLE 20.

DRIED AT 230°C FOR 3 HOURS. (UNCONTAMINATED).					
t.	p x 10^3.	t.	p x 10^3.	t.	p x 10^3.
0.5	0.0261	57.5	31.95	129	115.9
3	0.1743	63	35.43	135	123.5
6	1.050	69	41.24	141	129.9
9	2.534	75	46.27	147	134.5
12	4.095	81	52.53	153	137.4
15	5.750	87	58.37	159	140.6
21	8.450	93.5	65.79	166.5	142.5
27	12.08	99	73.65	171	143.8
33	15.47	105	81.23	177	144.7
39	18.59	111	90.12	186	145.2
45	23.15	113	99.91	195	145.7
51	26.77	123	107.4	p_f	146.1

TABLE 20. (continued)/...

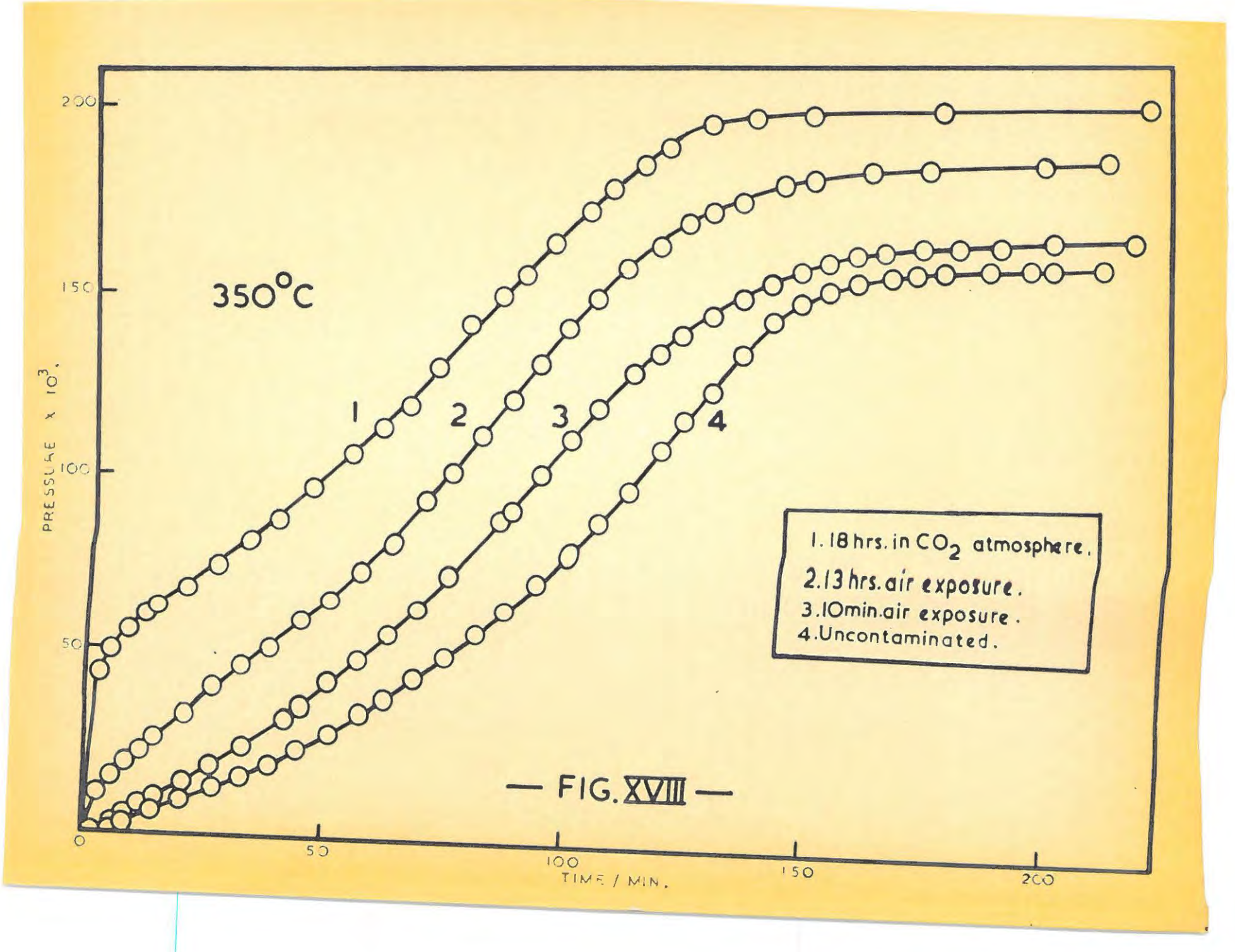
350°C
1
2
3
4
1. 18 hrs. in CO_2 atmosphere.
2. 13 hrs. air exposure.
3. 10 min. air exposure.
4. Uncontaminated.
PRESSURE x 10^3.
TIME / MIN.
0
50
100
150
200

— FIG. XVIII —

TABLE 20. (continued)

10 MINUTES ATMOSPHERIC CONTAMINATION.					
t.	$p \times 10^3$.	t.	$p \times 10^3$.	t.	$p \times 10^3$.
0.5	0.0116	57	45.30	129	133.6
3	0.1191	63	51.99	135	137.9
6	2.742	69	59.54	141	142.0
9	5.140	75	67.38	147	144.3
12	7.231	85	80.72	153	147.0
15	9.526	87	84.50	159	143.1
21	13.51	93	93.53	165	149.3
27	18.39	99	101.4	171	150.2
33	23.35	105	110.1	180	151.3
42	30.20	112	118.8	189	151.7
45	33.39	117.5	123.7	198	152.2
51	39.78	123.5	129.2	p_f	153.1

TABLE 20. (continued)/...

TABLE 20. (continued)

13 HOURS ATMOSPHERIC CONTAMINATION.					
t.	p x 10^3.	t.	p x 10^3.	t.	p x 10^3.
0.5	1.243	57	68.31	129	157.8
3	11.66	63	75.51	135	161.2
6	14.63	69.5	85.96	144	165.8
9	19.34	75	93.53	150	171.0
12	21.49	81	103.4	156	171.6
15	24.76	87	115.3	162	172.2
21	30.78	93	121.4	168	173.2
27	37.17	99	131.2	174	173.4
33	43.35	105	137.7	180	173.6
39	43.50	111	146.3	193	173.7
45	55.76	117	151.3	p_f	174.1
51	60.98	124	156.3		

TABLE 20. (continued)/...

TABLE 20. (continued)

13 HOURS SATURATED CARBON DIOXIDE CONTAMINATION.					
t.	$p \times 10^3$.	t.	$p \times 10^3$.	t.	$p \times 10^3$.
0.5	1.307	60	104.6	132	182.9
3	41.53	66	111.3	138	183.3
6	46.46	72	119.6	150	183.9
9	51.99	78	127.7	159	184.4
12	55.46	85.5	137.7	165	184.7
15	57.60	90	144.1	174	184.8
21	63.59	96	151.3	180	184.9
27	69.93	102.5	159.2	189	185.0
33	75.03	103	165.2	198	185.1
39	81.39	114	170.2	p_f	185.2
46	88.86	120	175.4		
54	97.36	129	181.8		

Decompositions/...

Decompositions at 350°C were also interrupted at various stages, and the silver oxide was exposed to carbon dioxide (from a cylinder), at room temperature, for 15 minutes at atmospheric pressure. The runs were then continued, after evacuation, at 350°C. The results are illustrated in FIG.XIX, (TABLE 21), each contamination being done on a fresh run.

TABLE 21.

1.		2.	
t.	p x 10^3.	t.	p x 10^3.
CONTAMINATED AT t = 0		0.5	0.2036
		3	0.4356
0.5	0.2090	6	1.743
1	4.646	INTERRUPTED AND CONTAMINATED.	
3	5.307		
5	6.060	7	6.093
7.5	8.712	9	7.459
10.5	10.74	13	9.874

TABLE 21.(continued)/...

TABLE 21. (continued)

3.		4.	
t.	p x 10^3.	t.	p x 10^3.
0.5	0.1452	0.5	0.3282
6	2.120	6	1.597
9	3.427	9	3.629
12	5.780	16	9.583
15	8.132	21	12.20
INTERRUPTED AND		27	20.84
CONTAMINATED.		33	21.19
15.5	9.583	INTERRUPTED AND	
18	12.20	CONTAMINATED.	
21	14.81	36	26.13
		39	29.04
		42	31.95

TABLE 21. (continued)/...

TABLE 21. (continued)

5.		6.	
t.	p x 10^3.	t.	p x 10^3.
0.5	0.2817	0.5	0.3221
6	1.443	6	1.577
9	3.633	15	5.102
12	5.247	21	12.93
21	12.60	27	16.36
27	16.63	33	21.43
33	20.96	39	26.55
36	23.67	45	32.21
INTERRUPTED AND		51	36.38
CONTAMINATED.		58	43.56
39	26.13	63	49.03
42	28.58	INTERRUPTED AND	
45	31.55	CONTAMINATED.	
		64	50.53
		69	56.33
		70	57.22

6.12./...

6.12. THE EFFECT OF GRINDING.

40 mg. of silver oxide was preheated in vacuo at 250°C for three hours, the sample removed in an atmosphere of nitrogen, and then ground in an agate mortar in a nitrogen-filled glove box. A 20 mg. sample was then weighed out in nitrogen, and decomposed at 350°C. The p/t plot corresponded with that obtained from an unground, protracted specimen. The results illustrated in FIG.XX, are tabulated below in TABLE 22.

TABLE 22.

t.	p x 10^3.	t.	p x 10^3.	t.	p x 10^3.
0.5	0.1321	57	42.98	129	155.7
3	1.199	63	49.37	135	161.5
6	3.401	69	55.76	141	175.4
9	3.526	75	63.89	147	182.4
12	6.961	81	72.02	153	183.2
15	8.357	87	80.72	159	189.5
21	12.80	93	89.45	165	195.7
27	17.43	99	99.91	174	196.3
33	22.10	105	110.4	180	196.9
39	26.13	111	122.0	189	197.0
45	31.78	117	134.3	198	197.2
51	37.17	123	147.0	p_f	197.5

6.13/...

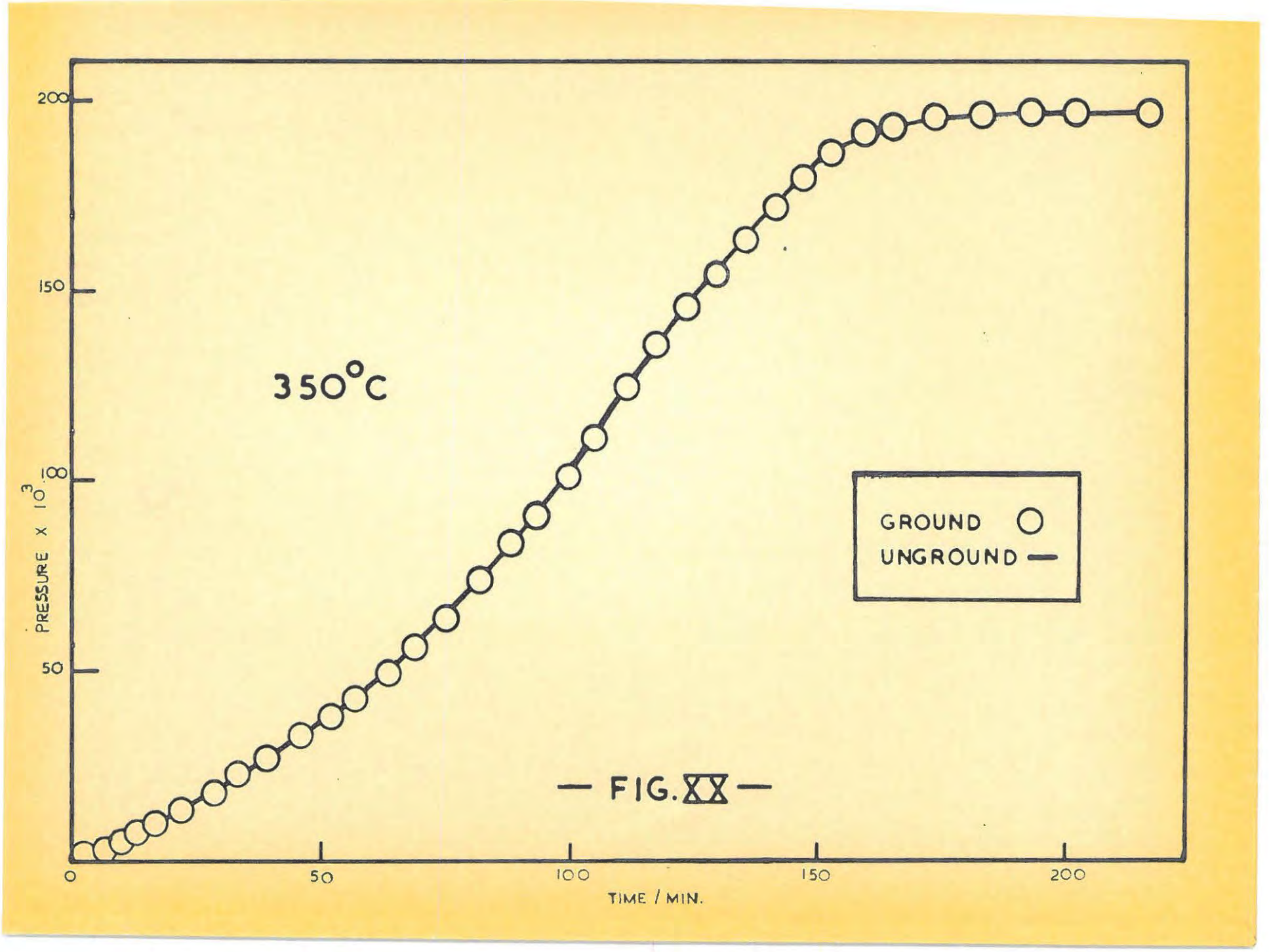
200
150
100
50
PRESSURE X 10^3
350°C
GROUND
UNGROUND
0
50
100
150
200
TIME / MIN.

— FIG. XX —

6.13. THE EFFECT OF CATHODE RAYS.

A cadmium trap was inserted between the McLeod gauge and the decomposition chamber to minimise the effects of the mercury vapour in the system (position N).

TABLE 23.

t.	p x 10^3.	t.	p x 10^3.	t.	p x 10^3.
0.5	0.3626	57	32.23	129	122.0
3	1.307	63	37.70	135	130.1
6	1.974	69	41.32	141	136.8
9	3.178	75	47.34	150	142.6
12	4.414	81	53.83	159	146.7
15	5.988	87	60.98	165	147.0
21	8.756	93	69.69	171	147.8
27	13.07	99	78.41	180	148.1
33	16.55	105	87.12	187	148.6
39	20.04	111	95.83	196	148.7
45	23.53	117	104.6	p_f	149.4
51	27.88	120	110.6		

The preheated salt was spread uniformly over the bottom of a quartz bucket of 5 mm. diameter, and irradiated for 6 minutes with bursts of 18-20 sec. duration, and with 10 sec. intervals between

bursts/...

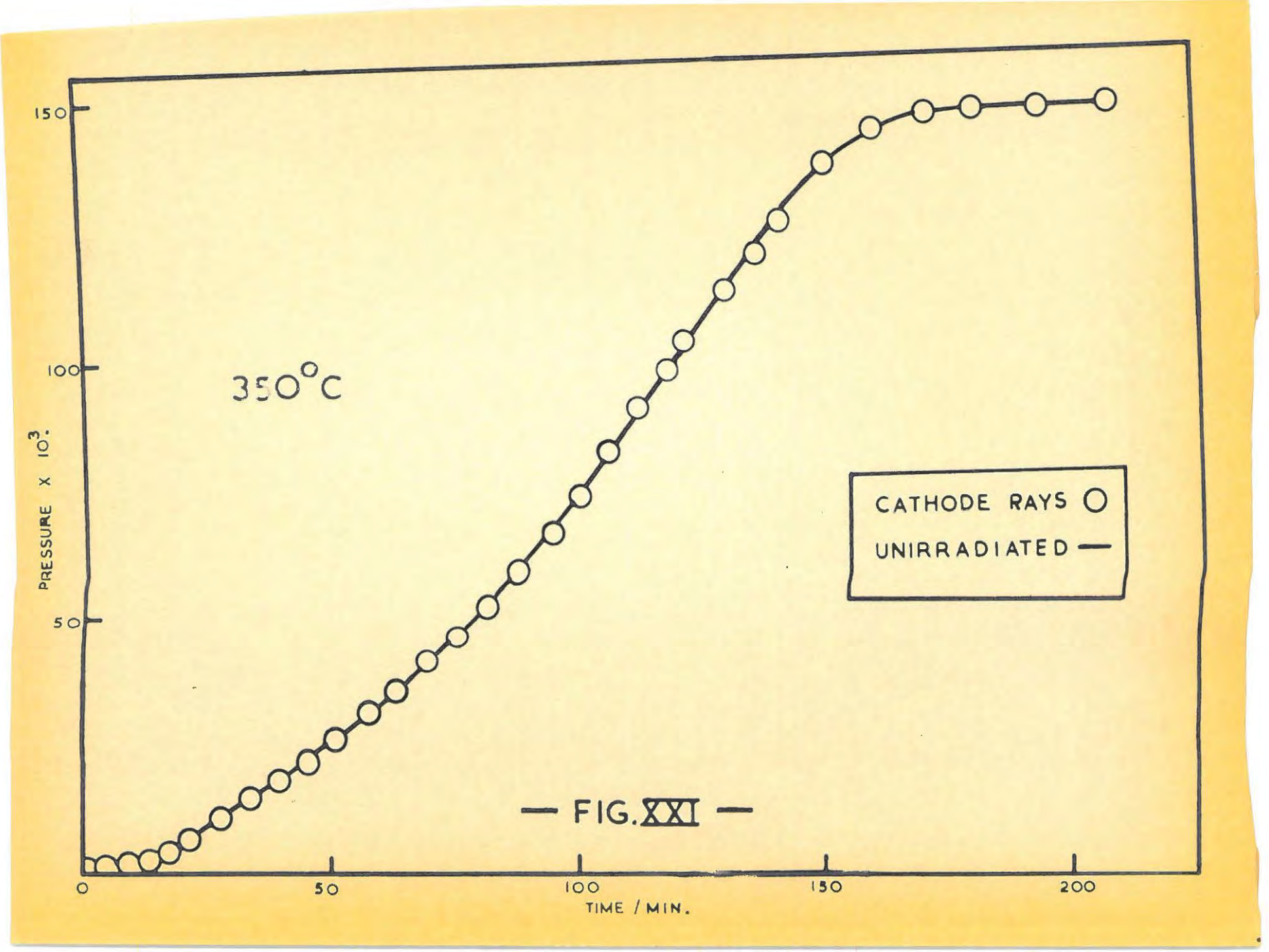
150
100
50
350°C
PRESSURE X 10³.
CATHODE RAYS O
UNIRRADIATED —
0
50
100
150
200
TIME / MIN.

— FIG. XXI —

bursts to prevent excessive heating of the bucket by the cathode rays.

The p/t plot for the decomposition at 350°C is given in FIG.XXI, and it can be seen that no effect occurred. The results, presented in TABLE 23, are corrected to a constant weight of 23 mg.

6.14. THE EFFECT OF MIXING WITH PRODUCT.

An intimate mixture of the product from the decomposition of 20 mg. of silver oxide at 380°C and 20 mg. of silver oxide preheated at 230°C for three hours was made. The mixing was done in the platinum bucket containing the preheated specimen.

TABLE 24.

t.	p x 10^3.	t.	p x 10^3.	t.	p x 10^3.
0.5	0.9419	47	32.60	122	146.7
3	1.751	54	40.83	132	165.1
6	3.709	60	46.46	140	136.0
9	5.513	66	54.03	150	194.3
12	6.934	72	61.06	162.5	196.9
15	8.369	81	72.06	174	197.1
21	12.05	90	85.27	183	197.2
28	17.69	97	93.61	190	197.4
33	21.39	103	117.4	199	197.5
39.5	25.93	114	130.3	p_f	197.5

An/...

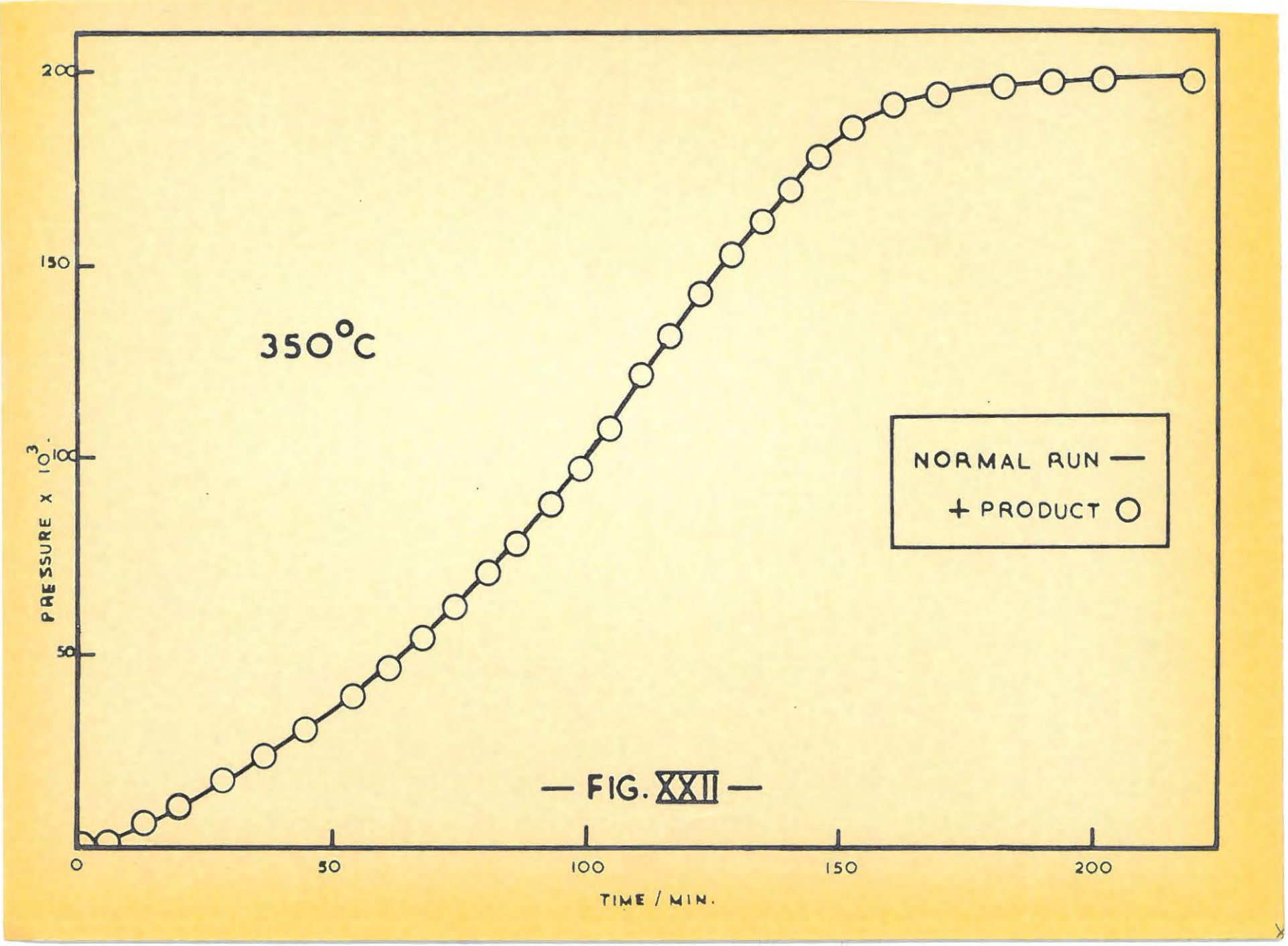
200
150
100
50
PRESSURE X 10^3.
350°C
NORMAL RUN —
+ PRODUCT O
0
50
100
150
200
TIME / MIN.

— FIG. XXII —

An atmosphere of nitrogen was maintained throughout the mixing. No change from the usual decomposition was obtained on decomposing the mixture at 350°C. The results, tabulated above in TABLE 24, are shown in FIG.XXII.

6.15. THE EFFECT OF OXYGEN.

Cylinder oxygen was not used in these runs since Garner and Reeves[59] have shown that, in such oxygen, organic impurities facilitate the decomposition of silver oxide, even at 100°C.

A specimen was pretreated for three hours at 280°C in vacuo. Prior to decomposition, 20 mg. of preheated silver oxide was heated at 400°C in an evacuated side arm, connected to the vacuum line, and the released oxygen created a pressure of approximately 2×10^{-1} cm. mercury in the decomposition line. The decomposition of the specimen was then carried out at 350°C in this atmosphere. No change from the normal decomposition occurred. The results are tabulated in TABLE 25 below, where the pressure values given represent the pressure of evolved oxygen only.

As well, a sample was preheated for three hours at 280°C in oxygen at 1 atmosphere pressure, (similar to Lewis[53]). The oxygen was prepared by heating a mixture of A.R. potassium chlorate and A.R. manganese dioxide. The decomposition at 350°C, in vacuo, was unchanged by this treatment. The results are given in TABLE 26.

TABLE 25./...

TABLE 25.

t.	p x 10^3.	t.	p x 10^3.	t.	p x 10^3.
0.5	0.0139	51	35.95	123	146.0
3	0.4131	57	42.59	129	156.4
6	1.504	63	49.04	135	168.6
9	2.564	69	56.20	141	175.8
12	5.204	78	68.29	150	185.3
15	7.155	90	85.27	159	192.3
21	11.61	94	92.37	171	196.1
27	16.17	101	104.6	177	196.6
33.5	21.79	105	110.9	195	197.3
39.5	25.73	111	123.5	p_f	197.5
45	31.24	117	136.7		

TABLE 26./...

TABLE 26.

t.	p x 10^3.	t.	p x 10^3.	t.	p x 10^3.
0.5	0.0076	60	47.98	132	159.2
3	0.0227	66	54.59	135	163.6
6	1.364	72.5	63.10	144	174.4
9	3.137	78	70.63	150.5	181.9
12	5.341	84	77.78	156	187.7
15	7.759	90	87.96	162	191.5
21	12.43	97	99.86	168	195.4
28	18.05	102	103.0	174	195.9
33	22.04	108	118.3	180	196.4
39	27.38	114	128.9	198	197.3
45	30.70	120	139.5	p_f	197.5
55	43.21	126	149.4		

6.16./...

6.16. VISUAL OBSERVATIONS.

The decomposition at 350°C was interrupted at various time intervals, and the resulting product observed microscopically, (magnification, x 400). A fresh sample was used in each case. The following results were obtained, (TABLE 27).

TABLE 27.

TIME, t.	MICROSCOPICAL OBSERVATION.
Undecomposed sample.	A dull, chocolate-brown coloured mass of very small particles. No silver spots were present.
Dried at 250°C for three hours. t = 0.	The same dull chocolate-brown colour as above.
15 minutes.	Black in colour, tending to form a coherent mass with quite a large number of minute silver specks; occasional regions where agglomerates of silver occur.
55 minutes.	Black, not very different from above - perhaps a slight increase in the number of pinpoints of silver.
97 minutes.	Black colour remains, but the pinpoints of silver now appear clearly visible.
130 minutes.	Surfaces all covered with silver.
154 minutes. (completeness).	Only pure silver present - it has a structure resembling silver filigree.

6.17. PERCENTAGE DECOMPOSITION.

The percentage decomposition was determined assuming the reaction:-

$2Ag_2$/...

$$2\,Ag_2O \longrightarrow 4\,Ag + O_2 \quad \ldots\ldots\ldots\ldots\ldots\ldots\ldots\ldots \quad (6.01).$$

The percentage was determined by weighing a sample, preheated at 250°C for three hours, in nitrogen, which was then decomposed into the known volume of the line (569 cos.), and the final pressure determined. The values of the decomposition temperature and room temperature were noted. The values for the percentage decomposition at 350°C were:-

84.11, 88.15, 91.36, 85.50 %.

MEAN : 87.4%.

6.13. THE REPEAT OF HOOD AND MURPHY'S METHOD.

A sample of 20 mg. of silver oxide was intimately mixed with approximately 5.0 mg. of silver obtained by heating silver oxide at 400°C for several hours with pumping. After weighing the 20 mg. sample in air, the mixing was done in air and no special precautions were observed. The mixing was done three hours before the run and the specimen was allowed to stand in air. The p/t plot for the decomposition at 350°C is shown in FIG.XXIII, (TABLE 28).

The pressure of the gas at one stage was at the limit of the McLeod gauge and, consequently, the run had to be interrupted and a portion of the gas pumped off.

TABLE 28./...

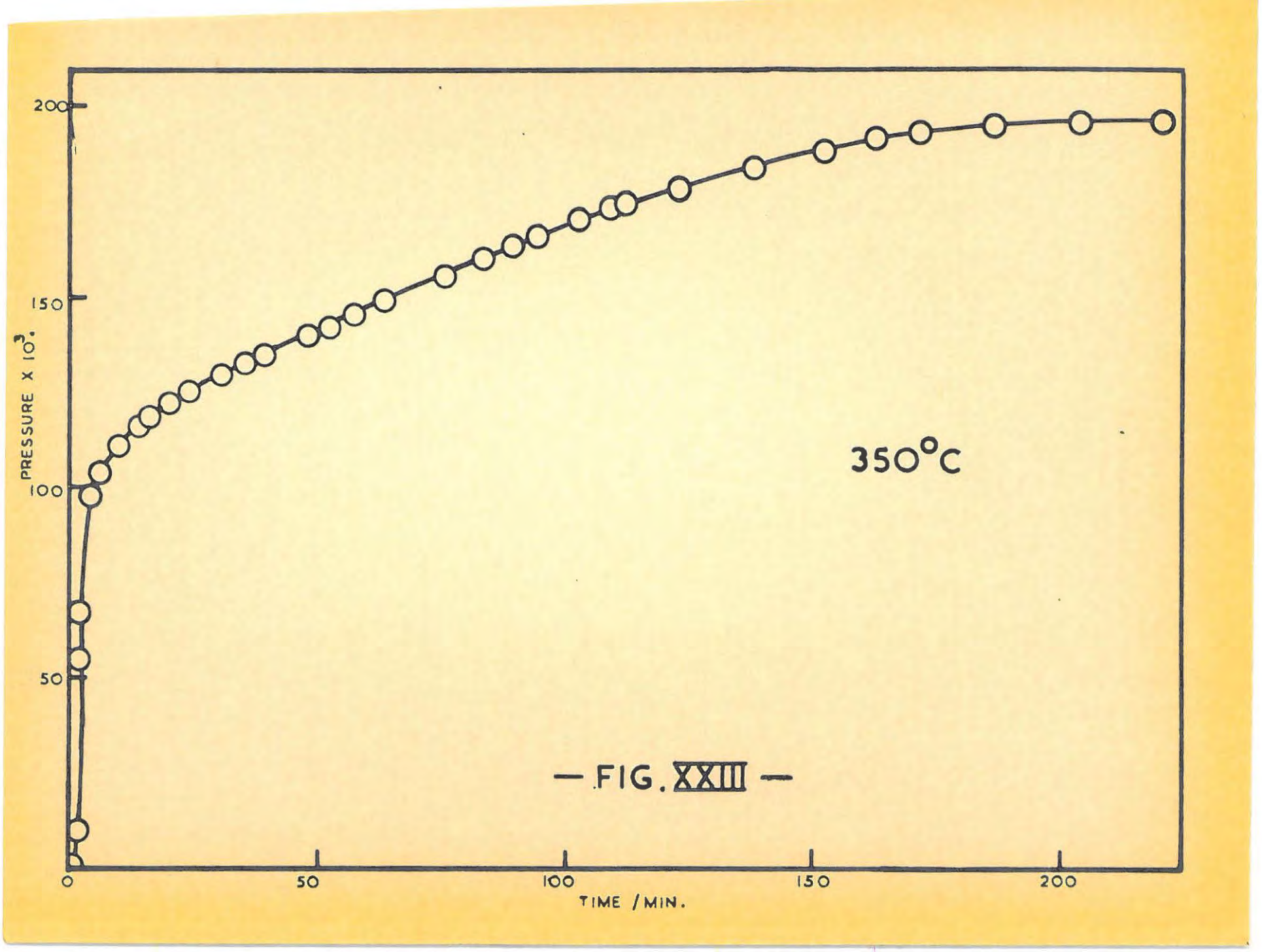

— FIG. XXIII —

TABLE 28.

t.	$p \times 10^3$.	t.	$p \times 10^3$.	t.	$p \times 10^3$.
0.5	4.581	36	134.6	109	174.8
2	59.02	39	135.6	112	176.0
4	97.47	47	140.3	121	179.5
6	105.5	51	142.7	136	185.7
10	112.6	57	146.2	153	191.0
14	116.7	63	149.8	163	192.6
16	119.3	75	156.7	170	193.9
20	122.5	82	161.0	185.5	196.9
24	125.5	89	164.5	194	197.2
30	133.0	94	167.3	p_f	197.5
35	134.2	102	164.5		

6.19. THE EFFECT OF TEMPERATURE.

A constant mass of 20.0 mg. was decomposed at various temperatures after the usual pre-treatment at 280° for three hours; to obtain the critical increment of the chemical process(es) occurring. These are discussed later. The following results were obtained where the volume of the line was 569 ccs. throughout, (TABLE 29).

TABLE 29./...

TABLE 29.

380°C.					
t.	p x 10^3.	t.	p x 10^3.	t.	p x 10^3.
0.5	0.1408	24	73.99	48	181.5
3	1.910	27	87.61	51	187.2
6	6.421	30	102.4	54	190.2
9	16.75	33	119.7	60	194.2
12	26.66	36	134.3	69	196.8
15	36.79	39	149.9	80	197.4
18	48.82	42	162.6	p_f	197.5
21	60.37	45	172.4		

370°C.					
t.	p x 10^3.	t.	p x 10^3.	t.	p x 10^3.
0.5	0.3093	30	52.18	60	140.7
3	1.980	33	59.53	66	162.2
6	4.681	36	67.23	69	170.8
9	9.874	39	75.33	72	179.0
12	15.60	42	83.37	75	185.0
15	21.22	45	92.26	81	192.5
18	27.37	48	100.8	87	196.7
21	33.40	51	110.8	93	197.1
24	39.17	54	121.2	102	197.4
27	45.45	57	130.8	p_f	197.5

TABLE 29. (continued)/...

TABLE 29. (continued)

360°C.					
t.	p x 10^3.	t.	p x 10^3.	t.	p x 10^3.
0.5	0.0302	33	37.11	87	151.6
3	1.154	36	42.11	93	173.4
6	2.891	39	47.04	99	182.0
9	6.426	42	50.56	107	190.1
12	9.321	45	57.41	111	191.7
15	13.77	51	68.62	117.5	194.3
18	17.37	57	81.69	126	195.6
21	20.68	63	96.56	135	196.5
24	25.16	70.5	116.4	144	197.1
27	28.11	75	128.2	p_f	197.5
30	32.96	81	144.7		

TABLE 29.(continued)/...

TABLE 29. (continued)

355°C.					
t.	$p \times 10^3$.	t.	$p \times 10^3$.	t.	$p \times 10^3$.
0.5	0.0255	36.5	37.46	103	161.3
3	1.679	43	45.36	108	170.8
6	3.255	48	53.03	114	180.3
9	6.421	54	62.44	120	187.0
12	10.43	60	72.80	126	192.7
15	13.40	67	85.87	132	195.4
18	16.72	71	94.61	138	196.9
21	19.39	73	108.6	144	197.1
24	23.30	85	121.5	153	197.3
27	26.74	90	134.6	p_f	197.5
30	30.03	96.5	149.9		

TABLE 29. (continued)/...

TABLE 29. (continued)

350°C.					
t.	p x 10^3.	t.	p x 10^3.	t.	p x 10^3.
0.5	0.0349	57.5	43.27	129	157.1
3	0.2323	63	43.21	135	167.6
6	1.452	69	56.05	141	176.0
9	3.514	75	62.73	147	132.4
12	5.547	81	71.15	153	186.2
15	7.312	87	79.28	159	190.5
21	11.47	93.5	89.15	166.5	193.4
27	16.38	99	99.90	171	194.8
33	21.00	105	110.1	177	196.3
39	25.21	111	122.0	186	196.6
45	31.36	118	135.6	195	197.2
51	36.30	123	145.5	p_f	197.5

TABLE 29. (continued)/...

TABLE 29. (continued)

345°C.					
t.	p x 10^3.	t.	p x 10^3.	t.	p x 10^3.
0.5	0.0451	60	47.05	138	154.1
3	0.8439	66	53.11	145.5	161.9
6	1.665	72	59.62	153	174.5
9	4.254	78.5	66.94	159	180.1
12	6.911	84	73.65	165	185.4
18	12.00	90.5	82.68	171	189.3
24	16.81	96	90.28	177	192.9
30	21.18	102	98.53	186	195.7
36	25.57	108	107.6	194	196.9
42	30.06	115.5	118.7	206	197.3
43	36.71	120	125.6	p_f	197.5
54.5	42.37	129	139.9		

TABLE 29.(continued)/...

TABLE 29. (continued)

340°C.					
t.	p x 10^3.	t.	p x 10^3.	t.	p x 10^3.
0.5	0.1211	63	41.27	162	151.6
3	1.766	72	47.80	171.5	164.6
6	2.711	81	54.13	177	172.1
9	4.693	90	61.36	186	181.9
17	9.662	99.5	70.80	201.5	190.8
21.5	12.66	108	78.41	207	192.3
27.5	16.29	117	89.01	213	193.5
33	19.52	128	100.4	222	196.5
39	23.90	135.5	112.4	235	197.2
45	27.99	144	123.3	p_f	197.5
54	33.69	153	137.3		

TABLE 29. (continued)/...

TABLE 29. (continued)

330°C.					
t.	p x 10^3.	t.	p x 10^3.	t.	p x 10^3.
0.5	0.0606	102	35.46	248	134.8
3	1.237	114	41.35	260	144.6
6	2.080	126	46.70	272	157.0
9	2.815	138	53.00	278	161.1
19	5.373	150	59.97	295	163.4
27	8.076	162	67.40	313	182.1
36	10.86	174	75.33	325	187.5
45	13.30	188	85.76	337	192.1
55	16.93	200.5	94.55	349	193.7
72	22.95	212	103.6	367	196.5
31	26.96	219	109.6	390	197.0
90	30.41	236	124.2	p_f	197.5

7. APPLICABILITY OF MATHEMATICAL EQUATIONS.

7.1. THE ACCELERATORY PERIOD.

7. 1. 1. The Prout-Tompkins equations.

The Prout-Tompkins equation,

$$\log_{10}\left[p/(p_f - p)\right] = k_1 t + c_1 \quad \ldots\ldots\ldots\ldots\ldots\ldots \quad (1.30).$$

was applied to the results. The equation was applicable to the limited extent shown in FIG.XXIV.

The values of k_1 are tabulated below in TABLE 30.

TABLE 30.

TEMPERATURE °C.	$1/T^{\circ}K \times 10^2$.	$k_1 \times 10^2$.
380	0.1531	3.905
370	0.1555	2.6[illegible]
360	0.1580	2.768
355	0.1593	1.733
350	0.1606	1.316
345	0.1619	1.241
340	0.1632	0.9101
330	0.1659	0.6325

However, as can be seen from FIG.XXIV, the equation does not describe the complete curve.

The fit of the modified Prout-Tompkins equation,

$\log_{10}$/...

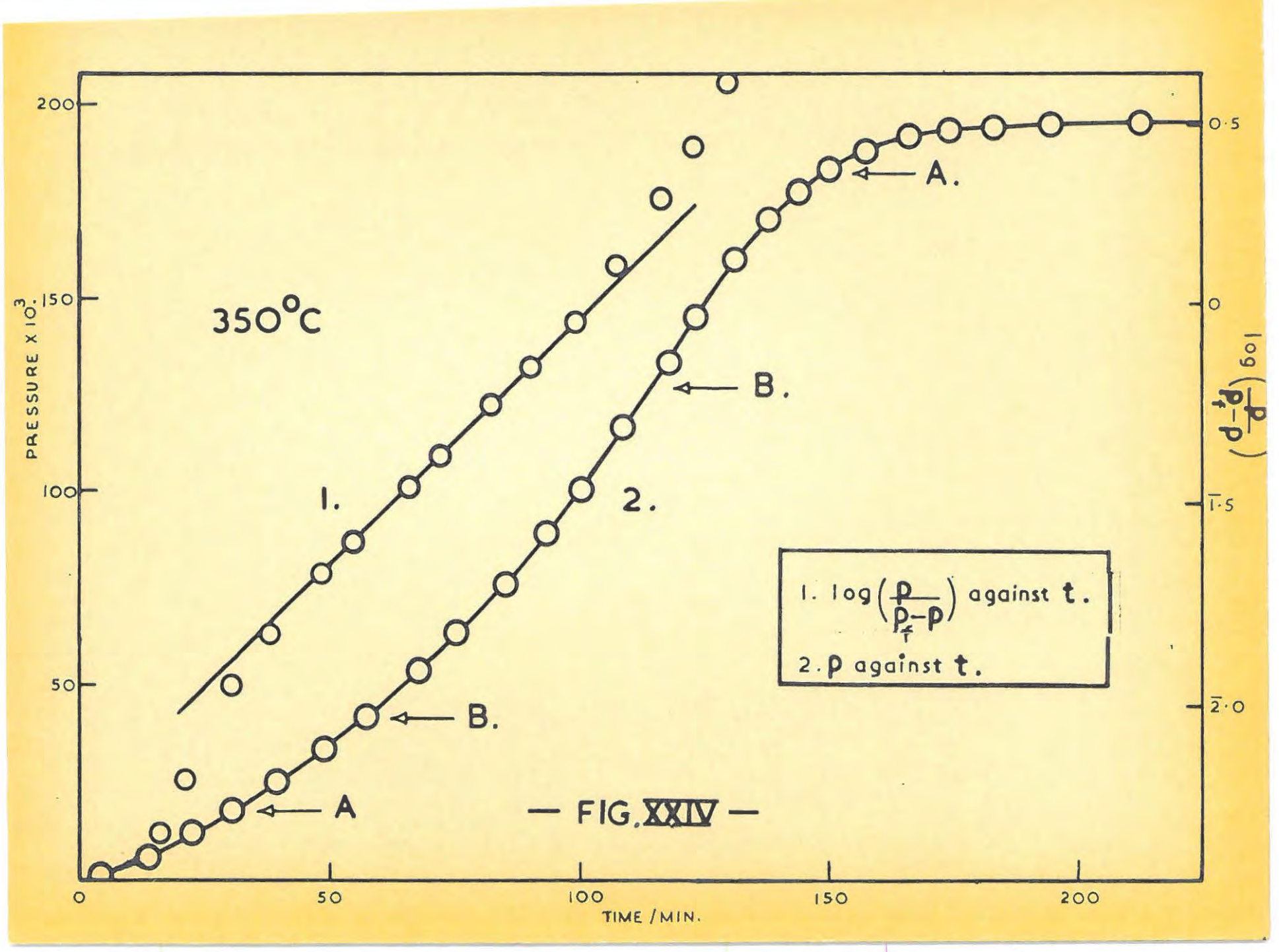
200
150
100
50
0
PRESSURE X 10^3.
350°C
1.
2.
A.
B.
B.
A
0
50
100
150
200
TIME / MIN.
0·5
0
$\bar{1}$·5
$\bar{2}$·0
$\log\left(\frac{p}{p_f - p}\right)$
1. $\log\left(\frac{p}{p_f - p}\right)$ against t.
2. p against t.

— FIG. XXIV —

$$\log_{10}\left[p/(p_f - p)\right] = k_2 \log t + C_2 \quad \ldots\ldots\ldots\ldots\ldots\ldots \quad (1.37).$$

was no better. (FIG.XXIV, AA).

7. 1. 2. The Exponential Law.

The equation,

$$\log p = k_3 t + C_3 \quad \ldots\ldots\ldots\ldots\ldots\ldots\ldots\ldots\ldots\ldots \quad (1.22).$$

was tested here. The fit is shown in FIG.XXIV, (BB), and does not cover the whole of the acceleration period.

7. 1. 3. The Power Law.

Garner and Reeves[59] found that their p/t plots over the acceleratory period could best be described by the expression,

$$p^{\frac{1}{3}} = k_4 t + C_4 \quad \ldots\ldots\ldots\ldots\ldots\ldots\ldots\ldots\ldots\ldots \quad (2.05).$$

Consequently, it was decided to apply this equation. The plots of $p^{\frac{1}{3}}$ against t for representative decompositions at 330°C, 350°C and 380°C are shown in FIGS.XXV, XXVI and XXVII respectively.

It can be clearly seen from these plots that, although the points approximate to a straight line at lower temperatures, this is not the case at higher temperatures.

Nevertheless, the best straight line was taken through the plots and the values of k_4 determined. (TABLE 31). These lines also give a negative intercept on the t axis, the value of which decreases with increasing temperature, as obtained by Garner and Reeves.

TABLE 31./...

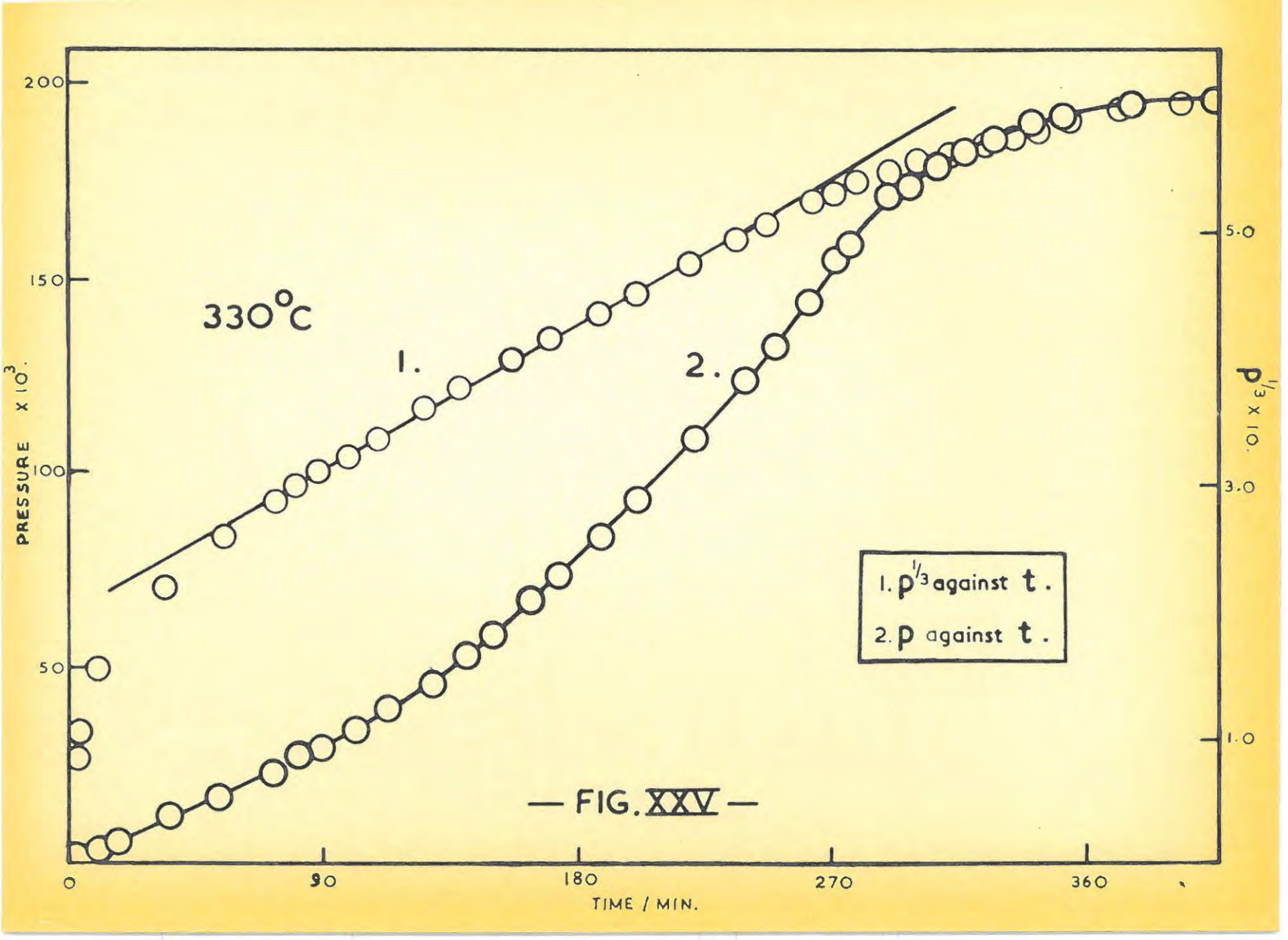
200
150
100
50
0
90
180
270
360
TIME / MIN.
PRESSURE x 10^3.
5.0
3.0
1.0
p^1/3 x 10.
330°C
1.
2.
1. p^1/3 against t.
2. p against t.

— FIG. XXV —

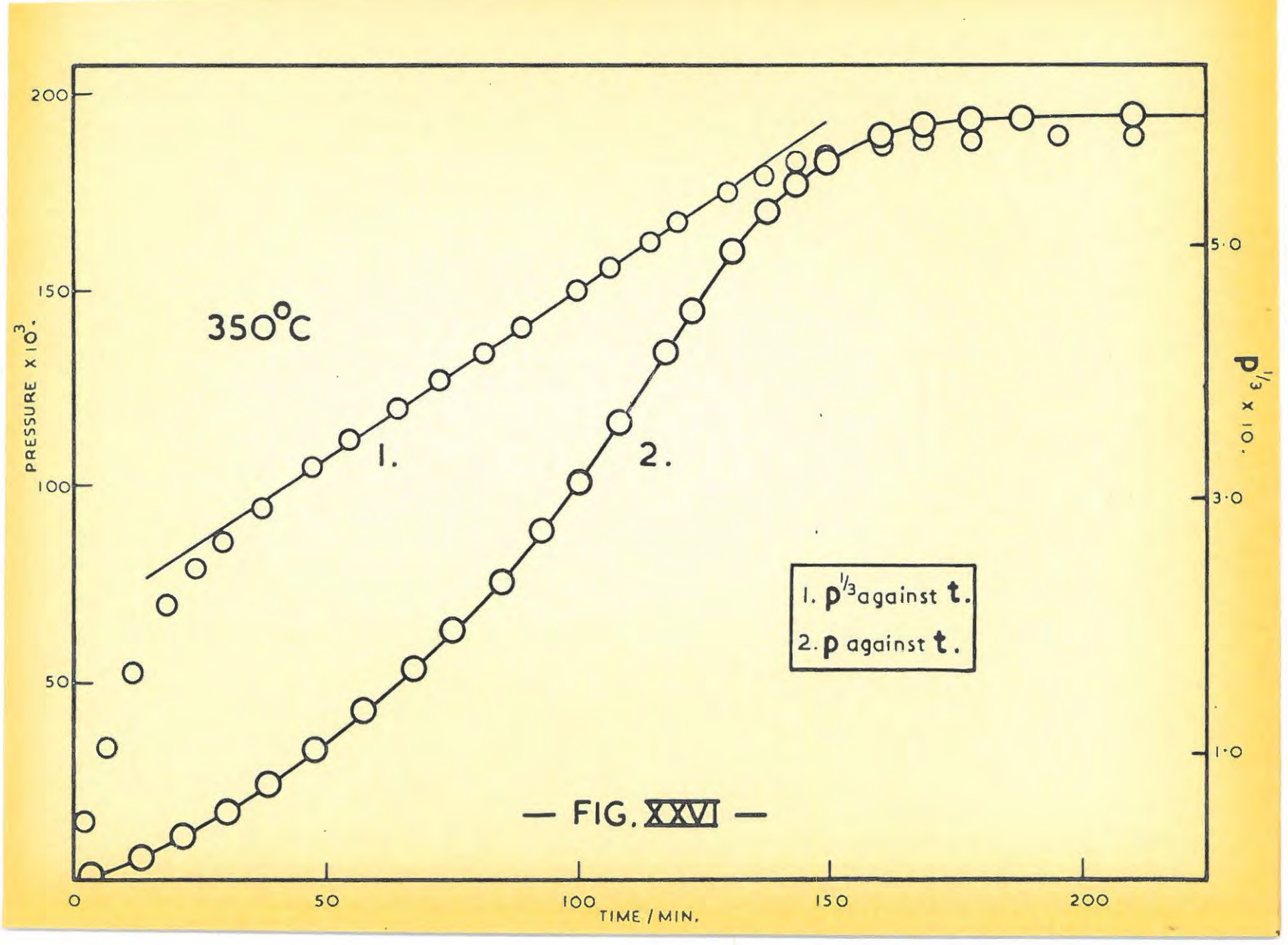
200
150
100
50
0
50
100
150
200
TIME / MIN.
PRESSURE X 10^3.
5·0
3·0
1·0
p^1/3 x 10.
350°C
1.
2.
1. p^1/3 against t.
2. p against t.

— FIG. XXVI —

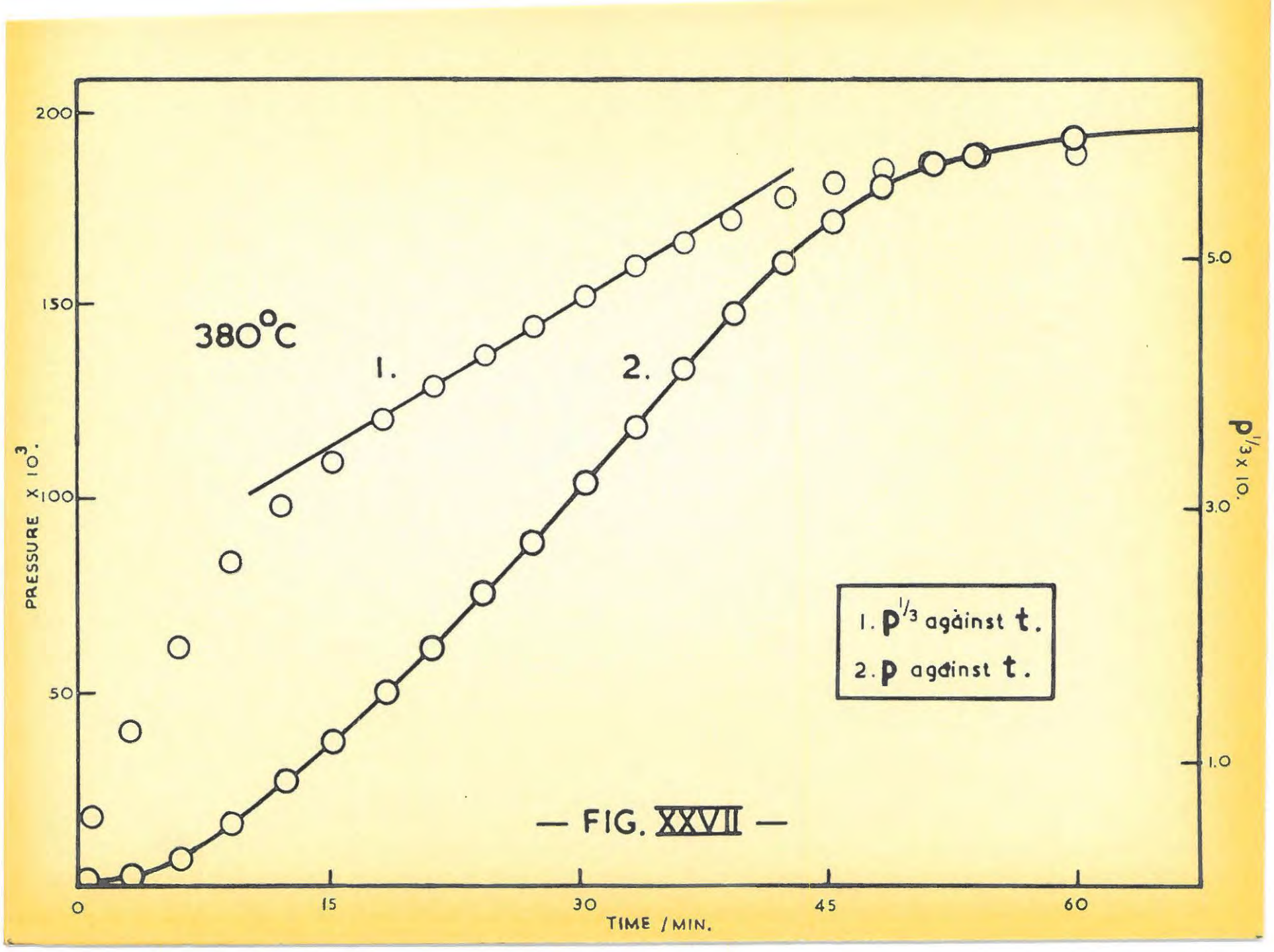
200
150
100
50
0
15
30
45
60
TIME / MIN.
PRESSURE X 10^3.
5.0
3.0
1.0
$p^{1/3}$ x 10.
380°C
1.
2.
1. $p^{1/3}$ against t.
2. p against t.

— FIG. XXVII —

TABLE 31.

TEMPERATURE °C.	$1/T°K \times 10^2$.	$k_4 \times 10$.
380	0.1531	1.239
370	0.1555	0.7732
360	0.1580	0.6082
355	0.1593	0.5022
350	0.1606	0.4047
345	0.1619	0.3398
340	0.1632	0.2879
330	0.1659	0.1939

In view of the poor fit of equation (2.05)., it was decided to test powers other than the cube root. It was found that the whole of the acceleratory period, except for a small initial portion, could be fitted by a square root plot i.e. by the equation

$$p^{\frac{1}{2}} = k_5 t + C_5 \quad \ldots\ldots\ldots\ldots\ldots\ldots\ldots\ldots\ldots\ldots\ldots\ldots \quad (7.01).$$

The plot of $p^{\frac{1}{2}}$ against t is shown in FIGS.XXVIII, XXIX and XXX. The linearity of this plot was maintained at all decomposition temperatures. The intercept on the abscissa is always negative.

The values of k_5 are tabulated in TABLE 32 below.

TABLE 32./...

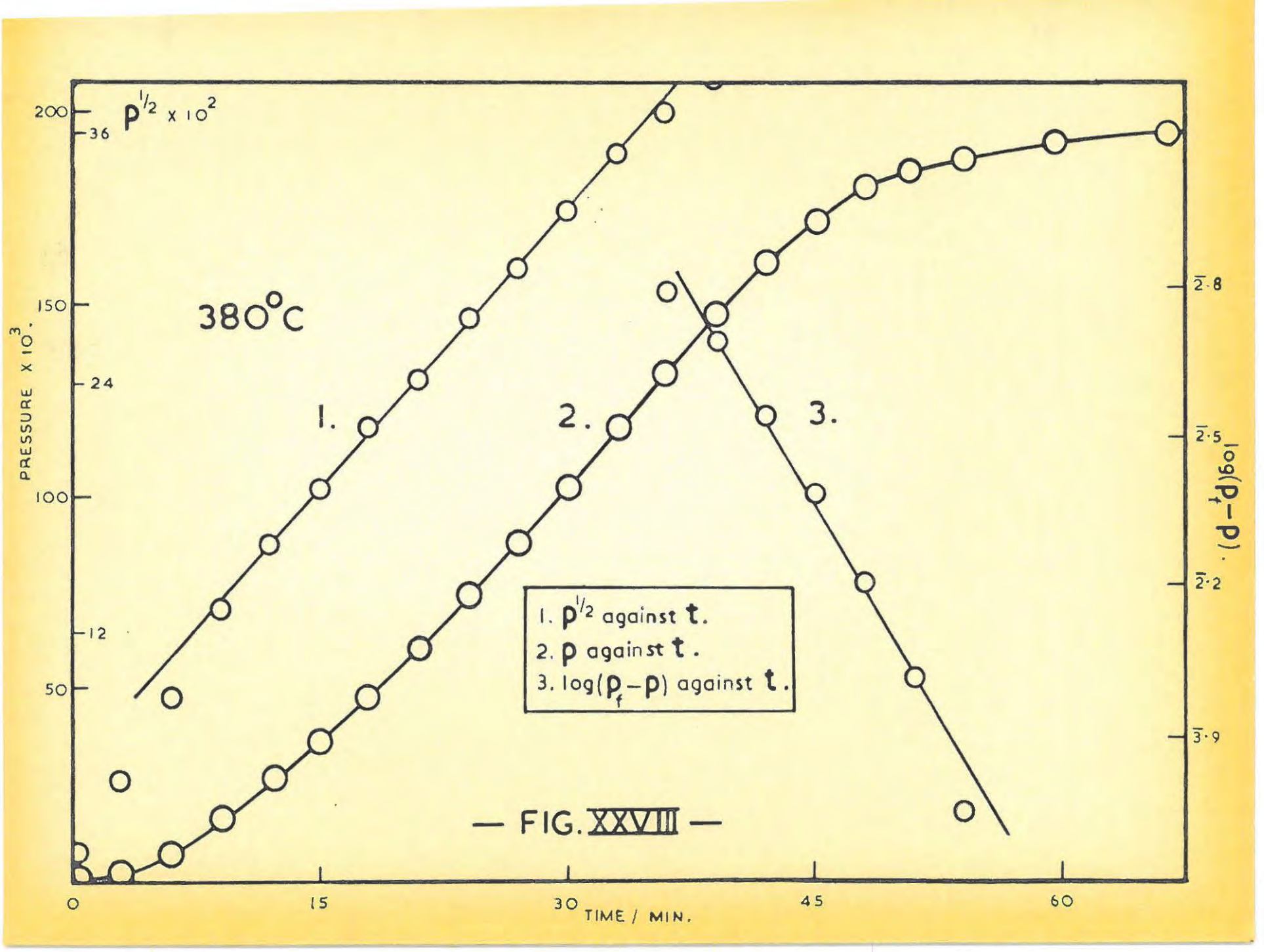
$p^{1/2} \times 10^2$
380°C
1.
2.
3.
1. $p^{1/2}$ against t.
2. p against t.
3. $\log(p_f - p)$ against t.
PRESSURE $\times 10^3$.
200
150
100
50
36
24
12
0
15
30
45
60
TIME / MIN.
$\bar{2}\cdot8$
$\bar{2}\cdot5$
$\bar{2}\cdot2$
$\bar{3}\cdot9$
$\log(p_f - p)$.

— FIG. XXVIII —

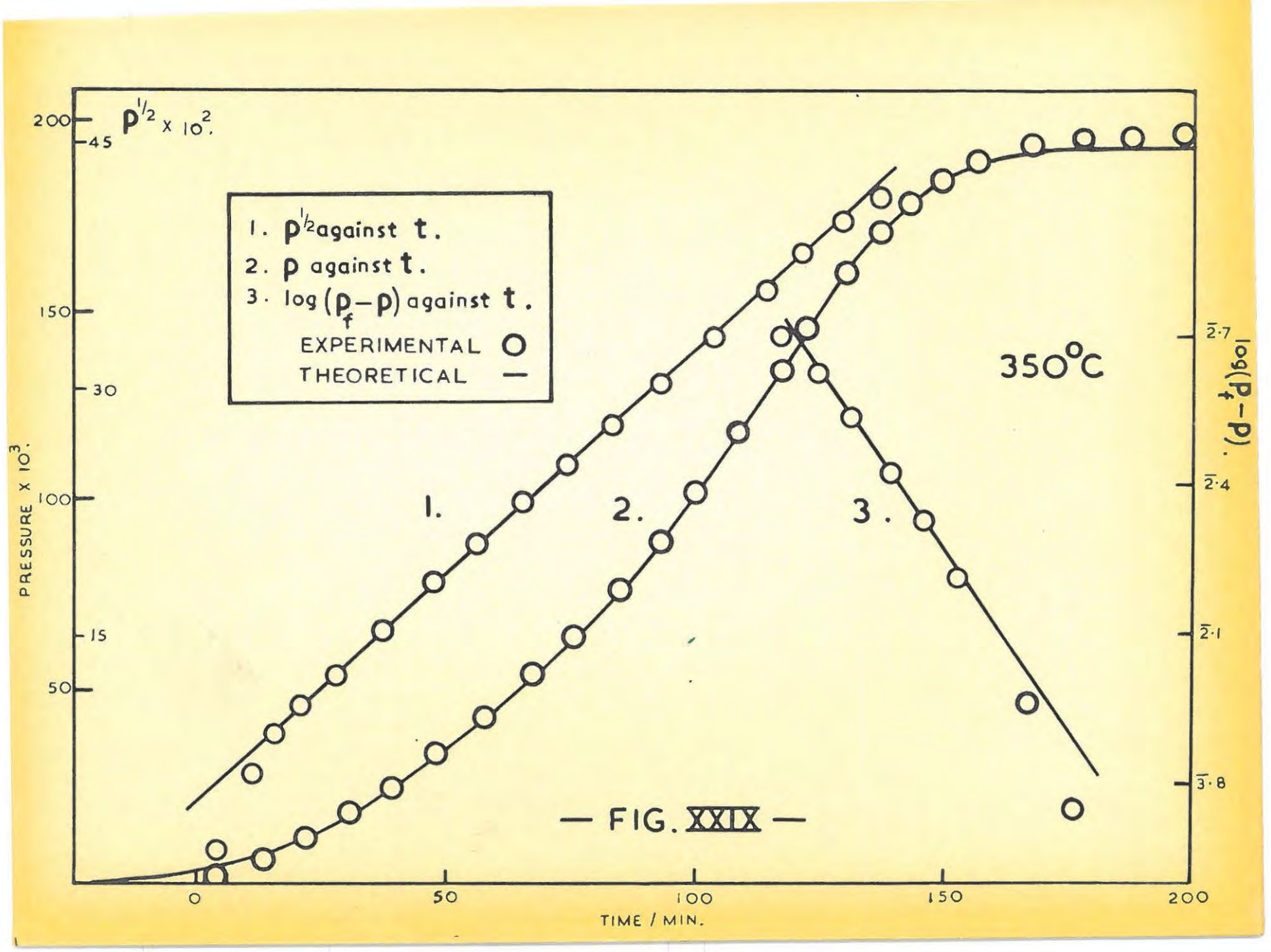
$P^{1/2} \times 10^2$.
1. $P^{1/2}$ against t.
2. P against t.
3. log $(P_f - P)$ against t.
EXPERIMENTAL O
THEORETICAL —
350°C
1.
2.
3.
PRESSURE X 10^3.
$\log(P_f - P)$.
TIME / MIN.
200
45
150
30
100
15
50
0
50
100
150
200
$\bar{2}\cdot7$
$\bar{2}\cdot4$
$\bar{2}\cdot1$
$\bar{3}\cdot8$

— FIG. XXIX —

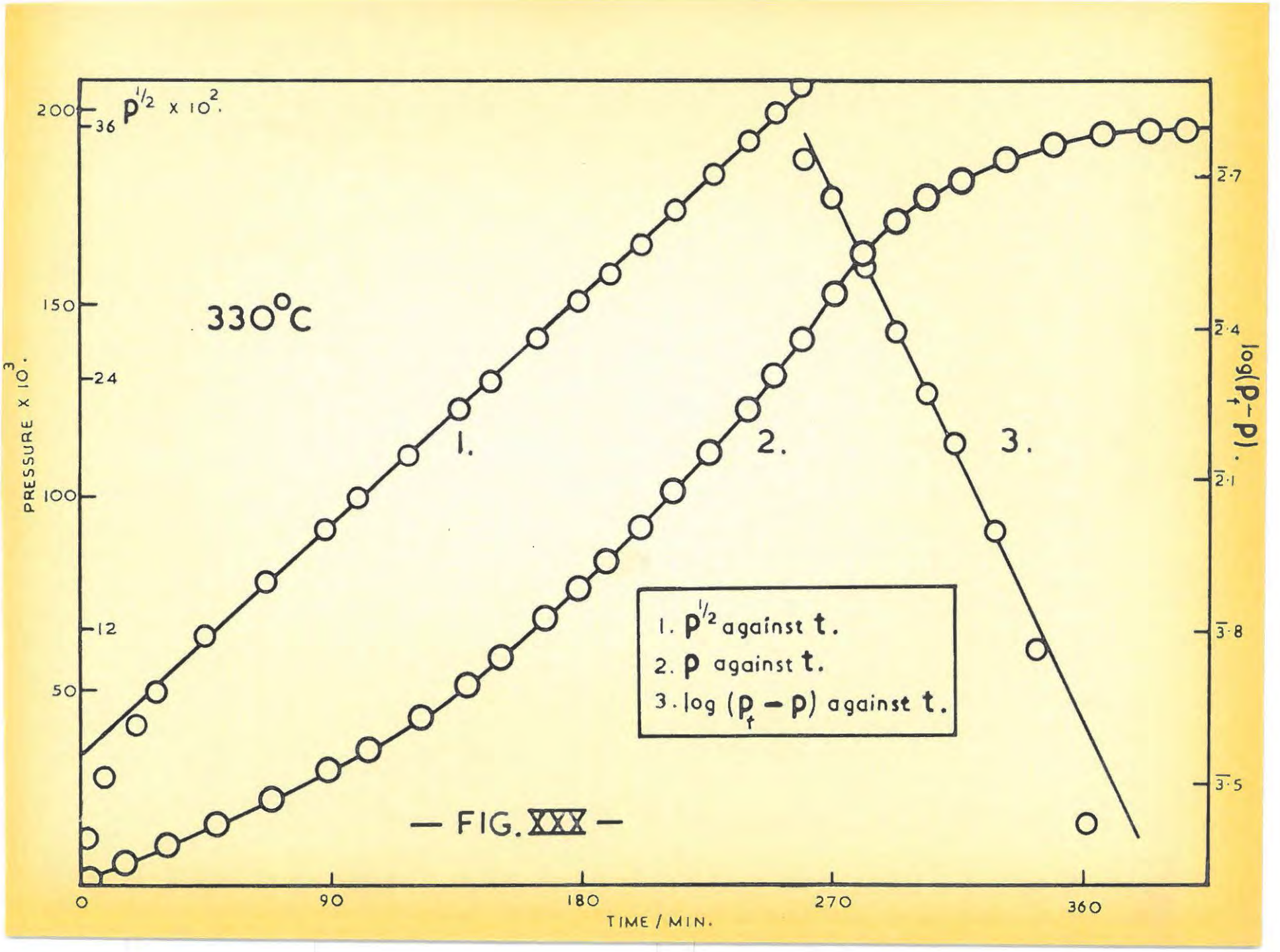
$p^{1/2} \times 10^2$.
330°C
1.
2.
3.
1. $p^{1/2}$ against t.
2. p against t.
3. log $(p_f - p)$ against t.
PRESSURE X 10^3.
200
36
150
24
100
12
50
0
90
180
270
360
TIME / MIN.
$\bar{2}\cdot7$
$\bar{2}\cdot4$
$\bar{2}\cdot1$
$\bar{3}\cdot8$
$\bar{3}\cdot5$
$\log(p_f - p)$.

— FIG. XXX —

TABLE 32.

TEMPERATURE °C.	k_5
380	0.4806
370	0.2921
360	0.2313
355	0.1921
350	0.1538
345	0.1365
340	0.1122
330	0.07178

7.2. THE DECAY PERIOD.

The fit of the Prout-Tompkins equations has already been shown to be confined to a small portion of the acceleratory period. No fit is obtained over the decay period. The applicability of the monomolecular law,

$$\log (p_f - p) = k_6 t + C_6 \quad \ldots\ldots\ldots\ldots\ldots\ldots\ldots\ldots\ldots (7.02).$$

over the decay period is shown in FIGS.XXVIII, XXIX and XXX.

The plot of the monomolecular law, although not fitting the p/t plot to its very end, gives a good straight line over the region of fit. (FIG.XXIX). The results are tabulated in TABLE 33 below.

TABLE 33./...

TABLE 33.

TEMPERATURE °C.	$1/T^{\circ}K \times 10^2$.	$k_6 \times 10$.
380	0.1531	0.6003
370	0.1555	0.5081
360	0.1580	0.3734
355	0.1593	0.3111
350	0.1606	0.2163
345	0.1619	0.1781
340	0.1633	0.1538
330	0.1659	0.0882

7.3. ACTIVATION ENERGIES.

The critical increment was determined from the equation,

$$2.303 \log_{10} k = \frac{E}{RT} + K \quad \ldots\ldots\ldots\ldots\ldots\ldots\ldots \quad (7.03).$$

where E = activation energy ($kcal.mole^{-1}$).

K = a constant.

T = the decomposition temperature in degrees Kelvin.

and R = 1.98 calories.,

by plotting the values of log k against 1/T, FIGS.XXXI and XXXII.

The values of E over the acceleratory period were; E_1 = 28.98 $kcals.mole^{-1}$, E_4 = 28.08 $kcals.mole^{-1}$, E_5 = 28.27 $kcals.mole^{-1}$, and over the decay period, E_6 = 29.64 $kcals.mole^{-1}$.

7.4./...

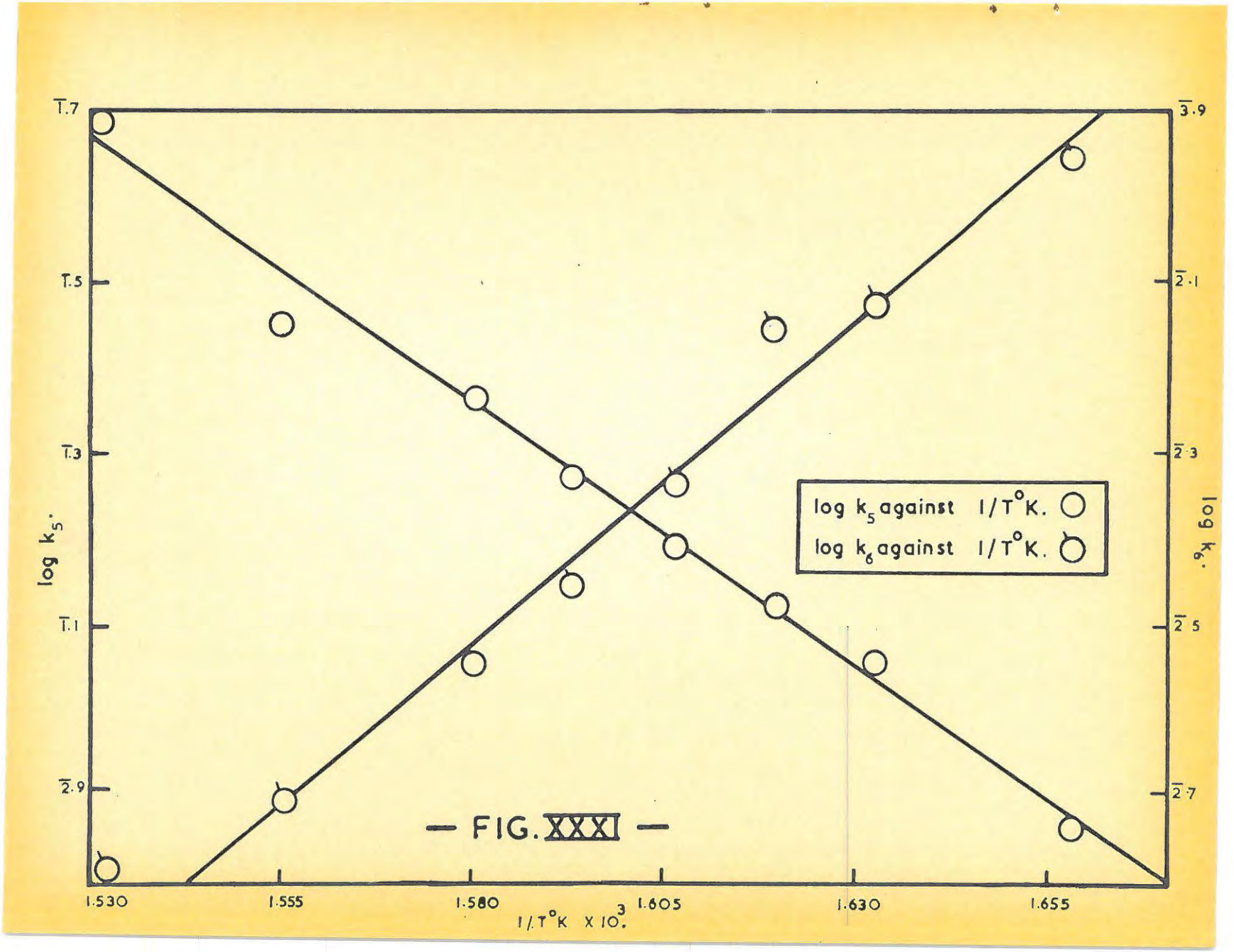
T.7
T.5
T.3
T.1
2.9
log k5.
3.9
2.1
2.3
2.5
2.7
log k6.
log k5 against 1/T°K.
log k6 against 1/T°K.
1.530
1.555
1.580
1.605
1.630
1.655
1/T°K X 10.3

— FIG. XXXI —

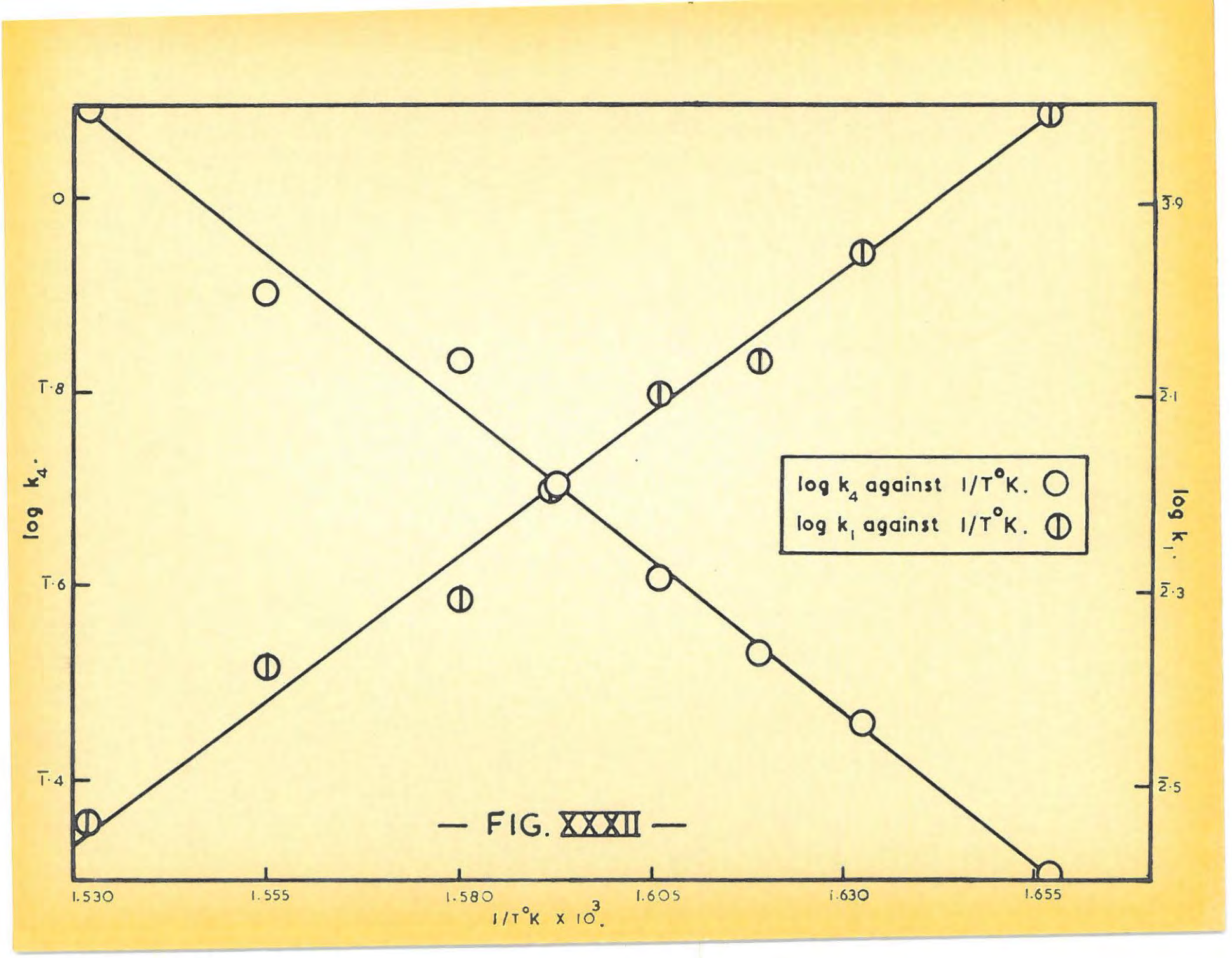
log k_4.
log k_1.
0
$\bar{1}\cdot8$
$\bar{1}\cdot6$
$\bar{1}\cdot4$
$\bar{3}\cdot9$
$\bar{2}\cdot1$
$\bar{2}\cdot3$
$\bar{2}\cdot5$
log k_4 against $1/T°K$.
log k_1 against $1/T°K$.
1.530
1.555
1.580
1.605
1.630
1.655
$1/T°K \times 10^3$.

— FIG. XXXII —

7.4. MATHEMATICAL ANALYSIS OF RESULTS FROM THE DECOMPOSITION OF SILVER OXIDE PREPARED FROM SILVER CARBONATE.

The oxide was preheated at 280°C for three hours, with pumping. The plot of $p^{\frac{1}{2}}$ against t was drawn for the decomposition at 330°C. (TABLE 34).

TABLE 34.

330°C.					
t.	p x 10^3.	t.	p x 10^3.	t.	p x 10^3.
0.5	0.1699	93	19.93	228	91.16
3	0.4722	102	22.36	237	99.32
6	1.150	113	26.39	246	106.5
9	2.036	120	29.01	258	113.5
12	2.560	130	32.70	270	130.2
18	3.221	138	36.21	282	142.0
24	4.420	147	40.34	294	159.7
30	5.471	156	44.37	309	169.4
36	6.450	165	49.34	321	179.9
42	7.786	174	54.31	336	189.2
48	8.814	186	61.33	351	193.0
57	10.59	192	64.70	370	195.3
66.5	12.95	203	72.22	400	196.7
75	15.01	210	77.84	p_f	197.4
84	17.22	219	84.01		

The/...

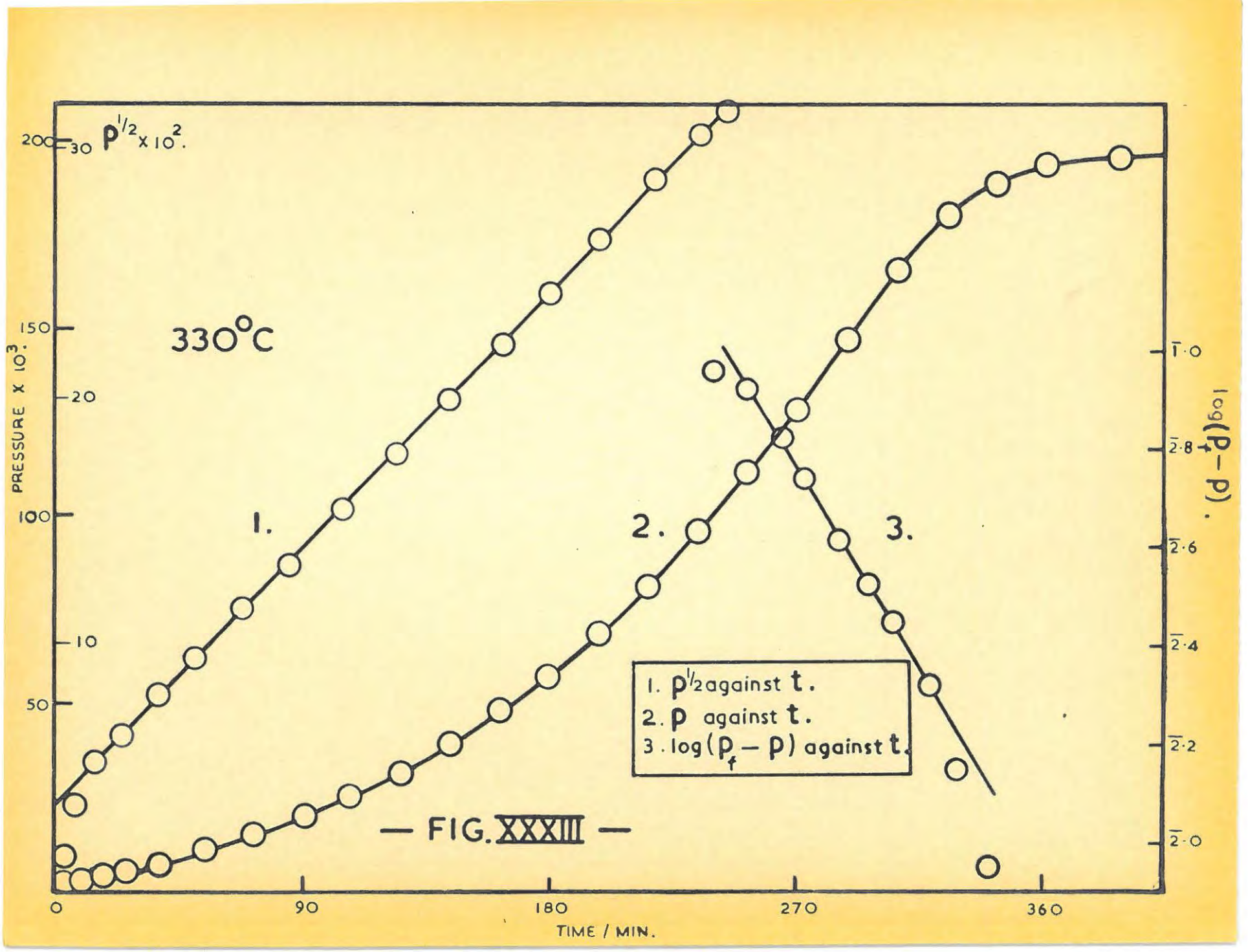
330°C
$p^{1/2} \times 10^2$.
PRESSURE X 10^3.
200
150
100
50
30
20
10
1.
2.
3.
1. $p^{1/2}$ against t.
2. p against t.
3. $\log(p_f - p)$ against t.
$\log(p_f - p)$.
$\bar{1}\cdot0$
$\bar{2}\cdot8$
$\bar{2}\cdot6$
$\bar{2}\cdot4$
$\bar{2}\cdot2$
$\bar{2}\cdot0$
0
90
180
270
360
TIME / MIN.

— FIG. XXXIII —

The fit was excellent as illustrated in FIG. XXXIII. The analysis of the decay period was also done. The fit of the unimolecular law was good and is exemplified as well in FIG. XXXIII.

8. DISCUSSION.

Contrary to previous reports, the results show that the decomposition of silver oxide is singularly reproducible. The requirement for this is that the oxide must be free from carbonate before decomposition. The decomposition of any contaminating silver carbonate during the decomposition of silver oxide will not give reproducible results, since the new surface may vary from specimen to specimen. Thus, even when a potassium hydroxide trap is present in the line, the results are not reproducible. However, after the pretreatment at 280°C for three hours in vacuo, the thermal annealing probably allows the silver oxide, formed from the decomposition of carbonate on the surface, to crystallise to its normal crystal structure, and reproducible, pressure-time curves result. The fast, initial decomposition of the silver oxide, prepared from silver carbonate, is possibly due to the fact that it is difficult to free the silver oxide from carbonate by normal heating[64].

The irreproducibility of results found by previous workers was apparently due to the reaction of the specimens with atmospheric carbon dioxide during handling and storage. The occurence of a maximum rate of decomposition at the commencement of the reaction, as found by Pavlyuchenko and Gurevich[56], and Garner and Reeves[59], is similar to that found for preparation B. It appears that Pavlyuchenko and Gurevich studied, in the main, the decomposition of silver carbonate in the relatively low temperature range 118°C - 220°C. A pressure-time curve for the thermal decomposition of silver carbonate[65] is shown in

FIG.XXXIV/...

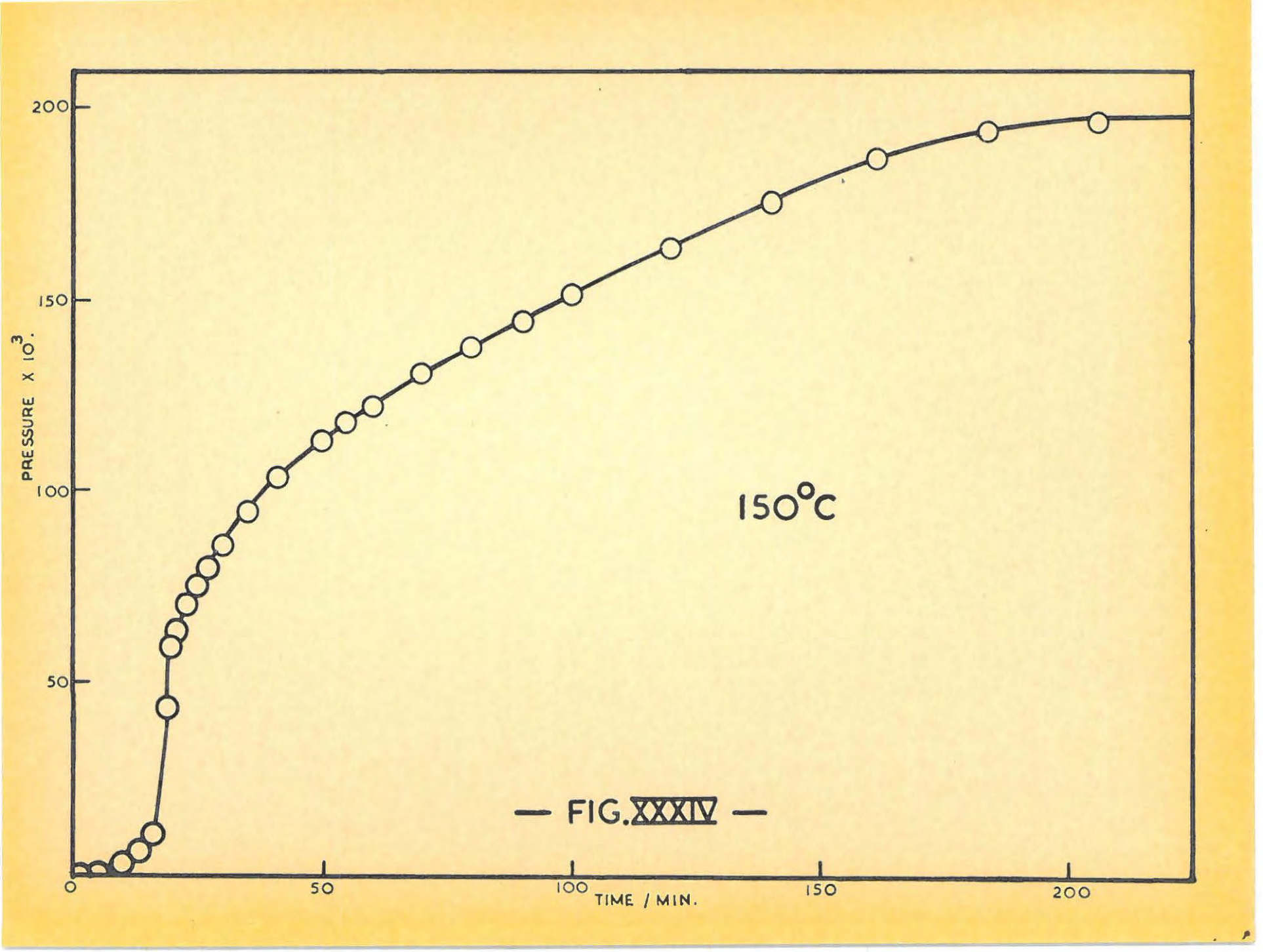

— FIG. XXXIV —

FIG.XXXIV. The reported sensitivity of the silver oxide to light was presumably due to the presence of silver carbonate, which does darken on exposure to light.

The pressure-time plots of Hood and Murphy resemble those shown by preparation C. Their pressure measurements were carried out by means of a differential water manometer; the evolved carbon dioxide thus fortuitously dissolving in the water, and only the pressure of the oxygen being recorded. The initial part of the curve was not shown. However, on producing the p/t plots back to t = 0, it appears that a small initial burst of gas may have occurred. This would be due to the rate of solution of the carbon dioxide being less than the rate of its evolution.

The sigmoid curves obtained by Garner and Reeves[59], using annealed silver oxide, do not show a maximum rate at the commencement of the reaction, and the plots resemble those found here for preheated specimens. The reason for this is not clear. However, during the annealing process, in addition to the large reduction in surface area of the silver oxide, decomposition of any silver carbonate present would have occurred. After this treatment, the large particles (approximate diameter, 0.3 mm.) would have formed less silver carbonate than the finely divided (approximate diameter 4×10^{-3} mm.) powder of the original preparation. As well, if the time of handling prior to decomposition was short, then very little contamination would have occurred. (N.B. The curves for carbon dioxide contamination show that no appreciable initial fast acceleration occurs even after 10 minutes exposure to air

after/...

after preheating). In our case, the preheating probably causes a slight sintering effect, and the particles will present a smaller surface area to the carbon dioxide gas, and thus be less contaminated by the carbon dioxide in the air than the original preparation.

Contrary to the finding here, Garner and Reeves reported an effect on the decomposition as a result of grinding. The fourfold increase in the velocity constant and the reduction of the maximum rate from 20% to 12% of the total decomposition would be consistent with a contamination of the specimen by carbon dioxide on grinding to a small particle size in air. Curves 2 and 4 in FIG.XVIII illustrate this point.

The possibility of reaction proceeding by a mechanism involving the production of effective intermediates must be considered. If these were comparatively stable, but changing at a high rate because of the rapid acceleration, the decomposition might proceed by chains with degenerate branching. However, the interruption of the reaction by sudden cooling and subsequent reheating after three hours, to the initial temperature, produced no change in the decomposition. Because irradiation with ultra-violet light and bombardment with high velocity electrons has no effect on the subsequent decomposition, a process based on a photochemical reduction, as with barium azide, is unlikely.

The accelerator stage of the decomposition is fitted by the square root plot;

$$p^{\frac{1}{2}} = kt + c \quad \ldots\ldots\ldots\ldots\ldots\ldots\ldots\ldots\ldots\ldots\ldots\ldots \quad (7.01)$$

This/...

This can arise from only one of two possibilities:-

(a). Linear chain reactions with the spontaneous generation of fresh nuclei or

(b). Reaction in two dimensions, from a fixed number of nuclei.

The first is improbable since such a mechanism would account for only a very small fraction of the decomposition, (with silver oxide, the expression holds to $\alpha \approx 0.75$), and, in addition, it has been shown that the number of nuclei cannot be further increased by physical means, such as grinding. Therefore, it is concluded that the reaction proceeds from a fixed number of centres, and that the silver nuclei grow in two dimensions. It is probable that with a precipitated solid such as silver oxide, the number of grain boundaries will be high. Two-dimensional nuclei may grow along these boundaries, thus resulting in a square root plot. The negative intercept on the abscissa of the plot of $p^{\frac{1}{2}}$ against t is of significance. In the decomposition of barium azide, Thomas and Tompkins[45] find an exponent of 6.0 with a positive intercept on the abscissa. This positive value was considered as being due to the fact that the nuclei (barium metal) grow more slowly when they are very small. With silver oxide, the negative intercept would thus signify very rapid growth of the nuclei in the early stages.

The absence of any effect after grinding suggests that the number of potential nuclei, prior to decomposition is high. This is also supported by the fact that, when points of silver become visible during the decomposition, there is a very large number per unit area. The potential sites for nucleus formation are not destroyed by

preheating/...

preheating in oxygen at one atmosphere pressure for three hours at 280°C.

In the light of the explanation of the initial fast reaction rate found with specimens contaminated by carbonate, it seems likely that Garner and Reeves' conclusion that their treatment with oxygen destroys silver nuclei and thus removes the initial fast acceleration with unannealed specimens, does not appear to be true. The sites for nuclear formation are more likely to be, not silver nuclei, but those points where the surface structure is disorganised. This is likely in a solid which is precipitated as almost colloidal sized particles. As well, nuclear formation will be favoured at dislocations. These will be high with a rapidly precipitated substance like silver oxide (approximately $10^9/cm^2$). This would explain the absence of any induction period, as found here, and by Garner and Reeves. Garner and Reeves' observation that Lewis' long induction period was due to the effect of oxygen on silver nuclei when small, is not valid since the runs in oxygen show no effect. In any case, too much stress is laid on these runs of Lewis', since neither Lewis nor any other workers were able to reproduce the long induction period.

Interrupting the decomposition at various times, exposing to carbon dioxide and then continuing the decomposition showed that reaction with carbon dioxide ceased at a time prior to the inflexion point. This would indicate surface coverage by the product at this point. However, the visual observations show that this is not so. The reason for this discrepancy is not clear, but may be due to a considerable decrease in the available silver oxide surface by the sintering of the small

silver/...

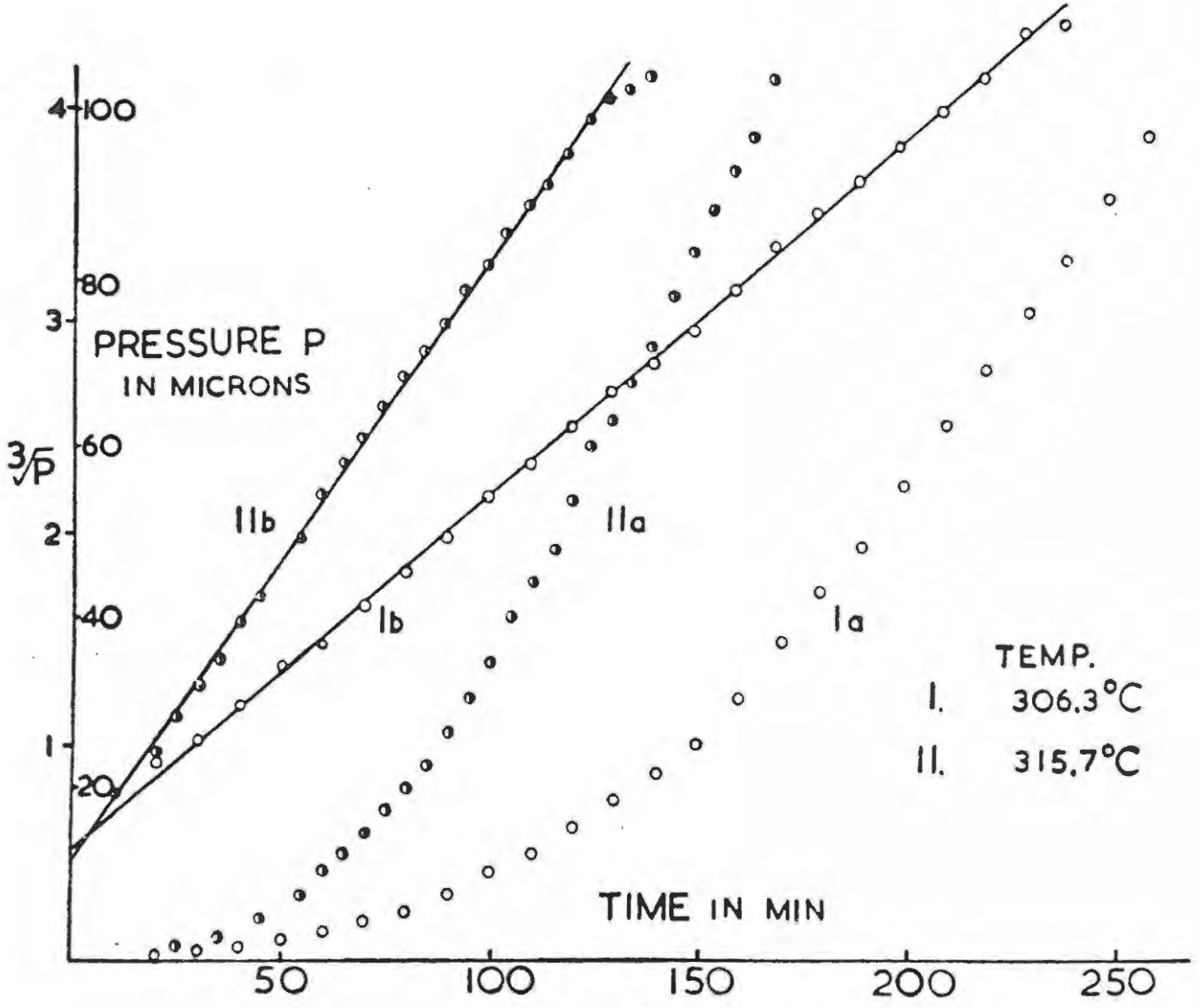
4
100
80
3
PRESSURE P
IN MICRONS
$\sqrt[3]{P}$
60
2
40
1
20
IIb
IIa
Ib
Ia
TEMP.
I. 306.3°C
II. 315.7°C
TIME IN MIN
50
100
150
200
250

FIG. 1.

silver oxide particles during decomposition.

The activation energy of 28.3 kcal.mole^{-1} approximates to the values found by Lewis[53] (31.3 kcal.mole^{-1}), Hood and Murphy[54] (25.6 kcal.mole^{-1}), and Averbukh and Chufarov[58] (29 kcal.mole^{-1}). Garner and Reeves, and Pavlyuchenko and Gurevich's values can be discredited. In any case, too few points were taken for the two activation energy plots of Garner and Reeves.

The conclusions here, and those of Garner and Reeves are at variance. The following observations might explain this. The cube root plot which they applied does not always appear to be linear. In FIG. 1. of their paper, the plot of $p^{\frac{1}{3}}$ against t for the decomposition at 315.7°C shows a distinct curvature of the line. The same applies to certain of the "split-run" curves in FIG.3. of the paper. A photographic enlargement of the plots for the decomposition at 315.7°C was made (see PLATE following page 132), and a straight line was obtained using the square root relationship (see FIG.XXXV). Another criticism of their work is that the p/t plots are not smooth curves, which would indicate a possible temperature variation.

The fit of the equations

$$\frac{dx}{dt} = k_8 x\,(1 - x) \quad \ldots\ldots\ldots\ldots\ldots\ldots\ldots\ldots\ldots\ldots \quad (2.01),$$

and

$$\ln x/(1 - x) = k_9 t + C_9 \quad \ldots\ldots\ldots\ldots\ldots\ldots\ldots\ldots\ldots\ldots \quad (2.02),$$

as found by Lewis and Hood and Murphy, respectively, is in accordance with the extent of applicability of the Prout-Tompkins' equation, since equations (2.01) and (2.02) may be transformed to the latter using the relationship $x = p/p_f$.

The/...

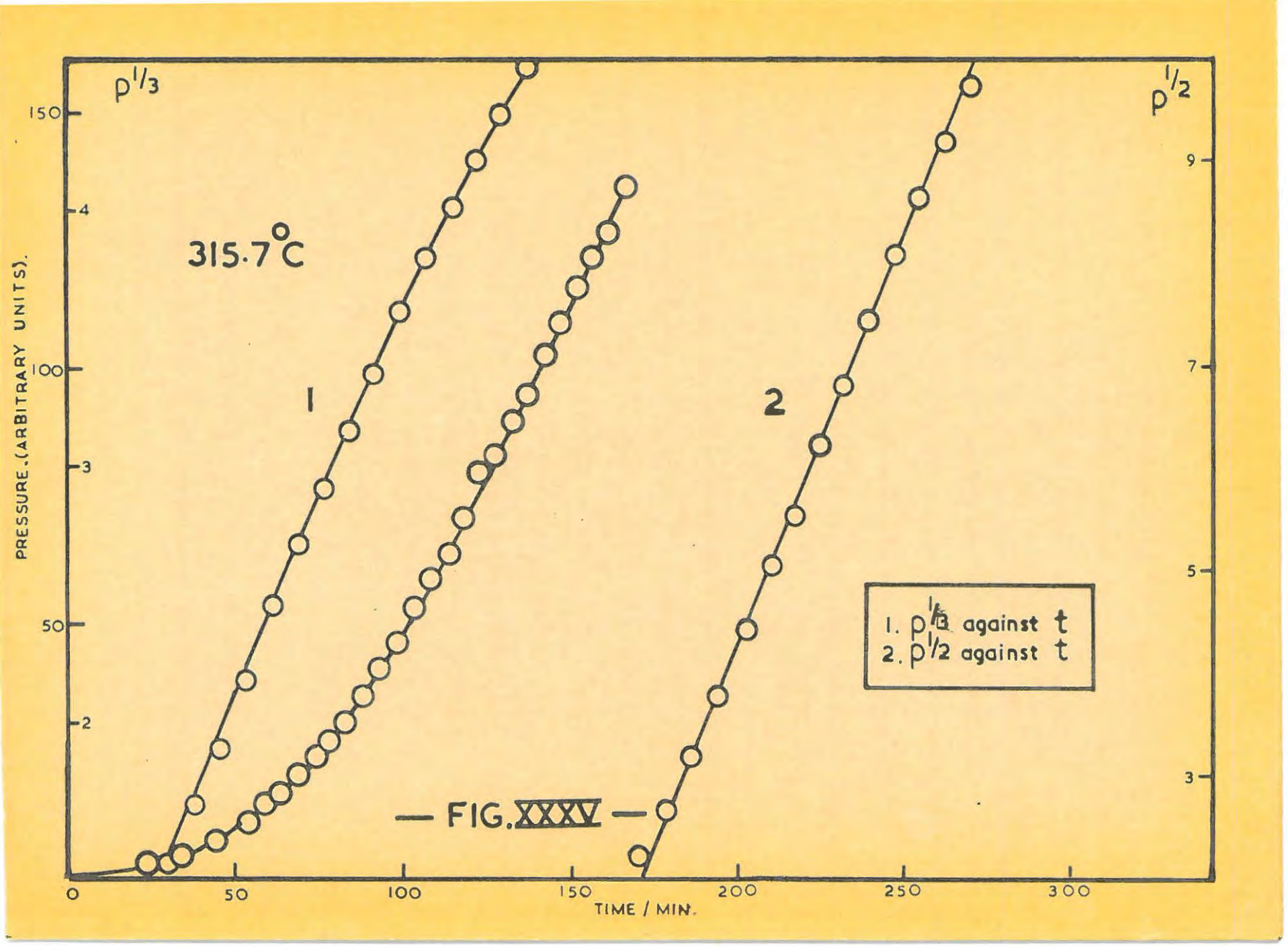
p^1/3
p^1/2
315.7°C
1
2
PRESSURE.(ARBITRARY UNITS).
TIME / MIN.
0
50
100
150
200
250
300
2
3
4
50
100
150
3
5
7
9
1. p^1/3 against t
2. p^1/2 against t

— FIG. XXXV —

The acceleratory stage of the decomposition proceeds by a mechanism of non-branching two dimensional reaction planes, and it is to be expected that, after interference of the planes, the undecomposed silver oxide will consist of isolated blocks of material in which no nuclei are present. In these blocks, if each molecule possesses an equal probability for decomposition, the rate of reaction will be proportional to the amount of substance undecomposed, consequently,

$$\frac{d\alpha}{dt} = k_9 (1 - \alpha) \quad \ldots\ldots\ldots\ldots\ldots\ldots\ldots\ldots \quad (3.01).$$

and therefore,

$$\log \frac{1}{1 - \alpha} = k_9 t + C_9 \quad \ldots\ldots\ldots\ldots\ldots\ldots\ldots\ldots \quad (3.02).$$

since $\alpha = p/p_f$,

$$\log \frac{p_f}{p_f - p} = k_9 t + C_9 \quad \ldots\ldots\ldots\ldots\ldots\ldots\ldots\ldots \quad (3.03).$$

and the plot of log $(p_f - p)$ against t will be linear. Equations (3.02) and (3.03) are referred to as the unimolecular decay law, and have been applied to several substances, e.g. by Hailes[17], to the decomposition of lead styphnate, by Garner and Gomm[19] to β- lead azide, by Harvey[8] to barium azide, by Marke[42] to calcium azide, by Centnerswer[67] and co-workers to the dissociation of magnesium, thallium, lead, cadmium, zinc and silver carbonates, by Slonim[63] to calcium carbonate, and by Hinschelwood and Macdonald[69] to silver oxalate. Silver oxide now becomes yet another substance to which the law applies.

Irradiation Effects.

The absence of irradiation effects can be accounted

for/...

for in the light of the theory advanced by Prout[7] for the decomposition of irradiated potassium permanganate. This theory was also applied to the decomposition of irradiated silver permanganate[52].

The p/t curves of whole crystals of potassium and silver permanganates, irradiated for increasing times, are characterized by:-

(a), A progressive shortening of the induction period,

(b), An increase in the maximum velocity until a "saturation velocity" is reached, and

(c), A lowering of the point of inflexion after this point.

These effects have been interpreted for irradiated potassium permanganate in terms of the production and annealing of cation vacancy-interstitial (V-I) pairs. Prout[7] irradiated potassium permanganate with 145 MeV protons, thermal neutrons and gamma-rays from ^{60}Co. The effective changes produced by the latter two radiations were considered to arise from the displacement of K^+ ions into interstitial positions, as a result of collisions with Compton electrons, generated by gamma-rays. These gamma-rays are those of capture, gamma-rays in the pile or those from the ^{60}Co "hot spot". Since collisions are heavily biased towards small energy transfer, the knocked-on atoms seldom have energies sufficient to produce secondaries, and so the damage will consist of isolated V-I pairs randomly distributed in the crystal, the separation of vacancies from interstitials being about four or five interatomic distances.

At the temperature of decomposition, there is annealing or recombination of vacancies and interstitials with the release

of/....

of the associated Wigner energy. This energy may be quite considerable. As the crystal is already at its decomposition temperature, and since the material in the region of recombination is temperature sensitive, a centre of decomposed material will result. The presence of decomposition product will cause deformation of the potassium permanganate lattice, and will result in a lowering of the activation energy for vacancy jump. There is, thus, preferential annealing around this region, which will increase in size to form a "decomposition spike".

During the induction period, annealing takes place and results in an increase in these "decomposition centres". A steady accumulation of strain in the crystal will result, and this is sufficient to produce physical fracture at the end of the induction period. Thereafter, reaction occurs on the newly formed surfaces and the reaction proceeds by the Prout-Tompkins mechanism of branching reaction chains.

The following must be considered when explaining the absence of any effect, after the oxide is irradiated in the pile or "hot spot". Firstly, annealing of the point defects at the temperature of decomposition may not occur. Silver oxide is a covalent compound[70] and in such compounds defects appear to be very stable. For example, heating irradiated (fast neutrons) quartz at 100°C for three weeks produces no observable recovery of the thermal conductivity change, and heating well above the $\alpha - \beta$ transition point, (573°C), is required before any major recovery occurs[71,72].

Secondly, if annealing does take place in silver oxide, the rapid formation and subsequent growth of the "normal" silver

nuclei/...

nuclei may destroy many of the sites at which interstitial-vacancy recombination would take place. Finally, the results after grinding show that the production of new surfaces does not increase the rate of decomposition.

Flanagan[73], in a study of irradiation effects (fast neutrons) on the dehydration of lead styphnate monohydrate, suggests that his results may be explained by the creation of massive damage in the specimens by thermal spikes. This raises the question as to whether an effect should have been obtained with specimens irradiated in the hollow uranium slug. Massive damage in the case of silver oxide would have meant the production of centres of decomposed material, i.e. silver nuclei. Reaction would then have taken place on heating from these centres. A possible answer is found to this problem if one considers the main features of the theory of thermal and displacement spikes.

Brinkman[74] suggested that, with the highly concentrated damage obtained with fast neutron bombardment of heavy elements, it was pointless to speak of individual collisions, and he proposed that the volume affected is melted for a short period, and then solidifies, in the main, with the same crystallographic orientation as the parent material. Such volumes he called "displacement spikes". The size of the displacement spike is determined as follows. As a moving atom slows down, the cross section for displacement collisions increases; at the point where one displacement collision occurs for every interatomic distance travelled, all the remaining energy of the moving atom is distributed in a displacement spike with an average energy of 1 e V per atom. The average

size/...

size of a displacement spike produced by 2 MeV neutrons in copper is thus estimated to be 75 Å in diameter, and contains 2×10^4 atoms.

Brinkman[75] further suggested that the main defects introduced by such spikes would be small dislocation loops, and a small number of interstitial atoms and vacancies quenched in on solidification.

The "thermal spike" model has been proposed by Seitz[76] in which a moving particle heats up the material surrounding its track through the solid for times of the order of 10^{-12} second. As in the case of displacement spikes, the consequences of the rapid heating and cooling cannot be predicted at all clearly[77]. Experimentally, it is observed that the ordered alloy Cu_3Au is disordered by neutron bombardment more rapidly than would be expected simply from the number of atoms displaced, and this is consistont with the displacement spike model.

The practical validity of these models depends on the limits of volume and time to which the macroscopic concepts of heat can be applied. The frequencies of atomic vibrations are in the range $10^{12} - 10^{13}$ sec^{-1}. During a time of 10^{-12} second, a disturbance to the lattice is propagated by elastic waves for distances between 10 - 50 Å, which is also about the mean free path of phonons in insulators at room temperature[78]. Consequently, in insulators, it is unsafe to apply the macroscopic concepts of heat for times shorter than 10^{-12} second, or to volumes with linear dimensions much less than 50 Å. In metals, where the free electrons play a dominant role in the transport of energy, elastic disturbances are mainly converted to disturbances of the free electrons in times of about 10^{-13} second[79].

From/...

From the above it would seem that there is a probability for the formation of thermal and/or displacement spikes in metals, but it is by no means likely in other substances such as silver oxide. In general, in silver oxide, the damage will consist of displaced atoms.

In addition to a study of the effects of irradiation on silver oxide, some preliminary studies have been made on the decomposition of irradiated and unirradiated caesium and rubidium permanganates. The detailed results do not form a part of this thesis and will be presented elsewhere. The Prout-Tompkins equation fits the p/t plots of the unirradiated specimens and the effects of pre-irradiation resemble those of potassium and silver permanganates.

Insufficient work has, as yet, been done in the field of the thermal decompositions of pre-irradiated solids to draw any definite conclusion as to the class of solids which will be affected by pre-irradiation. However, now that the decomposition of silver oxide and caesium and rubidium permanganates have been added to the number of substances which have been studied, certain characteristics are observable.

Prout[80] has reviewed the previous work and the work reported here on the decomposition of irradiated solids. He considers that substances which are likely to be affected by pre-irradiation, in the same way as the permanganates, will be those containing a simple cation and decomposing according to a branching-chain mechanism. He predicted that lead oxalate would fall into this class of solids. Preliminary/...

nary work by the author on this substance after irradiation in a ^{60}Co "hot spot", shows that this is the case. If this generalisation of Prout's is true, then the present study of silver oxide will have contributed to this deduction.

9. SUMMARY.

The results of the thermal decomposition of silver oxide, freed from silver carbonate by preheating at 280°C for three hours in vacuo, are highly reproducible. A study of the kinetics of the reaction in the range (330 - 380)°C has shown that the pressure-time curves over the acceleratory region are represented by the equation, $p^{\frac{1}{2}} = kt + c$. Reaction proceeds by the growth of two-dimensional nuclei with an activation energy of 28.3 kcal. $mole^{-1}$. The decay stage follows a unimolecular law and the activation energy is 29.6 kcal. $mole^{-1}$. Pre-irradiation by ultra-violet light, cathode rays, ^{60}Co gamma-rays, thermal and fast neutrons has no effect on the subsequent thermal decomposition.

10. BIBLIOGRAPHY.

(1). Gray and Waddington, Proc. Roy. Soc., A241, 110, (1957).

(2). Bright and Garner, J.C.S., 1872, (1934).

Garner and Pike, ibid, 1565, (1937).

(3). Garner and Tanner, ibid, 47, (1930).

(4). Garner and Maggs, Proc. Roy. Soc., A172, 299, (1939).

(5). Groocock and Tompkins, ibid, A223, 267, (1954).

(6). Bowden and Singh, ibid, A227, 22, (1954).

(7). Prout, J. Inorg. Nucl. Chem., 7, 363, (1958).

(8). Harvey, Trans. Faraday Soc., 29, 653, (1933).

(9). Macdonald, J.C.S., 832, (1936).

(10). Garner and Hailes, Proc. Roy. Soc., A139, 576, (1933).

(11). Garner and Southon, J.C.S., 1705, (1935).

(12). Cooper and Garner, Trans. Faraday Soc., 32, 1739, (1936).

(13). Wischen, Proc. Roy. Soc., A172, 314, (1939).

(14). Colvin and Hume, ibid, A125, 635, (1929).

(15). Prout and Tompkins, Trans. Faraday Soc., 40, 488, (1944).

(16). Finch, Jacobs and Tompkins, J.C.S., 2053, (1954).

(17). Hailes, Trans. Faraday Soc., 29, 544, (1933).

(18). Prout and Tompkins, ibid, 43, 148, (1947).

(19). Garner and Gomm, J.C.S., 2123, (1931).

(20). Garner and Marke, ibid, 657, (1937).

(21). Garner and Haycock, Proc. Roy. Soc., A211, 335, (1952).

(22). Mott and Gurney, ibid, A164, 151, (1938).

(22a). Garner, Chemistry of the Solid State, Butterworths Scientific Publications, (London), 1955.

(23)/...

(23). Benton and Cunningham, J. Amer. Chem. Soc., 57, 2227, (1935).

(24). Bartlett and Tompkins, unpublished work.

(25). Tompkins and Young, unpublished work.

(26). Smekal, Physik. Z., 26, 707, (1925); Roy., 45, 869, (1927).

(27). Birchmshaw and Edwards, J.C.S., 1800, (1950).

(28). Dode, Bull. Soc. Chim., 170, (1938).

(29). Herley and Prout, unpublished work.

(30). Prout and Tompkins, Trans. Faraday Soc., 42, 482, (1946).

(31). Sole, Thesis for M.Sc. degree, Rhodes University, S.A., (1959).

(32). Bagdassarian, Acta. phys-chim., U.R.R.S., 20, 441, (1945).

(33). Avrami, J. Chem. Phys., 7, 1103, (1939); 8, 212, (1940); 9, 177, (1941).

(34). Erofeyev, C.R. Acad. Sci., U.R.S.S., 52, 511, (1946).

(35). Groocock and Griffiths, J.C.S., 3330, (1957).

(36). Birchmshaw and Harris, ibid, 1398, (1948).

(37). Simpson, Taylor and Anderson, ibid, 2378, (1958).

(38). Colvin and Hume, Proc. Roy. Soc., A132, 48, (1931).

(39). Colvin and Hume, Phil. Mag., 8, 589, (1929).

(40). Bradley, Colvin and Hume, Proc. Roy. Soc., A137, 531, (1932).

(41). Mitchell, Phil. Mag., 40, 249, (1949).

(42). Sheppard, Photo. J., 65, 380, (1925).

(43). Sheppard and Hudson, J. Amer. Chem. Soc., 49, 1814, (1927).

(44). Mott, Proc. Roy. Soc., A172, 325, (1939).

(45). Thomas and Tompkins, Proc. Roy. Soc., A210, 111, (1951).

(46). Thomas and Tompkins, J. Chem. Phys., 20, 662, (1952).

(47)/...

(47). Singh, Trans. Faraday Soc., 55, 124, (1959).

(48). Garner and Moon, J.C.S., 1398, (1933).

(49). Maggs, Trans. Faraday Soc., 35, 433, (1939).

(50). Groocock. Abstracts of the Royal Society Discussion on Initiation and Growth of Explosions in Solids, (May.1957).

(51). Flanagan, Nature, 181, 42, (1958).

(52). Prout and Sole, J. Inorg. Nucl. Chem., 9, 232, (1959).

(53). Lewis, Zeit. Phys. Chem., 52, 310, (1905).

(54). Hood and Murphy, J. Chem. Educ., 26, 169, (1949).

(55). Benton and Drake, J. Amer. Chem. Soc., 56, 255, (1934).

(56). Pavlyuchenko and Gurevich, J. Gen. Chem., (Moscow), 21, 517, (1951).

(57). Iijima, Bull. Inst. Physic. Chem., (Japan), 21, 737, (1942).

(58). Averbukh and Chufarov, Zhur. Fiz. Khim., 23, 37, (1949).

(59). Garner and Reeves, Trans. Faraday Soc., 50, 254, (1954).

(60). Keyes and Hara, J. Amer. Chem. Soc., 44, 479, (1922).

(61). Eastwood, Nucleonics, 13, 52, (1955).

(62). Gledhill, J. of S.A. Chem. Inst. IV., 1, 19, (1951).

(63). Clur, Thesis for M.Sc. degree, Rhodes University, S.A., 14, (1959).

(64). Riley and Baker, J.C.S., 2510, (1926).

(65). Prout, private communication.

(66). Marke, Trans. Faraday Soc., 33, 770, (1937).

(67). Centnerswer, J. Chem. Phys., 9, 27, (1930).

(68). Slonim, Z. Electrochem., 36, 439, (1930).

(69)/...

(69). Hinschelwood and Macdonald, J.C.S., 2764, (1925).

(70). Sidgwick; Chemical Elements and their Compounds, (Oxford), I, 113, (1950).

(71). Berman, Klemens, Simon and Fry, Nature, 166, 864, (1950).

(72). Berman, Proc. Roy. Soc., A208, 90, (1951).

(73). Flanagan, Trans. Faraday Soc., 55, 114, (1959).

(74). Brinkman, J. Appl. Phys., 25, 961, (1954).

(75). Brinkman, Dixon and Meecham, Acta Metallurgica, 2, 38, (1954).

(76). Seitz, Disc. Faraday Soc., 5, 271, (1949).

(77). Kochler and Seitz, Z. Phys. 138, 238, (1954).

(78). Kittel, Introduction to Solid State Physics, (New York : Wiley), 82, (1953).

(79). Kittel, ibid, 243, (1953).

(80). Prout, Nature, 183, 884, (1959).